**M-Pos342**

**IMAGING ION MICROSCOPY EVIDENCE THAT LANTHANUM ENTERS THE CELLS AND RELEASES CALCIUM FROM THE GOLGI REGION.** ((X. Zha and G. H. Morrison)) Department of Chemistry, Cornell University, Ithaca, NY 14853.

The effect of $La^{3+}$ on LLC-$PK_1$ (porcine kidney epithelium derived) cells was investigated by ion microscopy, a quantitative imaging technique based on mass spectrometry. Cells were incubated with $LaCl_3$ for 10 min. (1 mM) or 30 min (0.1 mM), and intracellular calcium distributions were imaged by ion microscopy. Compared to control cells, a 10 min. incubation with 1 mM of $La^{3+}$ released more than 0.1 mM of calcium from the Golgi complex while other cellular regions, such as nucleus and cytoplasm, remained largely unchanged. A 30 min. incubation with 0.1 mM of $La^{3+}$ induced similar depletions in the Golgi calcium. These two experiments were repeated on cells that are pre-incubated with 1 mM ouabain. The presence of ouabain in the medium increased the loss of calcium from the Golgi by about 4 folds as compared to the one without ouabain. The $La^{3+}$ effect, therefore, was amplified by $Na^+$ loading, indicating a possible involvement of an $Na^+/La^{3+}$ exchanger. The integrity of the Golgi complex was maintained in all experiments as evidenced by NBD-ceramide fluorescence staining of the cells. Lanthanum was detected within cells by ion microscopy and its uptake was facilitated by the ouabain induced $Na^+$ loading. These results indicate that $La^{3+}$ may effect cellular calcium homeostasis by actions other than a simple calcium antagonist.

Supported by NIH grant GM 24314.

**M-Pos343**

SOME ASPECTS OF ZINC TRANSPORT INTO PIG SMALL INTESTINE BRUSH BORDER MEMBRANE VESICLES. ((F.Tacnet, F.Lauthier and P.Ripoche)) DBCM/SBCe, CE Saclay, 91191 Gif/Yvette Cedex, France .

A specific and saturable carrier mediated process for the essential trace element, zinc, was already described in the intestinal brush border membrane (for review see Cousins (1985) Physiol.Rev., 65:238-309 ; Tacnet et al. (1990) BBA, 1024:323-330). Here, we looked for possible zinc pathways through other transport systems by measuring time-courses of $^{65}$Zinc uptake across the intestinal apical membrane isolated in a vesicular form.

Although zinc uptake is strongly affected by pH ($pH_{opt}$=6.6), experiments in the presence or absence of proton gradients did not allow us to conclude in favor of a neutral $Zn^{2+}/_nH^+$ exchange mechanism.

A zinc uptake through the $Cl^-/HCO_3^-$ exchanger, as those shown in the red cell membrane, was studied. Although zinc transport was enhanced in the presence of bicarbonate ions (or other low-affinity zinc-binding anions such as thiocyanates), no DIDS or DPC sensitivity was detected indicating that the intestinal anion antiporter is not a major route for zinc reabsorption.

By using the tripeptide GlyGlyHis, expected to be a high-affinity zinc ligand, we showed that zinc could be transported as a $[(GlyGlyHis)_n\text{-}(Zn)_n]$ complex, utilizing the $H^+$/peptide cotransport system, i.e., in conditions necessary for the secondary active transport of the peptide: inwardly directed $H^+$ gradients and membrane potential "negative inside".

These results suggest that complexes of zinc could be reabsorbed through the brush border membrane either via a zinc specific pathway (saturable carrier) or via existing carriers such as a neutral anionic exchanger or peptide (or amino acid) transporters.

**M-Pos344**

MODULATION OF POTASSIUM CHANNELS AND CALCIUM INFLUX IN ENDOTHELIAL CELLS BY CYCLOPIAZONIC ACID, A SARCOPLASMIC RETICULUM $Ca^{2+}$-PUMP INHIBITOR. ((E. Pasyk and E.E. Daniel)) McMaster University, Hamilton, Ontario.

We have used cyclopiazonic acid (CPA), a selective inhibitor of the $Ca^{2+}$-pump in sarcoplasmic reticulum (SR) of cultured bovine pulmonary endothelial cells to elucidate the role of $Ca^{2+}$ stores in controlling $K^+$ channels and $Ca^{2+}$ entrance using patch-clamp technology. As a consequence of the action of CPA, unbalanced leakage of $Ca^{2+}$ from the intracellular stores occurs, causing transient elevation of cytosolic $Ca^{2+}$. This elevation is expressed by $[Ca^{2+}]_i$-induced outward $K^+$ current activation. Reduction of inwardly rectifying $K^+$ current also occurs. The effects of CPA on both $K^+$ currents shifts the membrane potential towards more negative values increasing the driving force for the external $Ca^{2+}$. We also showed that $Ca^{2+}$ may enter the bovine pulmonary artery endothelial cells through nonselective cation channels (permeable for $Na^+$, $K^+$, $Ca^{2+}$) activated by stretch. CPA stimulates an influx of $Ca^{2+}$ through these channels. CPA-induced increase of intracellular $Ca^{2+}$ due to emptying of $Ca^{2+}$ stores and subsequent influx of external $Ca^{2+}$ may lead to the production of EDRF by endothelial cells which contributes to the relaxation of vascular smooth muscle. (Supported by MRC and PMA of Canada.)

**M-Pos345**

CORTICOSTERONE STIMULATES AMILORIDE-SENSITIVE SODIUM ENTRY IN XENOPUS LAEVIS LUNG ((L.M. Baxendale)) The Johns Hopkins Univ. Sch. Nursing, Baltimore, Md. 21287-1316.

Sodium (Na) absorption is integral for alveolar fluid reabsorption essential for optimal lung function. Xenopus laevis lung (XLL) resembles mammalian alveolar type II epithelial cells (ATII) (Fischer et al 1989) morphologically and functionally. Both systems exhibit active Na absorption via entry through amiloride-sensitive apical Na channels and exit via basolateral Na-K ATPase pumps. Harvest and preparation of ATII monolayers is a time and labor intensive procedure. XLL has a single epithelial cell type and does not require manipulation for study. Contrary to previous reports, we have found that large adult XLL does respond to $\beta$ adrenergic agonists and other agents such as the glucocorticoid corticosterone (Corti) important in regulation of Na and fluid reabsorption in distal lung. Lungs of XL were excised, opened and mounted as a flat sheet on lucite rings in a modified Ussing chamber. Tissues were continuously perfused on both sides with a Ringer's solution containing (in mM): 100 Na, 2.4 K, 2.4 $HCO_3$, 2 Ca, 102 Cl, 5 D-glucose bubbled with room air pH 7.8 at 22° C. Initial values for open-circuit transepithelial voltage and resistance (Rt); and short-circuit current (Isc) were recorded. Essentially all of the Isc was amiloride sensitive (Ina). The tissues were short-circuited and Ina was allowed to equilibrate (7.1 ± 1.1 $\mu A/cm^2$). At this point, corticosterone (1 $\mu M$) was added to the basolateral bath. After several minutes,Ina increase to a plateau value of 13.7 ± 3.3 $\mu A/cm^2$ (t=192 minutes). Rt was slightly decreased in the presence of Corti (88.5 ± 2.5 % control). Glucocorticoid receptors are found on ATII cells and these data suggest XLL also shares this trait. These data indicate that XLL may be an alternative model system for ATII cells. Further, enhanced lung function observed in the presence of glucocorticoids (which enhance surfactant secretion) may also be augmented by stimulation of Na entry and therefore fluid reabsorption.

## MEMBRANE RECEPTORS

**M-Pos346**

**PURIFICATION AND CHARACTERIZATION OF THE HIGH AFFINITY HIT CELL SULFONYLUREA RECEPTORS** ((D.A. Nelson, L. Aguilar-Bryan, S.W. Wechsler, A.S. Rajan and J. Bryan)) Depts. of Medicine and Cell Biology, Baylor College of Medicine, Houston, TX 77030

Sulfonylureas stimulate insulin secretion from pancreatic beta cells by binding with high affinity to a membrane protein, presumably an ATP-sensitive $K^+$ channel. HIT cell membrane proteins were photolabeled with an $^{125}$I-labeled glyburide analog, solubilized with 1% digitonin and chromatographed on lectin, reactive dye and phenylboronate containing column beds. Further purification was done by electrophoresis. The major form of the receptor is a Con A-binding glycoprotein with an apparent MW of 140 kDa. This protein photolabels with an efficiency of ~1%. The 140 kDa band shifts mobility slightly upon digestion with Endoglycosidase F/N-glycosidase F (Endo F), yielding a polypeptide of ~137 kDa after N-linked carbohydrate removal. A second, minor, wheat germ agglutinin-binding form of the receptor is also present in HIT cells. This protein, with an apparent MW of 150 kDa, photolabels with low efficiency. Incubation of this form of the receptor with Endo F also yields a polypeptide of ~137 kDa, suggesting the two forms of the receptor contain similar polypeptides, but differ in carbohydrate content. This idea is supported by experiments in which each receptor is digested with Endo F, followed by V8 protease. The resultant peptides from each receptor have identical electrophoretic mobilities. Two radiolabeled peptides from the 140 kDa protein, of 49 and 66 kDa, are glycosylated at residue 9, the same position as in the intact polypeptide. This suggests that the N-terminus is extracellular, and that the sulfonylurea binding site is in the first one-third of the receptor protein.

**M-Pos347**

THE KINETICS OF RECEPTOR-MEDIATED CELL ADHESION UNDER FLUID FLOW. ((L.A. Tempelman, D. A. Hammer)) School of Chemical Engineering, Cornell University, Ithaca, NY 14853.

The physiological function of many cells is dependent on their ability to adhere via receptors to ligand-coated surfaces under fluid flow. For example, an early step in the leukocyte-mediated inflammatory response is the adhesion of neutrophils to endothelial cells under fluid stresses of 1 -5 dynes/$cm^2$. We have developed an experimental system to measure the kinetics of cell adhesion as a function of cell and surface chemistry and fluid flow. Using a parallel-plate flow chamber, we measure the binding of rat basophilic leukemia (RBL) cells preincubated with anti-DNP IgE to polyacrylamide gels to which 2,4 dinitrophenol (DNP) is covalently bound. We observe the spatial pattern of cell binding as cells travel from the DNP-free to the DNP-coated section of the chamber, as well as the total number of cells bound.

There is a rather narrow range of DNP densities, IgE coverages and shear rates for which the percentage of cells which bind changes. For example, with 4 x $10^4$ binding sites on the cells and a ligand density of approximately $10^{10}$ sites/$cm^2$, adhesion ranged from 99 to 2.4 % for shear rates from 30 to 120 $sec^{-1}$. The spacial patterns of adhesion indicate that adhesion is a probabilistic process. Results for adhesion as a function of receptor number and ligand density will also be presented. Finally, we measured the adhesion of RBL cells to DNP-coated gels which were preincubated with anti-DNP IgE. Adhesion in this system results from the binding of the $Fc_\varepsilon$ receptor to the Fc portion of IgE , a *higher* affinity interaction with a hundred fold *lower* forward reaction rate. Adhesion under flow in this system is very low, although static adhesion occurs readily. This demonstrates that the forward rate of reaction of the receptor-ligand pair is more important than its affinity in the regulation of adhesion under fluid flow.

**M-Pos348**
MEMBRANE FUSION MEDIATED BY HUMAN PARAINFLUENZA TYPE 3: RECEPTOR REQUIREMENTS FOR VIRAL INFECTION AND CELL-CELL FUSION.
Anne Moscona[1] and Richard Peluso[2], Mt Sinai School of Medicine, Departments of [1]Pediatrics & Cell Biology and [2]Microbiology, NY.

Human parainfluenza virus type 3 (HPF3), a member of the paramyxovirus group of viruses, is an important agent of respiratory disease in children. HPF3 establishes persistent infection in cell culture following high multiplicity infection. The persistently infected (pi) cells do not fuse with each other, yet rapidly fuse when seeded with uninfected cells. We have shown that the failure of the pi cells to fuse with each other is due to a lack of a receptor on these cells for the viral hemagglutinin-neuraminidase (HN) glycoprotein, and established that both the fusion (F) and HN proteins are needed for cell fusion mediated by HPF3. We now use this information to investigate the mechanism of membrane fusion mediated by HPF3. Low multiplicity infection with HPF3 normally results in extensive cell fusion. However, syncytium formation is prevented by the addition of neuraminidase to remove sialic acid, the receptor for the viral HN glycoprotein. While the infected cells do not fuse, the virus still spreads throughout the culture, and the cells become persistently infected. The finding that neuraminidase treatment of cells infected at a low moi allows spread of the virus without cell fusion suggests that there are different sialic acid receptor requirements for a virus to infect a cell (by fusing with the plasma membrane) than for fusion between cells. To investigate this, cells infected with low multiplicity were treated with several different amounts of bacterial neuraminidase. With low level neuraminidase treatment, there are sufficient sialic acid receptors for virus to infect a cell but not enough to allow cell fusion, while with higher level neuraminidase treatment there are insufficient sialic acid receptors even for virus infection. Our interpretation of these data is that there are different neuraminic acid requirements for a virus particle to infect a cell by fusion of the viral envelope with the plasma membrane than for fusion of an infected cell with an uninfected cell. These findings offer insight into virus-induced membrane fusion, the fundamental mechanism of pathogenesis by HPF3.

**M-Pos349**
ANALYSIS OF THE LIGAND BINDING SITE OF THE HUMAN N-FORMYL PEPTIDE RECEPTOR.
((J.-L. Gao and P.M. Murphy)) NIAID, NIH, Bethesda, MD 20892. (Spon. by Lesley McKinney).

The N-formyl peptide receptor (FPR) is a G protein-coupled receptor expressed in phagocytes of higher species. FPR mediates the activation of neutrophil microbicidal functions. A structurally related receptor FPRL1 (L=like) has 69% identity to FPR at the amino acid (aa) level. When expressed in Xenopus oocytes, FPRL1 has a $10^5$-fold higher threshold for activation by N-formyl-met-leu-phe (fmlp) compared with FPR. In order to understand the structural basis for this loss of ligand potency for FPRL1, we constructed FPR-FPRL1 receptor chimeras, and tested their ability to link fmlp to a $Ca^{2+}$ flux response in Xenopus oocytes. We found that: (1) switching the N-terminal domain of FPR to FPRL1 shifts the fmlp concentration-response curve 300-fold to the left; (2) switching individual extracellular loops of FPR to FPRL1 shifts the concentration-response curve about 10-fold to the left for each loop; (3) switching the C-terminal domains of FPRL1 to FPR does not shift the concentration-response curve. These results and sequence comparisons suggest that (1) the binding of fmlp to FPR involves all four extracellular domains; and (2) the loss of sensitivity of FPRL1 to fmlp is caused, at least in part, by acidic residues in the N-terminus of FPRL1.

**M-Pos350**
CHEMICAL CROSS-LINKING OF IgE-RECEPTOR COMPLEXES IN RBL-2H3 CELLS ((S.-Y. Mao and H. Metzger)) NIAMS, NIH, Bethesda, MD 20892 (Spon. by D.H.H. Tsao)

Aggregation of IgE-receptor complexes on mast cells by multivalent ligands activates a signal transduction pathway that leads to degranulation. The phosphorylation of aggregated receptors and cellular proteins is thought to play a role in intracellular signaling. Aggregated IgE-receptor complexes become associated with the Triton X-100 insoluble cytoskeleton or plasma membrane skeleton. This association is dependent on the degree of aggregation. We investigated whether cellular components interact preferentially with aggregated receptors and become temporarily trapped under conditions where the receptor-cytoskeleton interactions are promoted. Gel electrophoresis and western blot by anti-phosphotyrosine antibody showed that both the phosphorylated β and γ receptor subunits as well as a 85-kDa peptide (p85) become trapped in the detergent-insoluble skeleton. A cross-linking protocol was developed to stabilize the interaction between the receptor and proteins physically proximal to it. RBL cells were permeabilized with tetanolysin and proteins were cross-linked with the water-soluble chemical cross-linker, DTSSP. These experiments allowed confirmation of the interaction between the receptor, p85, and several additional proteins.

**M-Pos351**
**AUTOIMMUNE ANTIGEN GP330 IS IMMUNOLOGICALLY RELATED TO SKELETAL MUSCLE RYANODINE RECEPTOR.**
**((*John J. Mackrill, Abdul K. Sesay and F. Anthony Lai*))**
**MRC National Institute for Medical Research, Mill Hill, London, UK.**

Monoclonal antibodies raised against rabbit skeletal muscle ryanodine receptor (RyR) cross-react with a high molecular weight (HMW) protein in rabbit kidney microsomal preparations. This HMW kidney protein sediments as a complex with a similar apparent sedimentation coefficient (~30S) to the RyR upon sucrose density gradient centrifugation, but does not display high-affinity [$^3$H]ryanodine binding. The kidney HMW protein binds calcium more effectively than does skeletal muscle RyR, as assessed using a $^{45}Ca^{2+}$ overlay technique. Monoclonal antibodies and polyclonal antisera raised against the purified kidney HMW protein do not cross-react with skeletal muscle RyR. Lectin binding studies indicate that the kidney HMW protein is glycosylated, unlike skeletal muscle RyR. Nucleotide sequence analysis of a cDNA clone isolated from a rabbit kidney cDNA library using antisera to kidney HMW protein, indicates that the rabbit kidney HMW protein is related to gp330, a human glycoprotein autoantigen associated with Heymann's nephritis, an autoimmune disease of kidney. The epitope(s) involved in this immunological cross-reaction are as yet uncharacterized.

**M-Pos352**
EGF BINDING KINETICS AT THE SINGLE CELL LEVEL.
((J. Chung, N. Sciaky and D.J. Gross)) Program in Molecular and Cellular Biology, University of Massachusetts, Amherst, MA 01003 and CBMB, NICHD, National Institutes of Health, Bethesda, MD 20892.

Time lapse series of images of fluoresceinated-EGF (f-EGF) binding and debinding to EGF receptors (EGF-R) on individual A431 cells were collected via quantitative fluorescence imaging. Experiments were carried out at 4 °C to prevent endocytosis of f-EGF/EGF-R complexes. Binding curves (fluorescence vs. time) were generated for each cell. The data were fit to both one-site and two-site first order binding models; the two-site model fit the data much better for short (<1 min) binding/debinding times. Scatchard analysis of EGF binding has usually been interpreted as indicating that there are two affinity classes of EGF-R present on each cell, although direct evidence that both affinity classes exist on single cells has been lacking. Our data show that individual cells display both receptor affinity classes. Our data suggest that the density of EGF-R on A431 cells varies considerably from cell to cell, but that the range of EGF-R on- and off-rates for EGF binding is small.

Supported by NSF DCB-9105429.

**M-Pos353**
**CELL LENGTH DEPENDENT RECTIFICATION OF SURFACE RECEPTOR TRANSPORT IN SINUSOIDAL ELECTRIC FIELDS.**
**((T.R. Gowrishankar, and R.C. Lee))** The University of Chicago, Pritzker Sch. of Med., Chicago, IL 60637

The uniaxial resistance to receptor transport in an applied sinusoidal electric field causes a net time-average displacement, resulting in the rectification of receptor migration. Since the kinetics of receptor transport depends on electromigration and back-diffusion, the cell length affects the redistribution of receptors in a sinusoidal field. A finite difference model was formulated to simulate the receptor transport in an applied electric field. This model accounted for receptor crowding, excluded volume due to inter-protein interactions and the presence of immobile receptors. The simulation results show that under an applied sinusoidal electric field, the level of accumulation at the tapered ends of a cell increases as the cell length is reduced. Relative density of surface receptors at the two ends of the geometry (inset) is shown in the figure as a function of the cell length. The profile shown is for a 10 V/cm, 0.01 Hz sinusoidal electric field. A net relative accumulation of 20 times the initial concentration was observed at the leading edge of the geometry for cells of 50 μm length for receptors with a mobility of 1.2 $\times 10^{-6}$ cm$^2$/V-sec and a diffusion coefficient of $2.3 \times 10^{-9}$ cm$^2$/sec corresponding to MHC receptors. The level of accumulation was found to decrease by an order of magnitude for a corresponding decrease in receptor mobility. The simulation results also demonstrate that receptor transport rectification is observed at higher frequencies for cells shorter than 50 μm.

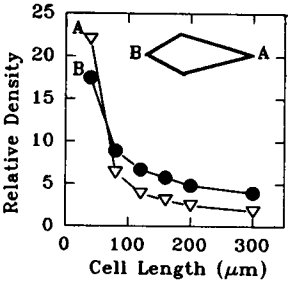

**M-Pos354**

GLUCAGON-LIKE PEPTIDE-1 MODULATES ß-CELL $[Ca]_i$ ONLY WHEN [GLUCOSE] IS ELEVATED. ((C.A. Cullinan, E.J. Brady, R. Saperstein, M.D. Leibowitz)) Merck Research Labs, P.O. Box 2000, RY80N-31C, Rahway, NJ 07065

Depolarizing concentrations of glucose produce characteristic, well documented alterations of intracellular free Ca ($[Ca]_i$) in pancreatic ß-cells. The effects of the proposed incretin, glucagon-like peptide-1 (7-36) amide (GLP-1) on $[Ca]_i$ were determined at 32-34° C from fura-2 fluorescence ratio imaging of individual ob/ob mouse pancreatic ß-cells after 3-6 days in culture. In control cells $[Ca]_i$ is low in 3 mM glucose; increasing [glucose] to 8 mM results in an initial dip in $[Ca]_i$ followed by slow oscillating increases in $[Ca]_i$ (**A**). GLP-1 (0.03-10,000 pM) does not alter $[Ca]_i$ when glucose is low (3 mM) but, in elevated glucose (8-10 mM) GLP-1 does change the $[Ca]_i$ response (**B**). The integral of the initial dip is reduced ([GLP-1]=10-100 pM). The integral of the "complete" Ca signal is increased for [GLP-1]≥1 pM. In addition, the peptide increases the frequency of both large, rapid spikes of increased $[Ca]_i$ ($ED_{50}$~1 pM) and sustained, stable plateau responses. Activation of the GLP-1 receptor leads to alterations in $[Ca]_i$ only when [glucose] is high.

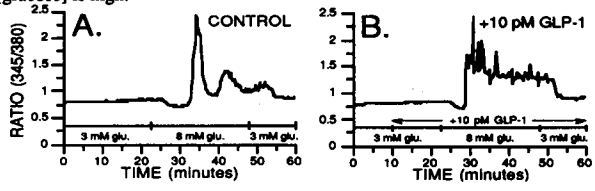


**M-Pos355**

SUBTYPE SELECTIVITY OF ISOPROTERENOL IN NEONATE AND ADULT RAT VENTRICLE CELLS. ((V. Kuznetsov, S.F. Steinberg and R.B. Robinson)) Dept. of Pharmacology, Columbia Univ., NY 10032.

Beta-adrenergic agonists are known to enhance cardiac contractility, relaxation and $[Ca]_i$. Although the heart is reported to contain both $ß_1$ and $ß_2$ receptors, their relative role in these actions of ß-adrenergic agonists is not fully defined. We used the $ß_1$ antagonist CGP 20712 and the $ß_2$ antagonist ICI 118551 (both 0.1 μM) to investigate if the contractile and $[Ca]_i$ effects of isoproterenol (ISO), in both nonatal and adult rat ventricle cells, can be fully accounted for by action at $ß_1$ receptors. In the presence of ICI, ISO 0.1 μM increased the amplitude of the calcium transient, measured as the fura2 ratio signal, by 27±14% and 18±14% in adult and neonate (x±SE). Cell shortening, measured with a video edge detection system, increased 39±17% and 40±25% in the two preparations. The maximum rate of relaxation of shortening increased 51±17% and 118±28%, respectively. In contrast, after exposure to CGP, the same concentration of isoproterenol had no significant effect (P>0.05) on the amplitude of either the fura2 or cell shortening signals, or the maximum rate of relaxation, both in the adult and neonate. It therefore appears that, with respect to the parameters studied, all effects of ISO can be accounted for by action at the $ß_1$ receptor, both in the neonatal and adult rat ventricle.

**M-Pos356**

CHARACTERIZATION AND FUNCTIONAL EXPRESSION OF THE ATP RECEPTOR IN VAS DEFERENS SMOOTH MUSCLE. ((S.N. Russell, M.A. Horner, D.P. Westfall, I.L.O Buxton and B. Horowitz)) Departments of Physiology and Pharmacology, University of Nevada School of Medicine, Reno, NV 89557.

ATP has been established as an excitatory co-neurotransmitter in the guinea-pig vas deferens. The direct characterization of the postsynaptic $P_2$ receptor involved has not been made. Rapid, reversible [$^{35}$S]ADPßS binding, and saturation isotherms demonstrating that the radioligand bound to 356 ± 46fmol/mg protein with high affinity ($K_D$ = 9.5 ± 1.2nM), suggested the presence of $P_2$ receptors. In vas deferens labeled with [$^3$H]*myo*-inositol and stimulated with ATP, the rapid dose-dependent appearance of agonist-stimulated $IP_3$ accumulation was mimicked by αß-methylene ATP>ATP>ADPßS and was blocked by pretreatment of tissues with ANAPP$_3$ suggesting the identity of $P_2$ sites as phospholipase C-coupled $P_2x$ receptors. Poly-A$^+$ mRNA extracted from guinea-pig vas deferens was injected into *Xenopus laevis* oocytes. Using the two electrode voltage clamp method the endogenous $Ca^{2+}$-activated $Cl^-$ current couldbe evoked by steps from a holding potential of -60mV to +20mV. In cells injected with mRNA addition of 5mM ATP to the bath solution significantly increased the amplitude of this current. This rise was assumed to be due to a receptor stimulated rise in intracellular $Ca^{2+}$. A similar significant 0.5mM ATP induced rise in the $Ca^{2+}$-activated $Cl^-$ current was seen in the absence of extracellular $Ca^{2+}$ suggesting an internal source for the $Ca^{2+}$ rise. *This work was supported by NIH HD26227 to ILOB and a grant from the American Heart Association.*

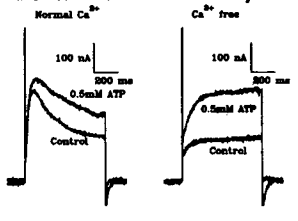


**M-Pos357**

FUNCTIONAL CHARACTERIZATION OF METABOTROPIC GLUTAMATE RECEPTOR SUBTYPES. (L. Simoncini, B.A. Haldeman, T. Yamagiwa, E. Mulvihill) ZymoGenetics, 4225 Roosevelt Way, NE Seattle, WA, 98105.(Spon. by A. Tse)

Metabotropic glutamate receptors (mGluR) represent a major glutamate receptor subtype in the brain. Using a recently isolated clone of the metabotropic glutamate receptor, type 1a (K.M. Houamed et al. Science 252:1318-1321 (1991)), as a probe, we have screened a total rat cDNA library and isolated five other clones which we term mGluR1b, mGlurR2, mGluR3, mGluR4a and mGluR4b. They are similar but not identical to clones of M. Masu, et al (Nature 349:760-765 (1991)). Each receptor type has been cloned into a mammalian expression vector and stably expressed in BHK570 cells. Clones containing functional receptors of the mGluR1a, mGluR1b, mRgluR4a and mGluR4b subtypes have been isolated and characterized using $Ca^{++}$ imaging, receptor binding and assays of second messenger levels. mGluR 1a and 1b both stimulate phosphatidyl inositol (PI) hydrolysis and increase intracellular $Ca^{++}$. However the $Ca^{++}$ responses are different. Exposure of cells expressing mGluR1a to constant 100 μM glutamate causes a single intracellular $Ca^{++}$ transient, lasting 50 to 100 sec. This contrasts with cells expressing mGluR1b. Glutamate stimulation gives rise to repeated $Ca^{++}$ spikes with a constant period that varies from 1.5 to 4 minutes in individual cells. mGluR4a is coupled to the inhibitory cAMP cascade. Both glutamate( 100 μM) and L-AP4 (100 μM) are potent agonists and cause intracellular $Ca^{++}$ responses. This recombinant metabotropic receptor is the first subtype to respond to L-AP4 and thus may represent the presynaptic L-AP4 receptor present in hippocampal dentate gyrus granule cells (I.D. Folsythe and J.D. Clements, J. Physiol. 429:1-16 (1990); C. Thomsen et al.J. Mol. Pharm, in press).

**M-VCR4**

TIME-LAPSE MOVIES OF ACETYLCHOLINE RECEPTOR CLUSTER FORMATION ON CULTURED RAT MYOTUBES. ((D. Wang & D. Axelrod)) Biophysics Res. Div. & Dept. of Physics, U. of Michigan, Ann Arbor, MI 48109.

We have made overlayed time-lapse movies of total internal reflection fluorescence (TIRF) and Schlieren transmitted light images of developing rat myotubes in primary culture, to study when and where acetylcholine receptor (AChR) clusters appear. The receptors, including newly incorporated ones, were labeled with rhodamine α-bungarotoxin continuously present in the medium. Since TIRF illuminates only cell-substrate contact regions where almost all of the AChR clusters are located, background fluorescence from fluorophores either in the bulk solution or inside of the cells can be suppressed. During the experiment, cells were kept alive on the microscope stage at 37°C in 10% $CO_2$ atmosphere. Two digital images were recorded by a CCD camera every 20 minutes: the Schlieren image of the cells and the TIRF image of the clusters. After background subtraction, the raw cluster image was displayed in pseudocolors, overlayed onto the cell image, and recorded as 3 frames on a video tape. The final movies are thus able to summarize a week long experiment in less than a minute. These movies and images show that clusters form often shortly after the myoblast fusion but sometimes much later, and the formation takes place very rapidly (in about an hour). The clusters have an average life time around an hour, much shorter than the lifetime of a typical myotube. The brightest and largest clusters tend to be the longest-lived. The cluster formation seems to be associated with the contacts of myotubes at the glass substrate, but not to be associated with cell-cell contacts or myoblast fusion into myotubes. Newly incorporated AChR continuously appear in pre-existing clusters: after photobleaching, the fluorescence of some clusters recovers within an hour. Spptd. by NIH NS 14565 and NSF DMB 8805296.

**M-Pos358**

A 3D MODEL OF A SELECTIVE RECOGNITION SITE IN THE HUMAN 5-$HT_{1D}$ RECEPTOR. **A. Smolyar and R. Osman.** Department of Physiology and Biophysics, Mount Sinai School of Medicine, CUNY, New York, NY 10029.

A three dimensional model of the 5-$HT_{1D}$ receptor, which is used to elucidate the structural basis for its selectivity, has been constructed using an extensive set of computational and computer modeling techniques. The amino acid sequences, which are involved in the putative transmembrane helical parts of the receptor, have been selected based on comparisons and sequence alignments with other G-protein coupled receptors. After ideal α-helical segments were constructed and minimized, three intervals of molecular dynamics simulations were conducted. First 10ps was conducted with constrained backbone followed by 10ps with constrained $C_\alpha$ followed by unconstrained dynamics. Total energy and RMS deviation plots were used to determine the time interval in which the helices approached an apparent stable structure. Last 10ps of the stable trajectory were used to generate an averaged minimized structure. The helical bundle was constructed on the topology of bacteriorhodopsin. Each helix was oriented with the most conserved residues facing the interhelical space and its backbone was fitted to the backbone of the corresponding helix of bacteriorhodopsin. The structure of the entire bundle was optimized again. Two 5-$HT_{1D}$ selective drugs (sumatriptan and 5-carboxamido-tryptamine) were docked inside the receptor model and the structures of the complexes were minimized. The force field parameters for these two drugs were obtained from *ab initio* quantum chemical calculations and atomic charges were obtained from natural orbital populations. The role of different amino acid residues that constitute the binding site in the receptor model will be analyzed.

*Supported by NIDA Training Grant DA-07135 and grant DA-06620.*

**M-Pos359**

COMPUTATIONAL SIMULATIONS OF THE STRUCTURE, DYNAMICS, AND SIGNAL TRANSDUCTION MECHANISM OF A 5-$HT_2$ RECEPTOR

**Daqun Zhang and Harel Weinstein.** Dept. Physiology and Biophysics, Mount Sinai School of Medicine, CUNY, New York, NY 10029

We have constructed a complete 3-D model of the transmembrane (TMB) domain of the G-protein coupled 5-$HT_2$ receptor (GPC-5-$HT_2$-R), at atomic resolution. Preliminary molecular dynamics simulations have also been carried out on the receptor model and its complexes with ligands including full agonists, partial agonists and antagonists. The model incorporates the following assumptions: 1) The TMB region consists of a seven helix bundle; 2) The length and orientation of the individual helical segments can be determined from considerations of homology across GPCR families - including the pattern of conservation of amino acids, the steric and physicochemical properties of the residues, and the characteristics of localized groups of residues with particular properties (e.g., "hydrophobic patches," "amphiphilic faces"); 3) The topology of the bundle is determined by helix-helix interactions rather than by constraints from the connecting loops. The construction guides for the model were: i) ligand structure-affinity relationships of pharmacologically well characterized ligands; ii) structural features of membrane proteins for which structures are available at atomic resolution; iii) results of studies on the molecular biology of GPCRs. Results from the simulations suggest a signal transduction mechanism based on the structural response of the TMB helix bundle to the binding of ligands. Local effects at the recognition site, which produce the activation trigger, and distal effects that are propagated from the recognition site into the receptor region that is responsible for coupling to the effector are identifiable from the analysis of the dynamic behavior of the ligand-receptor complex. Supported by DA-06620 from the National Institute on Drug Abuse, and Research Scientist Award DA-00060 (to HW).

## EPIDERMAL BIOPHYSICS

**M-Pos360**

Evidence for Protein-Lipid Interaction in Mammalian Stratum Corneum. S.J. Rehfeld and W.Z. Plachy, Dept. of Chem. and Biochem. SF State Univ. SF, CA., 94132.

The role of protein components in mammalian stratum corneum (SC) and their relationship to the lamellar bilayer phase in maintenance of structure and SC barrier functions remains unresolved. Magnetic resonance spectroscopy (EPR spin probe and $^1H$ NMR) studies as a function of temperature and hydration of mammalian stratum corneum revealed the following results. Both spectral methods revealed a major broad phase transition occurring in the physiologic region, $T_m$ at 35±5°C. This phase transition apparently was not dependent upon hydration of SC. Hydrated murine stratum corneum showed no significant change in the polarity of the spin probe nonpolar micro-environment (the lipid bilayers). However, $^1D_2O$ rehydration of SC resulted in a significant resolution of $^1H$ NMR spectra. The increase in spectral resolution may be due to the swelling of proteins in SC. $T_1$ and $T_2$ for the resolved peaks as a function of inverse temperature showed the same major phase transition, $T_m$. The broad phase transition, from approximately 20° to 50°C, may involve the hydration of lipid complexes, i.e., glycosphingolipid-cholesterol complexes. $^1H$ NMR spectra of rehydrated human SC did not significantly increase resolution. We propose that differences in mammalian keratin and/or other proteins results in species differences in SC barrier function.

**M-Pos361**

LATERAL DIFFUSION OF A LIPID PROBE IN THE MEMBRANES OF ESSENTIAL FATTY ACID DEFICIENT AND SUPPLEMENTED CULTURED HUMAN KERATINOCYTES. ((R.M. Fulbright, D. Axelrod, W.R. Dunham, L.M. Rhodes, and C.L. Marcelo)) Biophysics Research Division and Departments of Dermatology and Physics, University of Michigan, Ann Arbor, MI 48109.

Primary adult keratinocytes grown in serum free medium are essential fatty acid deficient (EFAD) and are missing the dietary derived fatty acids 20:4 ($\omega$-6) and 18:2 ($\omega$-6) in cellular lipids and lipid-dependent structures. Cells grown in serum free medium supplemented with 18:2, or serum free medium supplemented with 18:2 and 20:4, differ significantly from their EFAD counterparts in membrane fatty acid composition. Using the fluorescence recovery after photobleaching (FRAP) technique, we have measured the lateral diffusion rate of the fluorescent lipophilic probe 1,1'-dihexadecyl-3,3,3',3'-tetramethylindocarbocyanine ($diIC_{16}(3)$) in the membranes of EFAD and fatty acid supplemented (FAS) cells at 35-37 °C. Assuming a focused laser spot half-width at $e^{-2}$ height of 1.9 $\mu$m, apparent values of the lateral diffusion coefficient $D$ occur from about $6\times10^{-9}$ to $20\times10^{-9}$ $cm^2/s$ for both EFAD and FAS cells (with a very few cells having higher $D$ values). However, only FAS cell populations have cells (about 40 % of the total number) with $D$ values less than $6\times10^{-9}$ $cm^2/s$. In this slow mobility group, most of the $D$ values occur in the range $2\times10^{-9}$ to $4\times10^{-9}$ $cm^2/s$. The apparent probe mobile fraction is greater than 0.9 in over 70 % of both the EFAD and FAS cells. By comparison, EPR studies have shown that the rotational mobility of a spin-labeled probe embedded solely in the nonpolar region of the membrane is higher for FAS cells than for EFAD cells. Supported by NIH NS14565 and NSF DMB8805296 (to D.A.), NIH AM26009 (to C.L.M.), and a NRSA (to R.M.F.).

## SODIUM CHANNELS

**M-Pos362**

ENTROPY OF TWO DISTINCT CONFORMATIONAL TRANSITIONS OF SINGLE SODIUM CHANNEL MOLECULES.
((K. Benndorf)) Zentrum für Physiologie, Universität zu Köln, Robert-Koch-Str. 39, 5000 Köln 41, Germany.

Single Na channel currents were studied in cell-attached patches of ventricular heart cells of the mouse with a low noise patch clamp technique which allows to study open channel life time at bandwidths of up to 20 kHz. Currents were recorded at voltages between -50 and 0 mV at both 10°C and 25°C. At the higher temperature, the amplitudes of single channel currents were more heterogeneous than at the lower temperature (Benndorf, Pflügers Arch., 1992, in press). For evaluation of the mean open time $\tau_o$, the threshold for event detection was therefore set to the center of the baseline noise level. The resulting distribution of open channel life times could easily be separated from the distribution of the false noise events. In both single channel molecules and lumped data from 18 patches (54,000 sweeps), $1/\tau_o$ was found to be U-shaped between -50 and 0 mV at 25°C, whereas it only increased in the indicated voltage range toward less negative potentials at 10°C. Consequently, the temperature coefficient $Q_{10}$ was larger at -50 mV than at 0 mV to be 4.8 and 3.6, respectively. Following Eyring rate theory and assuming first order reactions for deactivation and inactivation, *simultaneous* fit of the data at both temperatures allowed separation of enthalpic, entropic, and voltage dependent part of activation energy in both reactions. Both entropies were found to be positive with deactivation entropy $\Delta S_C$=0.23 kJ $mol^{-1}K^{-1}$ (27.6 k) being more than twice larger than inactivation entropy $\Delta S_I$=0.10 kJ $mol^{-1}K^{-1}$ (11.6 k).
Conclusions: Entropy associated with deactivation and inactivation of Na channels may be measured in single molecules. The open state is more ordered than the last closed and the inactivated state. Deactivation proceeds with larger conformational change than inactivation.

**M-Pos363**

A HELIX-COIL TRANSITION IN THE S4 SEGMENTS AS A MODEL OF THE CLOSED-OPEN CONFORMATIONAL CHANGE IN THE Na CHANNEL.
((H. Richard Leuchtag)) Department of Biology, Texas Southern University, Houston, TX 77004.

The demonstration that squid-axon membrane obeys a Curie-Weiss law (HRL, BJ 59:11a, 1991) confirms the ferroelectric-superionic transition hypothesis (HRL, 1991 IEEE Northeast Bioeng. Conf., 169): that a unit of the channel when closed is in an ordered state with an outward dipole moment, and when open is disordered and ionically conducting. This unit may be identified with a central cluster of four S4 segments. Because of their distributed positive charges, the S4 segments can not stably exist in the $\alpha$-helix conformation without the compressive electrical forces (e.g., electrostriction) present at resting potential. Thus a threshold depolarization induces a cooperative transition to a random-coil conformation in the S4s, breaking the interloop hydrogen bonds and exposing binding sites for the permeant ions. When all sites are filled with $Na^+$, a continuous ion pathway supports $Na^+$ current. Channel closing requires the reformation of the S4 $\alpha$ helices, and so is stochastically slower than opening.

M-Pos364

## CAN A HELIX SCREW? A REPTATION MODEL FOR THE DYNAMICS OF AN ION CHANNEL α-HELIX VOLTAGE SENSOR.

((G. L. Millhauser† and R. E. Oswald*)) †Department of Chemistry and Biochemistry, University of California, Santa Cruz, CA 95064 and *Department of Pharmacology, NY State College of Veterinary Medicine, Cornell University, Ithaca, NY 14853

Molecular biological research has suggested that the gating charge associated with voltage-dependent ion channels involves helices with highly conserved charged amino acids. It has been proposed that charge movement may arise from a helix screw motion of this conserved segment. As yet, the dynamics of this motion is unexplored. We are presently using our reptation theory (Millhauser, *Biophys. J.*, 57 857-864, 1990) to simulate the dynamics of a helix screw voltage sensor. Initial simulations have shown that indeed a helix can screw on the time scale observed for the gating current. In fact, the gating charge movement occurs in milliseconds and the total integrated charge is about 3 unit charges per ion channel. Further, the time course of the gating charge is found to be exponential. All of these predictions from our reptation model match experimental findings. This reptation theory approach is the first model to correctly predict the dynamic details of gating currents.

M-Pos365

## $Ca^{++}$ EFFECTS ON Na CHANNEL GATING DEPEND ON $[Na^+]$.

((C.M. Armstrong and G. Cota)) Dept. of Physiology, Univ. Pennsylvania, Philadelphia, Pa. 19104-6085; MBL, Woods Hole, Mass; CINVESTAV, Mexico City.

We investigated the effects of sodium and calcium ions on Na channel gating kinetics in squid giant axons, by varying $[Na^+]$ at constant $[Ca^{++}]$, or the reverse. Axons were perfused internally with N-methyl-glucamine glutamate and fluoride, and bathed in $Na^+$ $Ca^{++}$ $Tris^+$ solutions. Series resistance compensation was employed. Increasing $[Na^+]$ from 50 to 400 mM shifted the closing-rate vs $V_m$ curve to the left by 23 mV in 15 Ca, but by only 6 mV in 100 Ca; i.e., high $[Na^+]$ slowed closing, most strongly in 15 Ca. Increasing $[Na^+]$ from 150 to 400 mM in 50 Ca caused a small (approximately 7 mV) left shift of the g-V curve: higher $[Na^+]$ appears to facilitate opening. Turning to $[Ca^{++}]$ variations, increasing $[Ca^{++}]$ from 15 to 100 mM shifted the closing rate curve 9 mV to the right in 50 Na, and 20 mV or more to the right in 400 Na. Gating current measured in 0 Na was virtually unaffected by Ca variations. These results suggest that a competition between Na and Ca for a gating site is involved in at least some of the effects of Ca, since Ca variations have little influence when Na is absent or present only at low concentration.

M-Pos366

## PROPERTIES OF A NONEQUILIBRIUM MODEL OF SODIUM CHANNEL GATING.

(( M.Bartoszkiewicz and S.Miękisz )) Dept. Biophys., Medical School, Wrocław, Poland.

The time and external electric field - dependent behavior of a system of charged particles ('voltage sensors') in a viscous, dielectric layer ('membrane') is modelled by a Fokker-Planck type equation. The particle is assumed to control the state of the adjacent macromolecule ('channel') in a position - dependent way.

The system response to a sudden change in the electric field strength within the layer is analysed. Two voltage dependent variables of the model : the fraction of open channels and the 'gating charge' (charge displacement in the external circuit, caused by the movement of the 'sensors') are examined. Also, the influence of the initial conditions on the model's predictions is discussed.

M-Pos367

## A SIMPLE MODEL FOR SURFACE CHARGES ON ION CHANNEL PROTEINS.

((David Naranjo, Ramón Latorre and Mark F. Schumaker)) Dept. of Neurobiology, SUNY Stony Brook, Stony Brook, NY 11794; Dpto. de Biologia-Fac. Ciencas, Univ. de Chile, Santiago, Chile and Dept. of Pure and Applied Mathematics, Washington State University, Pullman, WA 99164.

$Na^+$ channel conductances were measured in neutral lipid bilayers with bulk $Na^+$ concentrations as low as 400μM. Conductances were seen to decrease only gradually at the lowest values of bulk $Na^+$. These results appear to be inconsistent with the numerical computations of Cai and Jordan (Biophys. Jl. 57_883-891, 1990), suggesting a qualitatively different relationship between the channel entrance and surface charges than was investigated by those authors. We describe a very simple model in which the channel entrance is effectively surrounded by a spherical "shell" of surface charges and their images. Depending on parameter values, the ion concentration at the channel entrance may increase very rapidly as the bulk concentration increases from zero. As the bulk concentration increases further, the ion concentration at the channel entrance may then enter a "buffered" phase, even at Debye lengths much larger than the separation between the channel entrance and the surface charges. In the buffered phase, the ion concentration at the channel entrance depends only weakly on the bulk concentration.

M-Pos368

## MODELLING THE FASTEST RESOLVABLE DISPLACEMENT CHARGE COMPONENT AS AN ACTIVATION TRIGGER FOR THE SQUID SODIUM CHANNEL.

((Ian C. Forster and Nikolaus G. Greeff)) Physiologisches Institut, Universität Zürich-Irchel, CH-8057 Zürich, Switzerland.

When displacement currents of the squid Na channel are recorded with sufficiently high resolution in response to voltage clamp depolarizing command steps, a small current spike is seen superimposed on the main displacement current waveform, particularly for depolarizations above 0 mV membrane potential. We have shown that this spike is part of a non-artifactual displacement charge component which can be separated kinetically from the total current (Forster & Greeff, European Biophys. J., 41, 99-116, 1992). Our data also suggest that there is one fast charge transition per Na channel. The kinetic separation procedure reveals a significant rising phase in the main current lasting about 100 μs, the existence of which has two important implications for modelling the Na channel activation process. (i) If the fast component is functionally independent of the Na channel gating mechanism then the rising phase implies that the first steps in the activation process are slower than those following. (ii) Our findings would also be consistent with the fast component acting as a triggering transition for the activation process by actuating the forward transitions of the main activation steps only after it has changed state. The fast trigger transition can nevertheless occur independently of the channel state. We have incorporated this concept into a multistate model for Na channel activation which predicts gating currents having an early time course similar to those recorded from the squid.

Supported by Swiss Nat. Sci. Foundation grant 31.27788.89

M-Pos369

## OPTICAL ROTATION CHANGES AND NERVE ACTION POTENTIALS.

((David Landowne)) Univ. of Miami Sch. of Medicine Miami, FL 33101.

Optical rotation changes (Δ-OR) associated with the passage of action potentials were measured in squid fin nerves by two different methods. In both the nerves were illuminated with white (tungsten-halogen) light passing through an optical train which included a polarizer (-45°), a photo-elastic modulator (PEM, 0°), the nerve (0°), an analyzer and a photodetector. A lock-in amplifier with a 2f reference signal from the PEM detected the OR signal which was filtered at 1 kHz and led to a computer-based signal averager synchronized to the nerve stimulator. In the quarter-wave-xp method the PEM was driven with a peak-to-peak retardation change of 500 nm, slightly more than quarter-wave-modulation, and the analyzer was at +45°, crossed with the polarizer. For the half-wave-0° method the PEM was driven at 700 nm (approximately half-wave) and the analyzer set at 0°. Both methods gave similar results although the quarter-wave-xp method had a better signal/noise ratio and appeared less sensitive to small changes of the nerve azimuth.

The beginning of the Δ-OR is slightly delayed in comparison with the change in birefringence that accompanies the action potential (Δ-BRF). Both propagate with the same velocity as the electrically recorded action potential. In the half-wave-0° method there is contamination of the Δ-OR signal with the Δ-BRF which is sensitive to small changes in the nerve azimuth. With both methods Δ-OR signal reversal was observed when the direction of propagation was reversed whereas the sign of the Δ-BRF did not reverse.

By amplitude and time course it is reasonable to suggest that a sodium channel protein conformational changes could underlie the Δ-OR signals.

Supported by NIH grant NS26651.

**M-Pos370**

**DISSECTING "FAST INACTIVATION REMOVAL": 1) EFFECTS OF INTERNAL pH AND CHEMICAL MODIFIERS.**

((J.G. Starkus, M.D. Rayner and P.C. Ruben)) Bekesy Laboratory of Neurobiology, University of Hawaii, Honolulu, HI 96822.

In crayfish axons, pronase, N-bromoacetamide and chloramine-T affect sodium channels by: i) removing fast inactivation, ii) shifting the steady state inactivation curve about 20 mV to the right along the voltage axis and, iii) producing an irreversible loss of sodium conductance. The apparent channel loss is quite variable from agent to agent and appears to be a separate pharmacological action. But is the right-shift of steady state inactivation caused by fast inactivation removal, or are these effects also separately mediated? Trypsin causes a similar ~20 mV right-shift of steady state inactivation without significant removal of fast inactivation. Since the steady state inactivation curve can be right-shifted without fast inactivation removal, these two effects apparently result from separate pharmacological actions.

Similarly, changes in pH of the internal perfusate ($pH_i$) can affect the midpoint voltage for steady state inactivation, again without removing fast inactivation in crayfish axons. Increasing $pH_i$ to 10 *right*-shifts the midpoint of steady state inactivation. By contrast, reducing $pH_i$ to 5 causes a ~20 mV *left*-shift in this same parameter. We speculate that equivalent effects of $\Delta$ $pH_i$ in, for example, cardiac sodium channels might have substantial physiological consequences.

(Supported by PHS grants #NS-21151, #NS-29204, NIH RCMI grant #RR-03061 and American Heart Assoc. Hawaii Affiliate)

**M-Pos371**

**DISSECTING "FAST INACTIVATION REMOVAL": 2) PHOTODYNAMIC EFFECTS**

( J.G. Starkus, A. Fleig, M.D. Rayner and P.C. Ruben)) Bekesy Laboratory of Neurobiology, University of Hawaii, Honolulu, HI 96822.

Illumination of crayfish giant axons, during internal perfusion with 0.5 mM methylene blue (MB), produces photodynamic effects which include: i) reduction in total sodium conductance, ii) shifting of the curve for steady state inactivation to the right along the voltage axis, iii) reduction in the effective valence of steady state inactivation and, iv) potentially complete removal of fast inactivation. The two kinetic components of fast inactivation in crayfish axons ($\tau_{h1}$ and $\tau_{h2}$) are differentially affected during photodynamic fast inactivation removal. The intercept of the faster component ($\tau_{h1}$) is selectively reduced at shorter MB+Light exposure times. Neither $\tau$h1 nor the slower ($\tau_{h2}$) process was protected from MB+Light by prior steady state inactivation of sodium channels.

Carotenoids provide protection against some of these photodynamic effects. Effects of carotenoid exposure (30 m) on sodium channel kinetics persist unchanged for >15 m after carotenoid washout, and are associated with maintained carotenoid protection against photodynamic damage, indicating that these sparingly soluble agents remain preferentially sequestered in hydrophobic membrane regions. Futhermore, carotenoids provide different levels of protection against each of the photodynamic effects listed above, suggesting that each effect may be mediated by damage to a different region within the sodium channel molecule.

**M-Pos372**

**SODIUM CHANNEL IIA: CHANGES IN SENSITIVITY TO dV/dt FOLLOWING SINGLE POINT MUTATIONS IN IIS4.**

((P.C. Ruben, A. Fleig, M.D. Rayner, and J.G. Starkus)) Bekesy Laboratory of Neurobiology, University of Hawaii, Honolulu, HI 96822.

The kinetics of sodium channels expressed in *Xenopus* oocytes may not be readily characterizable by two-electrode clamp, due to the large membrane capacitance and resultant slow clamp settling time. To assess this problem, we have compared properties of wild type and mutant channels in excised macropatches, using ramp depolarizations with differing dV/dt. Single point mutations in IIS4 can produce dramatic changes in ramp sensitivity. The wildtype rat brain IIA channel shows similar kinetics (in steps from -100 to 0 mV) for ramps as fast as 0.2 ms and as slow as 2 ms, with no significant changes in peak $I_{Na}$. By contrast, the L860F mutant shows reductions in peak $I_{Na}$ to 75% of control for a 0.2 ms ramp, 50% for a 0.6 ms rise time and 25% at 1 ms. Reduction in peak $I_{Na}$ is associated with selective loss of the fast inactivation kinetic. This change can be interprteted as resulting from rapid, closed-state inactivation in a separate sub-population of "fast mode" channels, occuring during slow ramp depolarizations.

We speculate that sensitivity to dV/dt may be a parameter of considerable physiological significance, which should be assessed during routine characterization of channel properties.

(Supported by PHS grants #NS-21151, #NS-29204, NIH RCMI grant #RR-03061 and American Heart Assoc. Hawaii Affiliate)

**M-Pos373**

**SODIUM CHANNEL IIA: INTERACTIONS BETWEEN NEIGHBORING CHARGED AND UNCHARGED AMINO ACID RESIDUES IN S4 SEGMENTS.**

((A. Fleig, P.C. Ruben, M.D. Rayner, M. Estacion, and J.G. Starkus)) Bekesy Laboratory of Neurobiology, University of Hawaii, Honolulu, HI 96822.

We have studied effects of three sodium channel rat-brain IIA mutants (kindly supplied by A. Goldin) expressed in Xenopus oocytes, using excised inside-out macropatches. These mutants, K859R, K859Q and L860F, were initially chosen to assess the functional significance of the "4th charge" in IIS4 ($859^K$). Comparing G(V) curves from these mutants with wild type IIA channels, we find no significant changes in effective channel valence. However, midpoints for the G(V) curves were: wild type, -20 mV; K859R, -30 mV; K859Q and L860F, 0 mV. Thus the charge deletion mutant (K859Q) shows the same right shift as the supposedly neutral aromatic substitution (L860F). Considering the 5 residues centered on position 859 (bold type), the wild type shows ..VFKLA.. whereas the corresponding sequence for L860F is ..VFKFA.. We conclude that the induced dipole actions of the two F residues which flank the central $859^K$ charge must be functionally equivalent to the K859Q charge deletion. We further speculate that the frequent pairings of charged residues in the S4 segments with either aromatic (5 occurences, all F's) or polar residues (10 occurences, G, S or T) may be functionally significant in modifying and directing the electrostatic effects of the charged residue.

(Supported by PHS grants #NS-21151, #NS-29204, NIH RCMI grant #RR-03061 and American Heart Assoc. Hawaii Affiliate)

**M-Pos374**

SEQUENCE OF A PUTATIVE SODIUM CHANNEL FROM THE JELLYFISH *CYANEA CAPILLATA*. (P.A.V. Anderson, M.A. Holman, and R.M. Greenberg) Whitney Laboratory, Univ. of Florida, St. Augustine, FL 32086. (Spon. by M.S. Kilberg)

The distinction between voltage gated $Na^+$ and $Ca^{++}$ channels breaks down in *Cyanea*. Although the $Na^+$ current which underlies the action potential is physiologically a $Na^+$ current, it has the pharmacological properties of a $Ca^{++}$ current. We have used degenerate primers designed against sequences conserved in other $Na^+$ channels to amplify by PCR a ≈900 bp *Cyanea* cDNA fragment homologous to other $Na^+$ channels. Subsequently, we have cloned and sequenced a 6050 bp cDNA with a 5217 bp open reading frame. The deduced amino acid sequence encodes a protein with a calculated molecular weight of ≈198 kDa. It has high similarity (30-35% identity) with, and a secondary structure profile homologous to, other $Na^+$ channels. The amino acid sequence is especially conserved in the transmembrane regions (up to 80% identity with rat brain II). Because the *Cyanea* $Na^+$ channel can be considered a functional chimera, insights can be gained by comparing its structure in important regions of the channel with other $Na^+$ and $Ca^{++}$ channels. Of particular interest are the proposed verapamil binding site of $Ca^{++}$ channels and the proposed TTX binding site and selectivity filter of $Na^+$ channels. Supported by NSF grant #BNS-9109155, AHA grant #92GIA/855, and funds from the Univ. of Florida DSR.

**M-Pos375**

**PROBING THE STRUCTURE OF SODIUM CHANNEL CYTOPLASMIC DOMAINS.** ((Sidney A. Cohen, Weijing Sun, and Robert L. Barchi)) University of Pennsylvania School of Medicine, Phila., PA 19104

We are investigating the spatial relationships among segments of the skeletal muscle sodium channel (SkM1) that project from the cytoplasmic surface of the membrane by examining the interactions between antibodies to defined epitopes within these regions. Anti-peptide polyclonal antibodies I-31 (residues 31-46 in the N-terminus) and B-30 (residues 921-935 in the ID 2-3 region) and four monoclonal antibodies developed against detergent solubilized SkM1 protein were studied. The epitopes for monoclonal antibodies A/B2 and L/D3 had previously been localized to residues 1-6 and 18-24, respectively, in the N-terminus of SkM1 (J Memb Biol 128:219-226) while the epitopes for the two other monoclonal antibodies were localized to the ID 2-3 region of SkM1 by proteolytic mapping and binding to fusion proteins. Measurements were done both with solid-phase competition assays and with a solution-phase assay in which solubilized channel protein retains the ability to bind $^3$H-STX. No interaction was observed between I-31 and A/B2 or L/D3 while I-31 interfered with F/C11 and B/D6 binding. Conversely, B-30 reduced L/D3, F/C11, and, to a lesser extent, B/D6 binding but did not affect A/B2's interaction with the channel. Our results suggest that there is a fixed spatial relationship between epitopes in the N-terminus and the ID 2-3 region and that the N-terminus assumes a compact, folded structure.

**M-Pos376**

**RAT BRAIN ß1 Na CHANNEL SUBUNIT INTERACTS WITH RAT BRAIN IIa, SKELETAL MUSCLE (μ1), and RAT HEART (RH1) α-SUBUNITS**

((JW Kyle, SY Chang, J Satin, JM Fang, HA Fozzard*, and RB Rogart)) Cardiac Electrophysiology Lab, Univ. of Chicago, Chicago, IL 60637.

Rat brain IIa (BrIIa) and rat skeletal muscle (μ1) Na channel α-subunits have abnormally slow rates of current decay when expressed in *Xenopus* oocytes. We cloned the ß1 sodium channel subunit (Brß1) from rat brain cDNA libraries. Coexpression of Brß1 with BrIIa resulted in an increase in the rate of current decay, similar to that reported by Isom et al. (Science 256:839), and also increased the rate of recovery from inactivation. Brß1 had negligible effects on the voltage dependence of the BrIIa availability curve tested with a 10 ms prepulse. μ1 current in oocytes decayed and recovered from inactivation more slowly than BrIIa. Coexpression of Brß1 and skeletal muscle (μ1) resulted in faster current decay and faster recovery from inactivation than BrIIa current. We detected no shift on the voltage axis of the μ1 steady-state availability curve.

Coexpression of Brß1 with rat heart (RH1) showed no detectable change in either the rate of current decay or recovery from inactivation. We did detect a shift in the **depolarizing** direction of 6 mV for availability (Fig). Thus the ß1 subunit from brain affects gating of α-subunits from brain, skeletal muscle, and heart suggesting that Brß1 interacts with three different Na channel α-subunit isoforms.

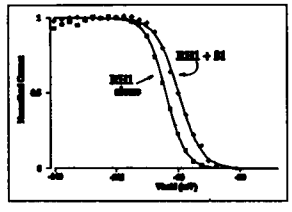

**M-Pos377**

**A CYSTEINE SUBSTITUTION IN THE P-REGION OF THE SKELETAL MUSCLE SODIUM CHANNEL ALTERS SENSITIVITY TO TETRODOTOXIN AND DIVALENT CATIONS.**

((*G.F. Tomaselli, H.B. Nuss, J.H. Lawrence, P.H. Backx, E. Marban*)) *Department of Medicine, Division of Cardiology, The Johns Hopkins University, Baltimore MD 21205*

A critically positioned cysteine (C) residue in the pore of the cardiac $Na^+$ channel has been implicated in determining the channel phenotype with respect to guanidinium toxin and group IIB divalent cation block. Replacement of tyrosine (Y) with C at position 52 in repeat I (I-Y52C) of the skeletal muscle $Na^+$ channel makes the channel insensitive to tetrodotoxin (TTX)($K_i$ 16 nM → >50 μM) and increases the affinity for $Cd^{2+}$ ($K_i$ 1.7 mM → 16.7 μM). Analysis of the voltage dependence is consistent with block within the pore of the channel. Replacement of the adjacent residue, tryptophan (W) with C (I-W53C) changes the phenotype of channel when expressed in *Xenopus* oocytes. This variant has an intermediate sensitivity to TTX ($K_i$=0.52 μM, n=3) and $Cd^{2+}$ ($K_i$=134 μM, n=3). The I-W53C mutant exhibited no other significant differences in permeation or gating from the wild type channel at the whole-cell level. These data are consistent with an intra-pore site of this residue and not consistent with a suggested ß-sheet structure of this region of the channel. Further, this suggests that $Cd^{2+}$ is loosely coordinated or bound to a single residue in this region of the channel.

**M-Pos378**

**THE LOCATION OF FUNCTIONAL SITES OF N-LINKED GLYCOSYLATION OF THE *Electrphorus electricus* Na CHANNEL DETERMINED BY *IN VITRO* TRANSLATION.**

((M. Macey ka, M. Stephan, C. Ukomadu, and W.S. Agnew*)) Depts Physiology and* Neuroscience, Johns Hopkins University, Baltimore, MD 21250

The α-peptide subunits of voltage-sensitive Na channels are heavily glycosylated, and exhibit a heterogeneous pattern of distribution of consensus sites for N-linked oligosaccharides. The channel from eel electroplax is 30 wt% carbohydrate and exhibits 10 consensus sites for N-glycosylation. This channel isoform contains both neutral and acidic chains, including one or more large unbranched polymers of α-2,8-linked polysialic acid containing a total of ~120 sialosyl residues. Hydrodynamic studies performed in our laboratory suggest these extended chains may reach as far as 600-1000 Å from the protein surface. To determine the number and location of functional glycosylation sites, serially truncated constructs of the electroplax cDNA were translated *in vitro* in the presence or absence of canine pancreatic microsomes. Acceptance of a neutral oligosaccharide core produced a molecular weight shift in the translated proteins of ~5 kDa. cDNA fragments encoding only one of each of the four subunit domains (I-IV) were used for production of serially truncated constructs which included or omitted each consensus site in succession. Of the 10 consensus sites, only four were observed to accept oligosaccharide core units during translation: asparagines 278, 328, 1160, and 1174. Topographically these four residues occur on the extracellular pedestals of domains I and III, between membrane spanning segment S5 and SS1-SS2 segments thought to form the mouth of the ion channel. We conclude that both neutral and negatively charged oligosaccharide chains must lie symmetrically disposed around the mouth of the ion channel, providing a striking simplification of the probable appearance of the molecule.

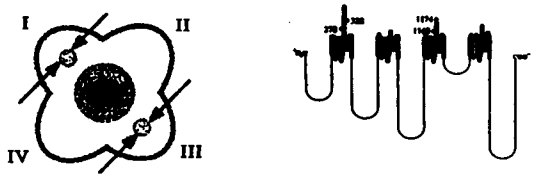


**M-Pos379**

STABLE EXPRESSION OF A HUMAN HEART Na CHANNEL GENE IN MAMMALIAN CELLS. ((P.H. Lalik, W.A. Volberg, L. Rapp, R.G. Kallen[1], D.S. Krafte, and R.B. Ciccarelli)) Sterling Winthrop, Rensselaer, NY and [1]The University of Pennsylvania, Philadelphia, PA. (Spon. C.C. Chadwick)

To prepare a mammalian cell line which stably expresses functional human cardiac Na channels, we subcloned the hH1 human cardiac Na channel gene into pRC/CMV and transfected CHO-K1 cells. Neomycin resistant cells were selected and cultured providing ~300 cell lines for further testing. The cell lines were initially screened at the DNA level by PCR analysis using primer sets corresponding to several regions of hH1 sequences. Cell lines having appropriately sized PCR-amplified DNA fragments were further characterized. RNA was isolated from individual lines and 1st strand cDNA prepared by reverse transcription. PCR analysis with the same primer sets as noted above suggested the presence of full-length mRNA transcripts. RNA positive cell lines were then screened with an antibody raised against a 20-mer peptide derived from amino acids 280 to 299 (domain I, S5-S6) of the hH1 protein. Immunoprecipitation demonstrated the presence of a protein in RNA-positive cell lines which was not present in control CHO-K1 cells. In addition, a higher MW band (approx. 260 kD) was also identified in both transfected and control CHO-K1 cells consistent with endogenous expression of the CHO-K1 Na channel. Cell lines producing the hH1 protein were subjected to voltage-clamp analysis to confirm functional expression of an hH1 Na channel. Endogenous CHO-K1 Na channels, similar to neuronal Na channels, were eliminated by inclusion of 50 nM tetrodotoxin (TTX) in the bath. Under these conditions, Na currents ranging from 1-10 nA were blocked 6 ± 5% by 300 nM TTX and 59 ± 6% by 3 μM TTX. Current-voltage curves had their maxima at -30 mV to -20 mV and the $V_h$ value for steady-state inactivation was -59 ± 2 mV. In conclusion, we have stably expressed the hH1 human heart Na channel gene in CHO-K1 cells which should facilitate the biophysical and biochemical characterization of human cardiac Na channels.

**M-Pos380**

**SLOW INACTIVATION OF SODIUM CURRENTS IN THE HCN-1A HUMAN CORTICAL CELL LINE.**

((R. E. Sheridan)) Neurotoxicology Br., Pathophysiology Div., USAMRICD, APG, MD 21010.

Slow inactivation is a process associated with sodium currents in many tissues. The HCN-1A human cortical cell line exhibits at least four types of sodium channel with different inactivation voltages and TTX/STX sensitivities. The characteristic voltages for steady-state inactivations that reach equilibrium within 50 msec can be either -94 ± 1.2 mV or -45 ± 1.5 mV. The proportions of these two channel types in each cell range from 0 to 100%. Unlike ganglionic neurons, which also exhibit a mix of sodium channel types, inactivation in HCN-1A cells was independent of TTX or STX sensitivity and all currents were half-maximally activated at the same -23 ± 1 mV potential. In HCN-1A cells, the population of sodium channels with the more positive fast inactivation voltage (-45 mV) also undergoes slow inactivation with a time constant of ~50 sec at -120 mV and a characteristic voltage of about -90 mV. By contrast, the fraction of sodium channels with the more negative fast inactivation voltage (-94 mV) does not appear to undergo the slow inactivation and recovery process. Like fast inactivation, the slow inactivation process in HCN-1A cells was independent of TTX sensitivity. None of these channel properties were altered by differentiation of HCN-1A cells in culture media containing either a mix of NGF, IBMX and dibutyryl-cAMP or Bottenstein N3 supplement.

**M-Pos381**

**EFFECTS OF AMINO ACID HYDROPHOBICITY AT POSITION 1489 ON SODIUM CHANNEL INACTIVATION**

((T. Scheuer, J.W. West, Y.L. Wang and W.A. Catterall))
Dept. of Pharmacology, University of Washington, Seattle WA 98195

Sodium channels respond to depolarization by activating and then inactivating. A variety of evidence now indicates that the intracellular loop between homogous domains III and IV ($L_{III/IV}$) of the sodium channel α subunit is involved in inactivation. It has recently been shown that mutation of Phe1489 of the rat brain type IIA sodium channel α subunit to Gln (F1489Q) dramatically inhibits inactivation (West et al , 1992, PNAS *in press* ). To further characterize the nature of this interaction we have substituted Phe 1489 with a variety of amino acids by site-directed mutagenesis and expressed the resulting constructs in Chinese hamster cells. Whole cell voltage clamp recording from these cells showed that the specific amino acid substitution at this position was indeed important. Whereas greater than 75% of the macroscopic current fails to inactivate in cells expressing F1489Q, current in cells expressing F1489W inactivated virtually completely with kinetics similar to those of the native channel. Currents in cells expressing F1489V were intermediate with approximately 40% of the current failing to inactivate. In general, inactivation was more complete when more hydrophobic amino acids were present at position 1489. The results are consistent with F1489 being responsible for the binding of the inactivation gate for its receptor. In the native channel this binding is virtually irreversible. In channels bearing amino acid substitutions at this position the binding becomes reversible and its affinity depends at least partially on the hydrophobicity of the substituted amino acid.

**M-Pos382**

FUNCTIONAL CONSEQUENCES OF A SODIUM CHANNEL MUTATION CAUSING HYPERKALEMIC PERIODIC PARALYSIS.((T.R. Cummins, J. Zhou, F.J. Sigworth, C. Ukomadu, M. Stephan, L.J. Ptacek*, M. Leppert* & W.S. Agnew+)) Yale Univ. Sch. of Med., New Haven, CT; *Univ. of Utah Health Sci. Ctr., Salt Lake City, UT; +The Johns Hopkins Univ. Sch. of Med., Baltimore MD. (Spon. by J. Friedman)

Hyperkalemic periodic paralysis, HYPP, one of several inheritable myotonic diseases, results from genetic defects in the skeletal muscle $Na^+$ channel. In some pedigrees, HYPP is correlated with a single base pair substitution resulting in a Met replacing $Thr^{704}$ in the fifth transmembrane segment of the second domain. This region is totally conserved between the human and rat channel; we have introduced the human mutation into the corresponding region of the rat muscle $Na^+$ channel cDNA and expressed it in human embryonic kidney 293 cells. Patch-clamp recordings show that this mutation shifts the voltage dependence of activation by 15 mV in the negative direction. This shift results in a persistent $Na^+$ current that activates near -70 mV, which could underlie the abnormal muscle activity observed in patients with HYPP. The other HYPP mutation identified (M1592V) also results in persistent $Na^+$ currents, but is reported to do so by altering channel inactivation through direct interaction with extracellular $K^+$. Thus, mutations at different sites of the skeletal muscle $Na^+$ channel alter distinct functional properties to elicit clinical symptoms of HYPP.

**M-Pos383**

Ca BLOCK AND PERMEABILITY OF SKELETAL MUSCLE Na CHANNEL ($\mu$1) AFTER SUBSTITUTION OF GLUTAMATE FOR LYSINE IN THE THIRD SS1-SS2 DOMAIN: SINGLE-CHANNEL AND WHOLE-CELL PROPERTIES

((M.S. deLeon and D.T. Yue)) Johns Hopkins University, Baltimore, MD 21205

A single amino acid substitution (K1422E) on the rat brain II Na channel confers both the property of external Ca block in the sub-millimolar range, and the ability to support appreciable Ca flux (Heinemann et al, Nature 356:441, 1992). This remarkable result not only builds the case that the ion-conducting pore is formed by four SS1-SS2 regions, but could also provide important clues as to the mechanism of Ca permeability. To extend our understanding of such "Ca-sensitive Na channels," we introduced a single amino acid substitution (K1237E) within the third SS1-SS2 region of the skeletal muscle Na channel $\mu$1 (analogous to K1422E in rat brain II). The $\mu$1 K1237E mutant in vector pGW1H was transiently expressed in mammalian HEK293 cells. Whole-cell recordings revealed potent block of Na current by external [Ca] in the 100$\mu$M range, compared to robust currents for wild-type $\mu$1 with up to 2 mM Ca. On-cell, single-channel patches of $\mu$1 K1237E (140 mM Na, 0-2 mM Ca in the pipette) demonstrated unitary currents similar to wild type, thereby making it unlikely that Ca block occurs on a submillisecond timescale. Furthermore, there were no discrete interruptions of single-channel currents by Ca, even when intrinsic openings were prolonged with 10$\mu$M fenvalerate (a toxin inhibitor of fast inactivation). This result argues against Ca blocking events lasting 1 to 10s of milliseconds. Hence, $\mu$1 K1237E appears to be characterized by long interruptions of current by Ca, lasting perhaps on the order of seconds. Ca permeability of $\mu$1 K1237E was tested on the whole-cell and single-channel levels (110 mM external Ca, 0 mM Na), but no currents were detected, in contrast to the results reported for rat brain II K1422E. Our findings suggest that Ca block of Ca-sensitive Na channels occurs on a timescale significantly slower than found in native Ca channels, and that one of only a few subtle differences in SS1-SS2 regions of the two Na channels may represent an important co-determinant of outright Ca permeability.

**M-Pos384**

CLONING OF A PUTATIVE SODIUM CHANNEL FROM SQUID GIANT AXON. ((J.J.C. Rosenthal, M.A. Perri and W.F. Gilly)) Hopkins Marine Station, Stanford University, Pacific Grove, CA 93950.

Although membrane sodium conductance has been studied more extensively in the squid giant axon than in any other system, the molecular structure of the underlying channels has not been determined. We have cloned a putative Na channel cDNA (pGFLN1) from Loligo opalescens by screening a stellate ganglia cDNA library with a partial clone isolated from giant fiber lobe (GFL) neurons using degenerate PCR primers. pGFLN1 has an open reading frame of 5352 nucleotides and encodes a protein of 1784 amino acids (203 kDa). Hydropathy analysis suggests that pGFLN1, like previously cloned Na channels, consists of four homologous domains each containing six putative membrane spans. The charged residues in the S4 membrane spans are conserved in both number and location between the squid sequence and those reported for several vertebrate Na channels. pGFLN1 shares 35%, 35%, 39% and 43% amino acid sequence identity with rat brain I, II, III and electric eel Na channels, respectively. The squid channel bears much higher homology to these other channels in the membrane spans and the putative inactivation loop (inter-domain loop III-IV). Northern blots and RNAse protection assays with probes containing 3' coding and untranslated sequence indicate that pGFLN1 mRNA is expressed in giant fiber lobes. Because the axons of GFL neurons fuse to form the giant axon, and because functional Na channels are not normally expressed in their cell bodies, we propose that pGFLN1 codes for a Na channel in the giant axon. Attempts to complement this assertion through expression studies are underway.

**M-Pos385**

PHASIC BLOCK OF CARDIAC AND NERVE NA CHANNELS BY LIDOCAINE UNDER UNIFORM CONDITIONS.

((Jonathan C. Makielski and Zheng Fan))Cardiac Electrophysiology Labs, University of Chicago, Chicago Il, 60637.

Cardiac tissue is more sensitive to lidocaine than nerve, but it is unclear whether the difference can be attributed to a greater affinity of the cardiac Na channel isoform binding site for lidocaine (lido), or whether state dependence and/or study conditions account for the differences. We voltage clamped Na current in rat ventricular (rv) cells and neuroblastoma (nb) cells using identical solutions (in mM 45 Na, 1.0 Ca, 1.2 Mg, 90 Cs, 135 Cl, 20 HEPES pH 7.3 outside, 140 CsF, 5.0 EGTA, 20 HEPES pH 7.3 inside) at 23 °C and identical pulse train protocols of 10 ms duration depolarizations from $V_h$=-150 to -20 mV with interpulse intervals (int) of .05, .1, .2, and .5 s for lido=0.1 and 0.5 mM. At $V_h$=-150 mV tonic block was negligible for lido up to 0.5 mM. The phasic block was significantly greater in rv than nb for all intervals and doses. For int=.1 the ½ blocking dose was 0.52 mM for rv and 1.3 mM for nb. In control, the midpoint of the availability curve ($h_\infty$) for nb was -83±7 mV (n=8) and for rv was -93±8 mV (n=6). Block by lido can depend upon the holding potential. When pulse trains in nb were run at -140 mV, however, ½ blocking dose was still greater than for rv at -150 mV. These results suggest that the cardiac isoform may have an intrinsically greater affinity for lidocaine but that the difference is less than an order of magnitude.

**M-Pos386**

VOLTAGE-SENSITIVE CHANNELS AND PEPTIDE TOXINS THAT TARGET THEM SHARE AN INTERSUPERFAMILY STRUCTURAL RELATIONSHIP THAT IS COMPLEMENTARY. John A. Schetz*, Department of Neuroscience and The Whitney Laboratory of the University of Florida, Gainesville, Florida 32610.

$K^+$, $Na^+$ and $Ca^{++}$ channels form a superfamily of voltage-dependent cation channel (VDCC) proteins. Current structural models for VDCCs envisage a protein conformation that gates the transmembrane movement of ions through a central "pore". The putative "pore" region corresponds to the amino acids that interconnect the fifth (S5) and sixth (S6) transmembrane spanning $\alpha$-helices in each of the four S1-S6 domain repeats. Structures of these S5-S6 "pore" regions on $K^+$ and $Na^+$ channels that bind the peptide toxins charybdotoxin (CTX) and $\alpha$-scorpion toxin ($\alpha$-ScTX) were compared and quantified with the aid of SHC® (Statistical *H*ydrophobicity *C*omparator), pattern recognition software for statistical comparison of protein secondary structures. SHC quantities reveal that the pore of $K^+$ and $Na^+$ channels share a common structural motif targeted by structurally similar peptide toxins. To entertain any structural trends within the VDCC superfamily, structure within comparable S5-S6 pore regions on an L-type cardiac $Ca^{++}$ channel was compared with those on $K^+$ and $Na^+$ channels and found to be similar to $Na^+$ but not $K^+$ channels. CTX and $\alpha$-ScTX share a common 3-D structure and bind to comparable S5-S5 pore regions. Apamin blocks L-type cardiac $Ca^{++}$ channels, and a three-dimensional energy minimization model for apamin has been proposed on the basis of the core structure of scorpion toxins. SHC comparison quantities show that apamin shares a structural motif common to $\alpha$-ScTX but distinct from charybdotoxin. On the basis of the complementary structural relationship between the VDCC superfamily and the "pore"-targeting peptide toxin superfamily, I predict apamin's binding site to L-type cardiac $Ca^{++}$ channels to be in S5-S5 of domain I.

**M-Pos387**

NA-CHANNEL ANTAGONISTS DETECTED IN CRUDE EXTRACT OF BULLFROG LIVER BY SINGLE-CHANNEL ASSAY. ((L. E. Llewellyn, P. Bell and E. Moczydlowski)) Dept. of Pharmacology, Yale Univ. School of Medicine, New Haven, CT 06510.

The North American bullfrog, *Rana catesbeiana*, contains high levels of a 90 kDa plasma protein called saxiphilin which is homologous to transferrin but binds saxitoxin and its derivatives with high affinity. The existence of saxiphilin raised the question of whether this amphibian also possesses an endogenous blocker of Na-channels. Various bullfrog tissues were extracted with acidic 50% methanol. The solvent was removed by rotary evaporation and lyophilization and the crude residue dissolved in $H_2O$ was assayed on single BTX-activated Na-channels from rat skeletal muscle (high affinity for TTX/STX) and calf heart (low affinity for TTX/STX) in planar lipid bilayers. Bullfrog liver proved to be a potent source of Na-channel blocking activity, whereas skin extract was ineffective. The liver extract contains at least two different compounds that block Na-channels as deduced from histogram analysis of discrete blocking events on rat muscle Na-channels. One component of the mixture induced long duration blocking events with mean dwell times of 5.3 sec and 23.8 sec at +50 mV and -50 mV respectively, while the other induced shorter mean dwell times of 0.25 sec at +50 mV and 0.78 sec at -50 mV. The apparent voltage dependence of blocking activity is similar to that of STX/TTX in this assay. Based on relative blocking activity, we estimate that the extract corresponds to an effective TTX content of 76 pmole / g liver. Like STX/TTX, the liver extract was a much less effective blocker of cardiac Na-channels. When tested in a binding competition assay, liver extract displaced [$^3$H]STX from rat brain membranes, but not from saxiphilin which does not recognize TTX. This result is consistent with the possibility that the liver extract contains TTX-like compounds. *R. catesbeiana* has not previously been recognized as a source of STX or TTX and the approach taken here has proven to be a sensitive means of identifying the presence of such blockers in a complex mixture. The chemical identity and functional significance of the TTX-like activity remains to be determined. Is it endogenously produced as a Na-channel modulator, is it a hazardous secondary metabolite or is it accumulated from microbial flora?

**M-Pos388**

**MODAL GATING KINETICS OF CARDIAC NA CHANNEL INDUCED BY ANTHOPLEURIN-A**

((D. Qin, E.B. Caref, and N. El-Sherif)) SUNY Health Science and V.A. Medical Centers, Brooklyn, NY 11209. (Spon. by N. El-Sherif)

Effects of sea anemone toxin anthopleurin-A (AP-A) on single channel Na current in rabbit ventricular myocytes were studied using cell-attached patch-clamp technique at 20-22C°. At a holding potential of -120 mV and test pulse of -20 mV, burst durations prolonged with increasing concentration of AP-A. Control open time histograms were best fitted with a monoexponential function, and the open time constant ($\tau_o$) was 0.4±0.1 ms (n=7). However, patches exposed to concentrations of 10, 100 or 1000 nM AP-A required 2 exponentials to fit open time histograms. The time constants of the fast component ($\tau_{o1}$) were the same as $\tau_o$ measured in control. The additional slow component of open time had a time constant ($\tau_{o2}$) of 1.3±0.3 (n=5), 1.6±0.3 (n=7) and 1.8±0.2 ms (n=8) at 10, 100, and 1000 nM AP-A, respectively. While both $\tau_{o1}$ and $\tau_{o2}$ had no apparent change with increasing concentration of AP-A (p=0.69, 0.47, respectively), the weight of $\tau_{o2}$ increased significantly (p=0.01). Closed time durations also required biexponentials, however, both the time constants and weight ratios remained unchanged at increasing concentrations of AP-A. Ensemble currents relaxed monoexponentially in control and biexponentially in AP-A-exposed patches. Weights of the AP-A-induced slow component increased with increasing concentration of AP-A (p<0.01). To estimate the dose-dependent modulation of AP-A on Na channels, the slow component weight changes of open time and ensemble current were used as response indicators, and described an $ED_{50}$ of 39 nM and 59 nM at -20 mV, respectively. These findings suggest that the modulation of cardiac Na channel by AP-A may be explained with a two-mode gating kinetic model, in which the modified mode has both a slower closing rate constant and a slower inactivation.

**M-Pos389**

**CONDUCTANCE PROPERTIES OF A SYNTHETIC 34-MER PEPTIDE ENCOMPASSING S4 AND S45 SEGMENTS OF THE VOLTAGE-SENSITIVE SODIUM CHANNEL.**

*O. Helluin, J.Y. Dugast, M. Brullemans, G. Molle and H. Duclohier.* URA 500 CNRS, Université de Rouen, BP 118, 76134 Mont-Saint-Aignan (France).

Segment S4 is recognized to be implicated in the voltage-dependence of ionic channels. More recently, Durell & Guy (1992) assumed that the contiguous segment, S45, could play a role in the gating process as well as forming the inner part of the pore lining (Biophys. J. 62: 238-250.). We thus synthesized by solid phase method a peptide of 34 residues encompassing the S4 and S45 regions of the domain IV of the eel sodium channel sequence: TLFRVIRLARIARVLRLIRAAKGIRTLLFAL (positions 1414 to 1447). The peptide was checked by electron-spray mass spectroscopy and circular dichroism spectra of the peptide in methanol yield a helical content of 55%. Then, the reincorporation of the 34-mer peptide was made into symmetric preformed Montal-Mueller or "tip-dip" bilayers (POPC-DOPE 7:3) bathed both sides by NaCl 500 mM, HEPES 10 mM, pH 7.4 solutions. From the concentration dependence (in the $10^{-8}$ M range) of the macroscopic I-V curves, the apparent mean number of monomers in a conducting aggregate can be estimated to 4-5. The most probable single-channel conductance (9 pS) is significantly lower than those reported for the S4 peptide reconstituted in negatively-charged planar bilayers (Tosteson *et al.* 1989. P.N.A.S.(USA) 86: 707-710).

[ Supported by GDR 0964 (C.N.R.S.). M.B. acknowledges the N.S.E.R.C. (Canada) for a postdoctoral fellowship. ]

**M-Pos390**

**STATE-DEPENDENT INTERACTION OF BUPIVACAINE STEREOISOMERS WITH CARDIAC SODIUM CHANNELS.**

(( C. Valenzuela, E. Délpon, J. Tamargo, L.M. Hondeghem, P.B. Bennett and D.J. Snyders ))
Univ. Complutense, Madrid, Spain and Vanderbilt Univ.,Nashville, TN 37232.

Block of cardiac $Na^+$ channels by bupivacaine (Bupi, 1μM) has been considered to derive from a high affinity of the inactivated state. To further determine the mechanism and stereoselectivity of block, experiments were performed on enzymatically isolated guinea pig ventricular myocytes. $Na^+$ currents were recorded with reduced $Na^+$ gradient at 16°C using the whole cell variant of the patch clamp technique under ionic conditions to eliminate non-$Na^+$ currents. Tonic block was <5% for both isomers (10μM). During depolarization to 0 mV block developed slowly with τ of 3.0±0.6 (S) and 1.8 ±0.5 s (R) (p<0.01), reaching 58±11% (S) and 72±6% (R) in 5 s (p<0.05). Recovery from block induced by 10 s steps proceeded with τ of 4.6 (S) and 5.6 s (R) at -120 mV. Simulations using apparent rate constants based on these data predicted the following levels of block during 3 Hz pulse trains: with 100 ms steps 27% (S) and 42% (R) and with 10 ms steps 4% (S) and 8% (R). Substantially more block was observed experimentally (16 pulses, 3Hz): 100 ms step 51±11% (S), 55±13% (R) and 10 ms step 33±8% (S), 34±13% (R). This high level of block with 10 ms steps, and the failure of the inactivated state interaction rate constants to predict the observed levels of block during trains indicate that both isomers also interact with an activated and/or open state of the cardiac $Na^+$ channel (at 10 μM). The similar level of pulse dependent block indicates that activated state interactions may not be stereoselective, in contrast to the interaction with the inactivated state.

Supported by CICYT SAF92-0157,Salud2000, and NIH HL40608 and HL47599.

**M-Pos391**

**BIOPHYSICAL CHARACTERIZATION OF Na CHANNEL BLOCK BY THE QUATERNARY PHENYLALKYLAMINE D890.**

((D.S. Ragsdale, W.A. Catterall and T. Scheuer)) Department of Pharmacology, SJ-30, University of Washington, School of Medicine, Seattle WA 98195. (Spon. by W.A. Catterall)

We have previously shown that phenylalkylamines, like verapamil and D600, are potent voltage and frequency dependent blockers of rat brain Na channel alpha subunits expressed in the CHO cell line CNaIIA-1. In this study we characterize Na channel block by the quaternary, positively charged, phenylalkylamine D890. Intracellular D890 blocked Na currents in a use-dependent manner (EC50 = 55 uM), but was ineffective extracellularly. Drug binding was rapid when channels were open, but not when they were resting or inactivated. Block was enhanced by strong depolarizations and antagonized by external Na ions. Repriming of drug bound channels at hyperpolarized potentials was extremely slow, with complete recovery taking more than 30 minutes, but recovery occurred within seconds when blocked channels were opened by trains of "unblocking" depolarizations to moderate potentials. Rate parameters were determined for the drug binding and unbinding reactions based on the rate of development of block during a train of pulses. The results suggest that D890 binds to a site within the channel pore, part way through the membrane electric field. The drug enters and leaves its binding site by a hydrophillic, intracellular pathway that is only available when the channel is open, not when it is closed or inactivated. Block of Na channels by quaternary local anesthetics and Ca channels by quaternary phenylalkylamines has similar characteristics, suggesting a similar site of action for these drugs on these two related channel types.

**M-Pos392**

**MODIFICATION OF SODIUM CHANNEL INACTIVATION BY ANTHOPLEURIN-A TOXIN IN CARDIAC PURKINJE CELLS.**

((M.F. Sheets and D.A. Hanck)), Departments of Medicine
University of Chicago and Northwestern Univ., Chicago, IL 60637 and 60611

Several lines of evidence have suggested that inactivation in cardiac Na channels is more voltage dependent than in TTX-sensitive channels. Because removal of inactivation by toxins and enzymes has been useful for gaining insight into inactivation and its coupling to activation, we investigated the action of the type 3 toxin anthopleurin-A (AP-A) on Na channels in single canine cardiac Purkinje cells. Macroscopic sodium currents ($I_{Na}$) and gating currents ($I_g$) were measured in cells that were voltage clamped and internally perfused via a large-bore pipette (13-15°C) before and after modifications by 1 μM extracellular AP-A. This toxin dramatically slowed decay of $I_{Na}$ in response to step depolarizations. However, in contrast to TTX-sensitive mammalian $I_{Na}$ where removal of inactivation has been reported to produce a dramatic increase in the size of $I_{Na}$ at threshold potentials secondary to a prominent negative shift in conductance, for cardiac $I_{Na}$ AP-A toxin produced only a minimal negative shift (-2.4 mV±1.5 mV S.D., n=8) of the potential ($V_{1/2}$) of half-maximal conductance. Similarly, there was no significant shift in the $V_{1/2}$ of the charge-voltage (Q-V) relationship or in its slope factor of the Boltzmann fit to the Q-V data. Although peak conductance ($G_{max}$) increased by 26%±13% (n=8), maximum charge ($Q_{max}$) was reduced by 30% ± 10% (n=9). All effects of toxin were reversible. These data suggest that inactivation is slow near $I_{Na}$ threshold, playing little role in determining $V_{1/2}$ for cardiac $I_{Na}$ and $Q_{1/2}$. At positive potentials, however, where it is more rapid, modification of inactivation produces marked slowing of a transition to an absorbing state (O→I) which reduces $Q_{max}$.

**M-Pos393**

**ATRIAL NATRIURETIC PEPTIDE MODULATES THE $Na^+$ AND $Ca^{2+}$ CHANNELS OF CULTURED BOVINE CHROMAFFIN CELLS.**

((L.A. Sorbera, L. Gandía and M. Morad)) Department of Physiology, University of Pennsylvania, Philadelphia, PA 19104.

Atrial natriuretic peptides (ANP) are a family of peptides produced predominately by the heart and brain and are also synthesized, stored and secreted in the adrenal gland (Ong et al. Biochem. Biophys. Res. Commun. 147:957,1987). In cardiac myocytes, we have reported the existence of two pathways for the regulation of ionic channels by ANP. While $Ca^{2+}$ channels are inhibited by a cGMP mediated pathway (Gisbert & Fischmeister, Circ. Res. 62:660,1988; Sorbera & Morad, Science 247:969,1990), the $Na^+$ channel is suppressed by ANP-induced enhancement of its $Ca^{2+}$ selectivity independent of the cGMP pathway (Sorbera & Morad 247:969,1990). We examined the effect of ANP (rat, 1-28 a.a.) in adrenergic 2-8 day cultured and whole cell clamped bovine chromaffin cells. Cell capacitances of the cultured cells ranged between 9-20 pF making it possible to control the $Na^+$ current and examine its regulation by ANP. 10-100nM ANP suppressed both $I_{Na}$ and $I_{Ca}$ consistent with its effects on cardiac myocytes. While the suppression of the $Ca^{2+}$ channel by ANP was slow (t½ 20 s), $Na^+$ channel was suppressed rapidly within 1-2 s. ANP failed to suppress $I_{Na}$ if $Ca^{2+}$ was omitted from the external solution, suggesting that the ANP effect was $Ca^{2+}$ dependent. When external $Na^+$ was replaced by $Cs^+$ or n-methyl glucamine, ANP induced a rapidly activating and inactivating current with kinetics and voltage dependency similar to that of the $Na^+$ channel (Fig. 1). This $Na^+$ channel current was blocked by 5μM TTX, and was completely suppressed in the absence of $Ca^{2+}$ suggesting that $Ca^{2+}$ was the charge carrier through the $Na^+$ channel. Thus, the regulation of the $Na^+$ channel by ANP appears to involve alteration of the $Ca^{2+}$ selectivity of the channel. Although ANP suppressed both $Na^+$ and $Ca^{2+}$ channels, only the suppression of the $Ca^{2+}$ channel was mediated by activation of guanylate cyclase. (Supported by NIH grant no. HL16152)

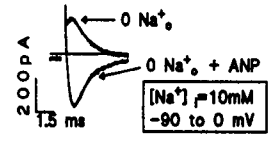

**M-Pos394**

**ATRIAL NATRIURETIC PEPTIDE ENHANCES $Ca^{2+}$ AND $Ba^{2+}$ SELECTIVITY OF THE CARDIAC AND SKELETAL $Na^+$ CHANNELS EXPRESSED IN A HUMAN KIDNEY CELL LINE.** ((L.A. Sorbera, R. Horn$^+$, R.G. Kallen and M. Morad)) Dept. Physiology & Biochemistry, University of Penn. and Physiology Dept., Jefferson Med. Coll.$^+$, Philadelphia, PA.

Cloned $Na^+$ channels were expressed transiently in a human kidney cell line (tsA201) under control of a CMV promotor. Two different isoforms were expressed: hH1, a TTX-resistant isoform from human heart and rSKM1, the TTX-sensitive isoform from rat skeletal muscle. $I_{Na}$ was measured in the whole cell configuration. Both isoforms produced large (>1nA) rapidly inactivating currents under control conditions (external solution in mM: 137 NaCl; 5.4 KCl; 1.0 $MgCl_2$; 2 $CaCl_2$ at pH 7.4) 1 to 2 days after transfection. Cells were dialyzed with 120 mM n-methyl glucamine (NMG), 5 mM MgATP, 20 mM HEPES, 14 mM EGTA and 0,10, or 20 mM NaCl. Extracellular $Na^+$ concentration were appropriately changed to 0, 10, and 20 mM $Na^+$ ($Na^+$ was replaced with NMG) to control $E_{rev}$ close to 0 mV. In hH1 cells, rapid (<50 ms) application of 100 nM ANP in 0, 10 or 20 mM $Na^+$ and 5 mM $Ca^{2+}$ or $Ba^{2+}$ containing solutions, enhanced the $Na^+$ current by 50-100%. ANP shifted the reversal potential of $I_{Na}$ by a minimum of 10-20 mV irrespective of whether the cells were dialyzed with 0, 10 or 20 mM $Na^+$. Trace by trace subtraction of $I_{Na}$ at different potentials showed a shift of the peak current from -20 mV by 5-10 mV toward positive potentials and significant inward currents positive to $E_{rev}$. There was no change in the kinetics of the $Na^+$ channel after addition of ANP. ANP similarly increased $I_{Na}$ and shifted the reversal potential in rSKM1 cells. Dialysis of the cells with 150 mM CsF blocked the enhancing effect of ANP on $I_{Na}$. These results show that ANP enhances the selectivity of the $Na^+$ channel to $Ca^{2+}$ or $Ba^{2+}$ in a manner similar to the effect observed in cardiac (Sorbera & Morad, Science 247:969,1990; Sorbera & Morad, Science 252:449,1991) and chromaffin cells. Since the current is enhanced both in hH1 and rSKM1, the data suggest that the ANP effect is not mediated through the TTX-sensitive site of the $Na^+$ channel. (Supported by NIH grant no. HL16152)

**M-Pos395**

**HYDROGEN PEROXIDE-INDUCED ALTERATIONS IN THE KINETICS OF THE CARDIAC SODIUM CURRENT.**

((Aruni Bhatnagar)), Physiology and Biophysics, University of Texas Medical Branch, Galveston, TX 77550

The effects of hydrogen peroxide on the sodium currents of isolated rat ventricular myocytes were studied using the whole cell configuration of the patch-clamp technique in low Na, Cs-Ringers solution. Superfusion with Cs-Ringers led to a progressive decline in the sodium current elicited on depolarization from a holding potential of -100 mV. This decline was accelerated on exposure to 100 $\mu$M hydrogen peroxide. Superfusion with Cs-Ringers solution also led to a time-dependent hyperpolarizing shift in the voltage dependence of the steady-state activation ($m_\infty$) (0.16 $\pm$ 0.04 mV/min) and inactivation ($h_\infty$) (0.14 $\pm$ 0.02 mV/min) parameters and slight increase in the time constants of current activation and decay. Exposure to 100 $\mu$M hydrogen peroxide accelerated the hyperpolarizing shifts in the voltage dependence of $m_\infty$, and $h_\infty$, which in the presence of the peroxide were 0.22 $\pm$ 0.06 and 0.33 $\pm$ 0.07 mV/min, respectively. The peroxide also increased the time constant for current decay more than 3 fold with little or no effect on the time constant for activation of the current. On the basis of these results it is suggested that reduction in the amplitude and the rate of inactivation of the sodium currents may be partly responsible for the arrhythmogenic effects of oxidative stress.

**M-Pos396**

**SUPPRESSION OF SODIUM CURRENTS BY 2,3-BUTANEDIONE MONOXIME IN RAT SINGLE CARDIAC MYOCYTES.**

((Y.-F. Xiao and J.J. McArdle)) Dept. of Pharmacology & Toxicology, New Jersey Medical School-UMDNJ, Newark, NJ 07103-2714. (Spon. by K. Friedman)

Our previous data show that a chemical phosphatase, 2,3-butanedione monoxime (BDM) could inhibit the L-type $Ca^{2+}$ current and the transient $K^+$ current in rat cardiac cells. In this study, effects of BDM on sodium channels were investigated by using the whole-cell recording method in rat single cardiac myocytes. Superfusion of 20 mM BDM elicited a strong inhibition of the inward $Na^+$ current ($I_{Na}$). For example, the peak $I_{Na}$ (a voltage-step to -30 mV from the membrane holding potential of -80 mV) was significantly inhibited from the control value of 6.51 $\pm$ 0.61 nA (n = 5) to 3.43 $\pm$ 0.92 nA ($p < 0.05$) following application of 20 mM BDM. Furthermore, 20 mM BDM increased the inactivation time constant of $I_{Na}$ from 2.21 $\pm$ 0.19 ms (control, n = 5) to 4.23 $\pm$ 0.53 ms ($p < 0.05$). The current-voltage relationship was not changed. The present data indicate that BDM has a strong inhibitory effect on the activity of cardiac sodium channels. In view of our previous and present data, it is proposed that BDM is a non-selective inhibitor of ion channels and its mechanism is probably related to channel dephosphorylation. Supported by grants NIAAA AA08025, AMA 90-G-027, and NIH NS31040.

**M-Pos397**

**EXTERNAL AND INTERNAL BLOCKERS OF THE HUMAN HEART SODIUM CHANNEL.** ((M.E. O'Leary, M. Chahine, L.-Q. Chen, R.G. Kallen and R. Horn)) Physiol. Dept., Jefferson Med. Coll., Philadelphia, PA 19107, Dept. Biochem. & Biophys., Univ. of Penn., Phila., PA 19104.

The cloned human heart Na channel (hH1), a tetrodotoxin-resistant isoform, was expressed heterologously in *Xenopus* oocytes and in human kidney cell lines. We examined the effects of putative extracellular ($Ca^{2+}$ and $Mg^{2+}$) and intracellular (tetraalkyl-ammonium cations) blockers on whole cell and single channel currents. The block by extracellular divalents was studied in outside-out patches from Na channels in which the fast inactivation had been removed by a Catterallian mutation in the cytoplasmic loop connecting the 3rd and 4th domain. Neither $Ca^{2+}$ nor $Mg^{2+}$ affected the amplitude of single channel currents between 0 and 1.5 mM, in contrast with data from TTX-sensitive isoforms. Intracellular tetraethylammonium (TEA) and tetrabutylammonium (TBA) both reduced outward more than inward currents and acted like fast open-channel blockers, i.e. reducing the amplitude of single channel current. TBA was more potent ($K_i$~0.5 mM at 0 mV); its apparent blocking site was located ~64% of the way into the membrane field from the inside.

**M-Pos398**

**ANGIOTENSIN II SUPPRESSES $Na^+$ CURRENTS IN BOVINE ADRENAL CHROMAFFIN CELLS.** ((Y. Cui and R.Y.K. Pun)) Dept of Physiol. & Biophys., Univ. of Cincinnati, Cincinnati, OH 45267. (Spon. by Dr. L.K. Lane )

We investigated the effects of angiotensin II (AII) on the voltage-dependent, TTX-sensitive $Na^+$ currents ($I_{Na}$) recorded from bovine adrenal medullary chromaffin cells (BCC) under whole-cell voltage clamp. AII reversibly reduced the peak $I_{Na}$ in a dose-dependent fashion. Inhibition was observed at a concentration of 1 nM (6.3±1.4%, mean±sem, n=7) and reached a maximum at 1 $\mu$M (34.2±3.8%, n=10), with a half-maximal effect at 11.6 nM. The AII-induced inhibition resulted from a significant reduction in peak conductance (control, 7.2±0.1 nS; AII, 4.3±0.1 nS; $p<0.01$, n=7). AII had no effect on the reversal potential (+53 mV for both control and AII) or the decay time of $I_{Na}$ (at +10 mV; control, $\tau$=1.1±0.1 msec; AII, $\tau$=1.1±0.1 msec, $p>0.05$, n=7). In addition, the $V_{1/2}$ and k values, two parameters that describe the voltage dependence of $I_{Na}$ for both steady-state activation and inactivation, were not affected by AII. The response to AII (1$\mu$M) had a delay and took 0.9±0.2 min (n=10) to attain maximum inhibition. Recovery from the effect was slow and took 3.5±0.8 min (n=10) after the application of AII had been terminated. The inhibitory effects of AII were blocked by the AII-receptor antagonist, [Sar$^1$, Val$^5$, Ala$^8$]-angiotensin II (10$\mu$M). The present study demonstrates that AII inhibits voltage-dependent $Na^+$ channels in BCC via a specific receptor-coupled mechanism. The prolonged time course of the AII response indicates the possible involvement of a second messenger mediating this inhibition. [Supported by AHA (Ohio Affiliate) SW-91-18]

**M-Pos399**

**The Characterization of Slower Component of Recovery Kinetics from Use-Dependent Block on Sodium Channel with Disopyramide**

Ryoichi Sato, Ichiro Hisatome*, Hiroyuki Takai, Yoshiki Aida, Sumio Matsuno, Senya Karasaki, Miki Oyaizu, Shin-ichi Koumi**, and Ryo Katori, Kinki University, Osaka, Japan, *Tottori University, Yonago, Japan,**Nippon Medical School, Tokyo, Japan

The recovery process from use-dependent block of sodium current ($I_{Na}$) by antiarrythmic drugs is composed of tow phase, i.e., fast or slow component. Previously, we reported that the slow component indicated the dissociation of disopyramide from receptor through hydrophobic pathway, in the present study, we discovered the existence of slower component of dissociation of disopyramide (50$\mu$M) and characterized the nature of its slower component in guinea-pig ventricular myocytes using patch-clamp technique. Prolonging the iterstimulus interval of the double pulse-protocal up to 5 minutes, the slower component of dissociation from use-dependent block of $I_{Na}$ by disopyramide have been observed at pH=7.4. This slower component was also observed after treated with 3 mM chloramine-T. The time constant of slower component ($\tau_{slower}$) was independent of hyperpolarizing the membrane(either HP=-100 or -140 mV), but this was dependent on the extracellular pH, i.e., $\tau_{slower}$ increased under aciditic condition (pH=6.8) and decreased under alkalic condition (pH=8.0). $\tau_{slower}$ was extremely larger than the deprotonation time constant(10pKa/[5X10$^8$]).

**M-Pos400**

**MODULATION OF THE VOLTAGE - DEPENDENT SODIUM CHANNEL BY INTRACELLULAR FREE CALCIUM AND FLUORIDE.**

**(( M. Egger and N.G. Greeff)) Physiologisches Institut, Universität Zürich, Winterthurerstr. 190, CH-8057 Zürich, Switzerland.**

**It has been shown that the intracellular free calcium concentration in N1E115 mouse neuroblastoma cells modulates the peak macroscopic sodium current, $I_{Na}$ (Bulatko & Greeff, Biophys.J 57: 308a, 1990). Under whole cell recording conditions an increase of the intracellular calcium concentration from pCa-9 to pCa-7 causes a significant enhancement of peak $I_{Na}$ of about 80%. This effect was not due to shifts in the current - voltage relation or the steady - state inactivation curves. Also the influence of cellular shape change, i.e. an increase of cellular membrane surface area accessible from the bath medium during osmotic swelling or exocytosis could be excluded by capacitance measurements. In order to study further the calcium induced modulation of $I_{Na}$ we used fluoride as the main internal anion which also keeps the free calcium concentration to about pCa-9 (given by solubility product). Nevertheless, the observed $I_{Na}$ was as large as in pCa-7 and showed similar kinetics. In addition, using non - stationary fluctuation analysis of $I_{Na}$ we could demonstrate the single channel conductance to be the same for both intracellular calcium concentrations as well as for fluoride. Therefore, the significantly higher current densities at pCa-7 and intracellular fluoride could be explained in terms of an increased number of activatable sodium channels. NaF is a well known G-protein activator and phosphatase inhibitor. Thus, our results suggest that the increase of $I_{Na}$ originates from an enhanced specific phosphorylation (probably via cAMP cascade) at the sodium channel. (Supported by Swiss National Fund 31-27788.89)**

**M-Pos401**

**DIFFERENCES BETWEEN SODIUM CHANNEL GATING AND DISTRIBUTION ON HUMAN FAST AND SLOW TWITCH SKELETAL MUSCLE FIBERS**

**((R.L. Ruff)) Neurology Service Cleveland VAMC and Depts. of Neurology and Neurosciences Case Western Reserve University School of Medicine, Cleveland OH 44106**

**Previous work suggested that human fast twitch fibers had a higher density of Na channels on the extrajunctional membrane and showed a greater increase in channel density near the endplate than slow twitch fibers. I examined whether the voltage gated properties and current amplitudes and the distribution of Na channels on 15 fast and 14 slow twitch histochemically classified human intercostal muscle fibers. Biopsies were obtained from 9 patients during thoracotomy. Muscles were enzymatically treated to aid in dissection and in identifying the nerve terminals. The maximum Na current density was measured at 3 or more sites in 2 different regions: 1) on the border of the endplate and 2) >200 μm from the endplate. For both fast and slow twitch fibers the Na current density at the border of the endplate was higher than it was >200 μm from the endplate (Table). The Na current density on fast twitch fibers was higher for both regions. In addition, fast twitch fibers manifest fast and slow inactivation of Na current at more negative potentials than slow twitch fibers. These results suggest that the Na channel distributions and voltage dependent gating are different on fast and slow twitch human skeletal muscle fibers. The differences between $I_{Na}$ on fast and slow twitch fibers might: 1) enable fast twitch fibers to phasically operate at high firing frequencies, and 2) enable slow twitch fibers to be tonically active at low firing frequencies. (Support: Department of Veterans Affairs)**

**Table:** Na Current Density and Inactivation of Fast and Slow Fibers

| | Na Current Density (mA/cm²)* | | | | | |
|---|---|---|---|---|---|---|
| Fiber Type | Endplate Border | Extrajunctional | $V_{h1/2}$* | $A_h$ | $V_{s1/2}$* | $A_s$ |
| Fast Twitch | 100±19 | 18.9±1.1 | -71±1 | 6.2 | -93.4 | 5.6 |
| Slow Twitch | 23.7±1.4 | 7.24±0.34 | -61±1 | 7.5 | -71.5 | 8.7 |

* Na current density of fast twitch fibers was greater than slow twitch fibers at each of the sites and fast twitch fibers manifest inacitivation at more negative potentials ($p<0.001$).

**M-Pos402**

DEVELOPMENTAL AND REGIONAL EXPRESSION OF RH1 mRNA IN THE RAT HEART. ((Sidney A. Cohen, Candace Mello, and Jane Yang)) Univ. of Penna. School of Medicine, Phila., PA. 19104

Cardiac sodium channels are essential for the initiation and propagation of rapid upstroke action potentials in the heart and are the major sites of action of Type 1 antiarrhythmic drugs. We sought to determine whether mRNA for the TTX-insensitive RH1 sodium channel is constitutively expressed or is developmentally or spatially regulated in cardiac tissues. Total RNA was prepared from 15 and 20 day gestational, 3, 7, and 15 week old male Wistar rats, and from different regions of the 15 week adult male heart and subjected to Northern blot analysis using a subtype-specific riboprobe. There was a slow but steady rise in the steady state RH1 mRNA level during the later portion of prenatal development. This was followed by a further increase from approximately half maximal levels in the juvenile heart to maximal levels in the adult rat heart. Adult left ventricular freewall, right ventricular freewall, interventricular septum, and atria all contained similar steady state levels of RH1 mRNA. These results are in contrast with previously reported $^3$H-STX binding assays of membranes prepared from rat hearts which reveal essentially invariant levels of TTX-insensitive sodium channel protein from birth and adulthood. These results suggest that RH1 mRNA expression is controlled at both the transcriptional and translational or post-translational levels in the rat heart.

**M-Pos403**

CHARACTERIZATION OF IONIC CHANNELS IN TROPICAL SQUID GIANT AXONS ((A. M. Correa, C. Caputo, R. Morales, F. Bezanilla)) Dept. of Physiol., UCLA, Los Angeles, CA, 90024 and Centro de Biofísica y Bioquímica, IVIC, Caracas, Venezuela.

Sodium and potassium channels from the giant axons of the tropical squids *Loligo plei* and *Sepioteuthis sepioidea* were characterized using the cut-open axon technique. Sodium channels were studied in external 540 NaCl, 10 HEPES-Na and internal 50 Na-Glutamate, 145 Cs-Glutamate, 10 CsCl, 20 CsF, 470 sucrose, 10 HEPES-Cs, 1 EGTA-Cs. Reconstruction of macroscopic currents from single channel data show regular Na channel kinetics (activation and inactivation). We also studied the conduction properties of the normal and the BTX-modified channels in *Sepioteuthis* in symmetrical Na solutions. The single channel conductance was reduced more than 50% by BTX within the range of concentrations studied (30 to 540 mM). This is similar to what has been found in *Loligo pealei* (Correa et al., J.G.P. 97:605). The single channel activity showed a marked temperature dependency in both species. The single channel conductance changed by about 20% lowering the temperature from 18 to 12 °C, and 30% from 12 to 5 °C. In records with few channel events, the product of $NP_o$ (N=number of channels; $P_o$=open probability) decreased dramatically with a decrease in temperature. Potassium channels were studied in external artificial sea water + TTX and in internal 560 mM K-Aspartate, 10 mM HEPES-K. K channels of both *Loligo* and *Sepioteuthis* showed a high temperature dependency. In *Sepioteuthis* along with the regular delayed rectifier K channels, we also found an inactivating K channel responsible for an inactivating K current. Although apparent at potentials between +20 and +40 mV the, inactivation becomes very striking at more positive potentials, showing an inactivation half time of 9.5 ms at +80 mV and 5 ms at +90 mV in the mean current traces. Supported by USPHS GM30376 and CONICIT S1-2148.

## CHANNELS (OTHER)

**M-Pos404**

**DELINEATION OF CHANNEL STRUCTURES BY THE OSMOTIC ACTION AND PENETRATION OF DIFFERENTLY SIZED NEUTRAL POLYMERS.**

((S.M.Bezrukov[a,b], I.Vodyanoy[c], V.A.Parsegian[a])) [a]National Institutes of Health, NIDDK; [b]St.Petersburg Nuclear Physics Institute, [c]Office of Naval Research.

By exposing ionic channels to neutral polyethyleneglycols of different molecular weight, we have been able to generalize the use of polymers to probe channel structure. Large excluded solutes in membrane-bathing solutions create an osmotic work of transition between different conductance states, a work proportional to the difference in polymer-inaccessible aqueous spaces of these states. Progressively smaller polymers begin to penetrate the channel space, to cause a decrease in channel conductance and to exert a correspondingly reduced effective osmotic pressure.

We find that the channel, a kind of ultimate molecular sieve, appears to exclude polymers on the basis of their rotational volume $(4/3)\pi R_g^3$ for radius of gyration $R_g$ (rather than the polymer cross-section $\pi R_g^2$ or diameter $2R_g$ typically used to gauge channel size).

In the particular case of the polypeptide alamethicin, polymer probing reveals a fixed (about 3,000 Å$^3$) aqueous volume change with each successive step between the five different conductance states. These states, then, are collections of conducting units of nearly the same conductance (but different access resistance) rather than pores of successively larger radius.

**M-Pos405**

HIGH-SALT WASH AND OSMOTIC SHOCK FLUID FROM *ESCHERICHIA COLI* RECONSTITUTED IN LIPOSOMES CONTAIN STRETCH-INACTIVATED ION CHANNELS. ((Boris Martinac*, Sergei I. Sukharev*, and Ching Kung*@)) Laboratory of Molecular Biology* and Department of Genetics@, University of Wisconsin, Madison, WI 53706

High-salt wash with NaCl-EDTA as well as osmotic down-shock with cold distilled $H_2O$ of *ompC⁻ ompF⁻* double mutant strain of *E. coli* (AW740) yielded soluble protein fractions which upon reconstitution into azolectin liposomes both contained activities of a stretch-inactivated (SI) ion channel when examined by patch clamp. The channel was permanently open at apparent zero pipette pressure. Application of positive pressure (blowing) caused the channel to gate reversibly between the open state and closed states of different size. The pressure-dependent closures were more prominent at positive pipette voltages than at negative voltages. Negative pressure (suction) above 80 mm Hg applied to the patch pipette inactivated the channel irreversibly. Pipette voltages larger than ±130 mV induced reversible porin-like closures of the channel. This SI channel behavior was similar to the behavior of porin-like channels we have found in the small-MS-channel-containing (SMSC) octylglucoside-solubilized membrane fractions obtained by gel filtration on the Superose 6 HR column. Our results suggest that the SI channel may be related to the SMSC and is most likely a porin-like protein from the outer membrane of *E. coli*. Supported by a grant from Markey Trust.

**M-Pos406**

RECONSTITUTION OF TWO DISTINCT TYPES OF MECHANO-SENSITIVE CHANNELS FROM THE *E. COLI* CELL ENVELOPE. ((Sergei I. Sukharev*, Boris Martinac*, and Ching Kung*@)) Laboratory of Molecular Biology* and Department of Genetics@, University of Wisconsin, Madison, WI 53706 (Spon. by B. Martinac)

Membrane patches of giant spheroplasts of the *ompC⁻ ompF⁻* double mutant (AW740) of *E. coli* contain two distinct types of mechanosensitive (MS) channels, the small (SMSC) and the large (LMSC) MS channel with conductances of 1.1 nS and 3.5 nS in 200 mM KCl, respectively. The membrane fraction from this mutant was solubilized in 3% octylglucoside and fractionated by gel filtration on the Superose 6 HR column. The individual fractions were reconstituted into azolectin liposomes, sampled by patch-clamp and found to contain functional SMSCs and LMSCs. Under non-denaturing conditions the profiles of MS channel activity showed an apparent molecular weight of about 60-80 kD for LMSC and 200-400 kD for SMSC. Both types of channels were more sensitive to suction in liposomes than in spheroplasts. At pipette voltages of 80-125 mV SMSCs closed reversibly to different subconducting levels in both, native and reconstituted membranes. Suction above 80 mm Hg inactivated these channels irreversibly. Porin-like channels which showed the typical three-step closures at voltages ±130 mV with a conductance comparable to that of the SMSCs also occurred in the SMSC-containing fraction. Our results show that LMSC and SMSC are distinct molecular entities with the latter one presumably being related to bacterial porins. Supported by a grant from Markey Trust.

**M-Pos407**

PATCH AND WHOLE-CELL MECHANOSENSITIVE CURRENTS RECORDED FROM BC3H-1 MUSCLE CELLS. ((O.P. Hamill and D.W. McBride, Jr.)) Neurobiology and Behavior, Cornell University, Ithaca, NY 14853.

Mechanosensitive (MS) channel currents were measured in membrane patches and whole BC3H-1 cells. A pressure clamp was used to apply pressure/suction pulses to activate MS currents. On cell-attached patches brief suction pulses activated single MS channel currents (5pA at -100 mV) that remained open for several seconds after the pulse (Fig, upper traces). After rupturing the patch, brief pressure pulses activated whole-cell MS currents (Fig, lower traces) that decayed with a time course similar to that seen in single MS channel ensembles (not shown). Whole-cell currents of 1 to 5 nA could be reproducibly activated in cells with estimated surface areas of 2000-3000 $\mu m^2$. These currents were rapidly and reversibly blocked by 100 µM gadolinium applied to the cell. Larger currents could be elicited by stronger pressure stimulation, however, such stimulation often resulted in irreversible current changes. Hysteresis in pressure-MS current response was often observed indicative of membrane-cytoskeleton decoupling. Supported by Muscular Dystrophy Association.

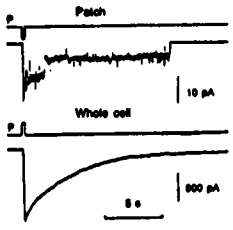


**M-Pos408**

MEMBRANE PATCH CAPACITANCE AND ADAPTATION OF MECHANOSENSITIVE CURRENTS IN RESPONSE TO PRESSURE-CLAMP STEPS. ((D.W. McBride, Jr. and O.P. Hamill)) Neurobiology and Behavior, Cornell University, Ithaca, NY 14853.

Recently it has been shown that mechanosensitive (MS) channels in Xenopus oocytes exhibit adaptive gating behavior in response to suction or pressure steps. Adaptation could arise because of a relaxation in the membrane area in response to the stimulation or because of a property intrinsic to the channel gating mechanism. The characteristics of adaptation such as its voltage dependence and fragility in the patch clamp configuration argue against a relaxation of the membrane area. In order to directly rule out this possibility we have monitored membrane patch area via capacitance during pressure clamp steps. Capacitances were measured by electrically stimulating the patch with a 10 kHz sine wave and measuring the response at the appropriate phase angle with a dual channel phase lock-in amplifier. Preliminary data suggest that both MS channel activation and subsequent adaptation can occur with no accompanying change in the patch capacitance.

**M-Pos409**

GADOLINIUM INHIBITS STRETCH INDUCED ALIGNMENT OF CULTURED ENDOTHELIAL CELLS.

((K. Naruse, H. Asano, and M. Sokabe)) Dept. Physiol. Nagoya Univ. Sch. Med., Nagoya 466 Japan

Endothelial cells in vivo align their longitude along the vessel. Although the mechanism of the alignment is completely unknown, shear stresses by blood flow or periodic stretches of the vessel wall may be one of the candidates to control the alignment. To test the effect of stretches on the alignment, we have grown vascular endothelial cells from human umbilical vein on elastic silicon membranes and applied cyclic sinusoidal stretches (60 c/min.) by 120 % in length at the peak. Within 4 hr. most of the cells aligned at 80 to 120 degree with respect to the direction of stretch. This alignment was dependent on the extracellular calcium and inhibited by gadolinium (10 - 100 uM), a potent blocker for the stretch activated (SA) channel. It is suggested that stretch dependent calcium influx through SA channels is involved in the alignment.

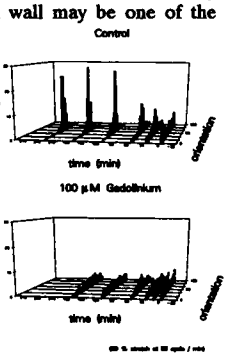


**M-Pos410**

DYNAMICS OF PATCH CLAMPED MEMBRANES: A MODEL ANALYSIS. ((M. Sokabe and K. Nunogaki)) Dept. Physiol. Nagoya Univ. Sch. Med. Nagoya 466, Japan

By using high power videomicroscopy, we could visualize patch clamped membranes in the pipette. When appiled a pressure pulse through the pipette, the area of the patch increased transiently, where both the rising and falling phases followed single exponential functions of time (Sokabe et al., Biophys. J. 59, 1991). Unexpectedly the falling phase was 1.2 to 1.6 times as fast as the rising phase. To explain this result we constructed a mechanical model of the patch that is composed of a viscoelastic element and a series viscose element describing the patch membrane and cytoplasm, respectively. This model could simulate the single exponential time course but failed to explain the faster falling phase. However, introducing an offset tension in the patch could successfully simulate it. Existence of offset tension in the patch was also suggested experimentally from a plot of tension in the patch as a function of area change of the patch. It is concievable that the offset tension is produced during seal formation proccess. After gigaseal formation most patch membranes at zero pressure are almost planar looking like to be stretched. This offset tension may partially explain the contradiction between the stretch activated (SA) single channel currents and macroscopic stretch activated currents, where the latter were harder to induce than the former (Morris and Horn, Science 251, 1991).

**M-Pos411**

**THE THREE - STATE MODEL FOR TRANSDUCTION - CHANNEL GATING IN HAIR CELLS.** ((V. S. Markin, F. Jaramillo and A. J. Hudspeth)) Neuroscience Research Center, University of Texas Southwestern Medical Center, Dallas, TX 75235-9039. (Sponsored by J. Albanesi)

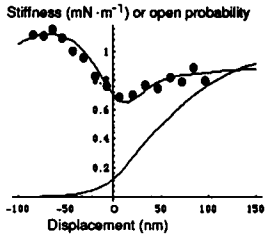


The mechanoelectrical transduction channels of a hair cell are gated by the application of force to the cell's receptive organelle, the hair bundle. A standard model for the gating process (Howard, J. & Hudspeth, A. J. [1988] *Neuron* 1:189-199), based upon two-state Boltzmann statistics, does not account for several experimental observations: 1) the difference in stiffness of a hair bundle before and after channel opening, 2) the different positions of mechanical and electrical manifestations of channel opening, and 3) the departure of the receptor potential from a simple Boltzmann dependence on displacement. To accommodate these results, we developed a three-state model for channel gating. The transduction channel is supposed to occupy any of three states - latched (L), closed (C), and open (O), related by the state diagram L ↔ C ↔ O. In the latched state a portion of a gating spring is immobilized so that the spring's tension is not passed to the gate; this state is accordingly less compliant. The theoretical curves for instantaneous bundle stiffness and open probability are presented in the figure together with experimental data from a bullfrog's hair cell. The model shows improved agreement with both mechanical and electrical data.

This work was supported by National Institutes of Health grant DC00317.

**M-Pos412**

**TWO-TONE DISTORTION PRODUCTS IN A SINGLE HAIR CELL.**

((F. Jaramillo, V. S. Markin and A. J. Hudspeth)) Neuroscience Research Center, University of Texas Southwestern Medical Center, Dallas, TX 75235-9039.

Stimulation of the auditory system with a pair of pure tones can give rise to the sensation of additional tones, or distortion products, that are not present in the stimulus. Prominent among these are the difference tone, $f_2 - f_1$, and combination tones such as $2f_1 - f_2$ and $2f_2 - f_1$. Distortion products originate within the cochlea, where they manifest themselves in the basilar membrane's vibration. We have found that distortion products are readily detectable at the level of individual hair cells, where they emerge from a nonlinearity intrinsic to the mechanoelectrical transduction process in the receptive organelles, or hair bundles. Deflection of a hair bundle acts through elastic gating springs to open mechanically sensitive ion channels. Over the narrow range of bundle displacements in which channels open and close, the hair bundle's stiffness decreases. This phenomenon, the gating compliance, makes the relationship between force and displacement strongly nonlinear. Using the displacement-clamp technique (Jaramillo, F. & Hudspeth, A. J. [1993] *Proc. Natl. Acad. Sci. USA*, in press), we performed a harmonic analysis of the force generated by the hair bundle in response to two-tone stimulation. We detected all the distortion products known in the psychophysics of hearing. A theoretical model based on the gating compliance accurately accounted for the amplitudes of the distortion products. Our results provide a plausible explanation for cochlear distortion products and suggest that the mechanical properties of hair bundles significantly influence the basilar membrane's motion.

This work was supported by National Institutes of Health grant DC00317.

**M-Pos413**

ION CHANNEL ACTIVITY OF THE $M_2$ PROTEIN OF INFLUENZA A VIRUS

((C. Wang#, K. Takeuchi, L. J. Holsinger, R. A. Lamb#, and L. H. Pinto*)) Dep't of Biochemistry, Molecular Biology and Cell Biology, #Howard Hughes Medical Institute, and *Dep't of Neurobiology and Physiology, Northwestern Univ. Evanston, IL 60208.

The single transmembrane domain of the $M_2$ ion channel of the Udorn, Rostock and Weybridge strains of influenza A virus differs in only 3 amino acids. Indirect evidence suggests that the pH-activation and amantadine block of these forms of $M_2$ might differ. We therefore measured these characteristics with 2 electrode voltage clamp in the oocyte expression system. All three channels were activated about equally (ca. 7- fold) by reducing pH from 7.5 to 6.2. However, the $K_i$ for the irreversible amantadine block differed for the channels and differed with pH. The $K_i$'s at pH 7.5 were: Udorn, 10 μM,; Weybridge, 20 μM; Rostock, 50 μM. The Ki's were higher at pH 6.2: 20, 30, and 100 μM, respectively. Analysis of single amino acid substitutions indicated that the difference between Rostock and Weybridge resulted from a difference in amino acid #27 (I and V, respectively). Amantadine attenuated inward and outward currents for all 3 ion channels at pH 6.2. Thus, the $K_i$ for amantadine block of the $M_2$ channel depends upon the amino acid composition of the transmembrane domain and the pH of the bathing medium.

**M-Pos414**

**CHANNELS IN LIPID BILAYERS INDUCED BY A FRAGMENT OF THE β-AMYLOID PEPTIDE.**

P. Marshall, T. Mirzabekov, W.L. Yuan, M. Carman*, I. Lieberburg*, and B. Kagan. Neuropsychiatric Institute of UCLA Medical School, Brentwood Veterans Administration Medical Center, Los Angeles, CA 90024, and *Athena Neurosciences, South San Francisco, CA.

Deposition of amyloid in senile plaques is one of the pathologic hallmarks of Alzheimer's disease. These plaques are composed of a 39-43 residue peptide known as β-amyloid, which is believed to play a role in the pathogenesis of Alzheimer's and which can be neurotoxic to cells in culture. We report that an 11-residue fragment of β-amyloid (residues 25-35) spontaneously forms ion-permeable channels when 3-15 μM concentrations are added to one side of a planar lipid bilayer. Channels open at positive voltages and close at negative voltages. In symmetrical solutions with 100 mM NaCl, 10 mM Tris-HCl, and 1mM $MgCl_2$ at pH of 7.5, channels were observed with conductances of approx. 10, 40, 60, 160, and 300 pS. Channels were also measured in a solution of 1M NaCl, 10 mM Tris-HCl, and 1mM $MgCl_2$ at pH of 7.2 and had conductances of approx. 50, 80, 150, 280, 660 pS, and rarely 1-3 nS. Ion selectivity of the channels was slightly cationic (10-12 mV at 10-fold gradient of NaCl). These results suggest that β-amyloid peptide may induce neurotoxicity through channel formation.

**M-Pos415**

SITE-SPECIFIC BIOTINYLATION OF COLICIN Ia: A PROBE FOR PROTEIN CONFORMATION IN THE MEMBRANE.

((Stephen Slatin, Xiao-Qing Qiu, Karen Jakes, Alan Finkelstein)) Dept. of Physiology & Biophysics, Albert Einstein Col.of Med., Bronx, N.Y. 10461.

Channel-forming colicins are *E. coli* proteins that form voltage-dependent channels in membranes and are lethal to sensitive strains of *E. coli*. Experiments with colicin E1 have led to a model of voltage dependence based on the insertion of alpha helical segments of the protein into the membrane in response to *cis* positive voltage. Here we report the use of biotinylation of colicin Ia at a specific site, followed by irreversible binding to streptavidin, as a technique for studying the orientation of the protein in the membrane. Lys 544 of colicin Ia was mutated to cysteine, using a plasmid generously provided by P. Ghosh (Ph.D. thesis, UCSF, 1992). This unique cysteine is at a site expected, by homology to colicin E1, to cross the membrane from the *cis* to the *trans* side in association with channel opening. The mutant channel differs somewhat from the wild-type (wt), but retains the ability to form voltage dependent channels and to kill target bacteria. Incubation of the mutant, but not the wt, with streptavidin, blocks killing. Channels formed by the mutant protein in planar lipid bilayers are abolished by streptavidin added to the *cis* side of the membrane, if they are closed, but not if they are open. *Trans* streptavidin has no effect on either open or closed channels. Evidently, residue 544 is accessible to *cis* streptavidin in the closed state, but the opening of the channel eliminates this accessibility. These results are consistent with the insertion model of gating proposed for colicin E1. (supported by NIH 299210-15)

**M-Pos416**

**COMPARATIVE STUDY OF IONIC CHANNELS FORMED BY CRYIA(A), CRYIA(B), CRYIA(C) AND CRYIC *BACILLUS THRURINGIENSIS* TOXINS IN PLANAR LIPID BILAYERS.**

((J.L. Schwartz, D. Savaria+, L. Masson, R. Brousseau and R. Laprade+)) B.R.I., National Research Council, Montreal, Que, Canada, H4P 2R2 and +G.R.T.M., University of Montreal, Montreal, Que, Canada, H3C 3J7.

Planar lipid bilayers (PLBs) experiments performed to investigate the formation of ionic channels by CryIC showed that: 1) the toxin forms ionic channels in PLBs at both acidic and alkaline pHs; 2) at acidic pHs (6-6.5), the channels are often chloride-selective; 3) at alkaline pHs (above 8.5), the channels are mainly potassium-selective and display subconductance levels not observed at acidic pHs (Schwartz et al., J. Membr. Biol., in press). We have extended these studies to the CryIA family of lepidopteran-specific Bt toxins in an attempt to relate the differences in toxicity between CryIA(a), CryIA(b) and CryIA(c) to the biophysical properties of the channels which may be formed by these toxins in PLBs. Our results show that the three CryIA toxins form ionic channels in PLBs at both alkaline and acidic pHs. At both pHs, channels are usually cation-selective. At acidic pH, the channels obtained for the three CryIA toxins have similar conductances and kinetics. At alkaline pH, the single channel conductances are in the following sequence: $G_{CryIA(a)} < G_{CryIA(b)} < G_{CryIA(c)}$. The three toxin channels possess substates at both acidic and alkaline pHs. Compared to CryIC channels, the CryIA channels display generally larger conductances and longer duration open states.

**M-Pos417**

*E. COLI* PORIN CHANNELS, FAST TRANSITIONS AND VOLTAGE DEPENDENCE

Edward J.A. Lea, Nicola D. Bishop and Jeremy H. Lakey, School of Biological Sciences, University of East Anglia, Norwich, NR4 7TJ UK and European Molecular Biology Laboratory, Meyerhofstrasse 1, Postfach 10.2209, D-6900 Heidelberg, Germany.

Mutant strains of *E. coli* which express OmpC and that grow on maltodextrins in the absence of LamB display channel sizes accountable for in terms of altered side chain bulk[2]. The typical voltage-dependence behaviour exhibited by porin channels is that they close in response to raised membrane p.d. and open again reversibly as p.d. is lowered. In this study, the voltage dependence of single trimer channel activity has been examined in planar bilayers formed by the method of Schindler[3]. Technical improvements have allowed data sampling intervals as small as 0.1 ms to be used. Open and closed time histograms have been constructed over a series of voltage steps up to 200 mV. Voltage dependent fast flicker occurs between the open and intermediate closed states. Results have been interpreted in terms of a model in which each of the three conducting states of a porin trimer unit passes from an open state to an inactivated state via an intermediate closed one.

1 Misra, R., Benson, S.A. (1988). J. Bacteriol 170, 3611-3617.
2 Lakey, J.H., Lea, E.J.A. & Pattus, F. (1991). FEBS Lett. 278, 31-34.
3 Schindler, H. (1980). FEBS Lett. 122, 77-79.

**M-Pos418**

## TWO DISTINCT SETS OF ION CHANNELS ARE FORMED BY NEUTRAL ALAMETHICIN F-50 POLYPEPTIDES

((Don-On Daniel Mak and Watt W. Webb)) Physics Department and School of Applied and Engineering Physics, Cornell University, Ithaca, NY 14853.

Voltage clamp recording of single-channel current of HPLC purified neutral alamethicin F-50 polypeptides in patch clamped pure lipid bilayers shows that alamethicin can form 2 distinct sets of conductance states regardless of the lipid and buffer used. The persistent channels that last for minutes have conductance states with higher conductance values than the corresponding states for the nonpersistent channels that appear more often but last a minute or less. The persistent channels show excess white conductance noise above the thermal and shot noise expected for the channel and associated spreading resistance. The excess noise increases with higher states. The nonpersistent channels show excess noise only in the 2nd and 3rd conductance states which have significantly shorter average dwell times and lower relative occupation probabilities than the other states. Simple models can account for the different kinetic characteristics and conductance values found in the 2 sets of channels by assuming that they have different packing arrangements for the alamethicin monomers in the channel assembly. The excess noise found in all persistent channel states is conjectured to be due to thermal fluctuation in the relative positions of the monomers in the channel. (ONR grant N00014-89-J-1656)

**M-Pos419**

## ALAMETHICIN CHANNEL CONDUCTANCE SUBSTATES

((Lorinda R. Opsahl and Watt W. Webb*)) Physics Dept. and School of Applied & Engineering Physics*, Cornell Univ., Ithaca, NY 14853

The channel forming peptide alamethicin has been studied extensively as a model ion channel system for over two decades, first for its voltage sensitive properties and more recently for its mechanical sensitivity. In spite of the relative simplicity of the 20 amino acid peptide there still exists considerable ambiguity concerning its switching mechanisms and inconsistency in experimental results. In order to clarify the structural changes involved in channel gating, we have analyzed the kinetics of switching between conductance levels in single channels formed by HPLC purified alamethicin. Dwell times for each conductance state are binned to create histograms which represent the conditional probability density functions of the conductance states. The dwell time histograms for events following upward transitions decay as a two exponential function while those corresponding to events following downward transitions decay as a power law at short times and exponentially at longer times. Plotting event amplitude as a function of dwell time reveals that the short time exponential behavior corresponds to brief transitions into substates with conductances that differ by 10-20 pS from the stable conductance states. The existence of two sets of conductance levels with kinetic rate constants which differ by several orders of magnitude offers a probable explanation for differences in observed channel behavior. This finding implies the existence of two weakly coupled sets of conductance states.

Financial support was provided by the ONR (N00014-895-1656), and facilities of the Developmental Resource for Biophysical Imaging Optoelectronics, NIH-(08-P1RR04-224A) and NSF-(DIR-8800278).

**M-Pos420**

## POTENT BLOCK OF $Cl^-$ CHANNELS BY THE ANTIALLERGIC DRUGS CROMOLYN AND RU 31156.

((M. E. Reinsprecht, I. Pecht*, H. Schindler, C. Romanin)) Institute for Biophysics, University of Linz, A-4040 Linz, Austria. * Department of Chemical Immunology, The Weizmann Institute of Science, Rehovot 76100, Israel.

We have recently reported (Romanin, C. et al., EMBO J. 10:3603-3608,1991) involvement of intermediate-conductance $Cl^-$ channels in the regulation of exocytosis from mucosal-type mast cells (line RBL-2H3) and blockade of these $Cl^-$ channels by the antiallergic drug disodium-1,3-bis(2'-carboxylate-chromone-5'-yloxy)-2-hydroxypropane (cromolyn). Based on the latter finding two questions have been addressed: (i) Is the action of cromolyn specific to intermediate-conductance $Cl^-$ channels of RBL-2H3 cells and (ii) do other antiallergic drugs also possess a $Cl^-$ channel blocking acticity? As an approach to the first question we compared the effects of cromolyn on intermediate-conductance $Cl^-$ channels of two unrelated cell types. For this, single $Cl^-$ channel activities in RBL-2H3 cells and alternatively, of colonic carcinoma cells ($HT_{29}$) were monitored employing the patch-clamp technique in the inside-out patch configuration. Intermediate-conductance $Cl^-$ channels were blocked by cromolyn ($IC_{50}$ ~ 15μM) in either cell type. $Cl^-$ channel inhibition occurred by a slow rather than a flickering block and with a Hill coefficient around 1. The second question was addressed by examining another antiallergic drug, 7-(S-methyl-sulphonimidoyl)-5-(n-hexyl)-xanthen-9-one-carboxylic acid (RU 31156). This compound was about one order of magnitude more potent ($IC_{50}$ ~ 1μM) than cromolyn. Chloride channel block occurred with a Hill coefficient about 1 and with similar characteristics as found for cromolyn. The $IC_{50}$ values for cromolyn and RU31156 were not significantly different ($p < 0.01$) in the two cell types. Our data provide evidence for a new class of $Cl^-$ channel blockers, which may be of further use in $Cl^-$ channel characterization as well as purification.

**M-Pos421**

## SINGLE HYPERPOLARIZATION-ACTIVATED CHLORIDE CHANNELS IN XENOPUS OOCYTES.

((S.J. Ackerman, G.C. Kowdley. J.E. John, L.R. Jones, J.R. Moorman)) University of Virginia, Charlottesville, VA 22908.

We have investigated the single channel characteristics of a hyperpolarization-activated $Cl^-$ conductance in Xenopus oocytes by recording unitary currents in cell-attached patches at 20° C. The bath solution was (mM): KCl 120, $MgCl_2$ 5, $KH_2PO_4$ 1, EGTA 5, glucose 5, HEPES 10 (pH 7.4). The pipette solution was NaCl 150, KCl 5.4, $MgCl_2$ 2, $CaCl_2$ 3, glucose 10, HEPES 10 (pH 7.5), and 50 μM $Gd^{+3}$ to block stretch-activated channels. No channel openings were detected at 0 mV, but nearly every patch had channel openings in 2 min recordings at potentials -50 to -140 mV. In this solution ($[Cl]_o$ 165 mM), the conductance was 13 pS and the extrapolated reversal potential was -58 mV (left). When $Cl^-$ was replaced by methanesulfonate to a final $[Cl]_o$ of 15 mM, the conductance was 32 pS and the extrapolated reversal potential was -13 mV. This identifies $Cl^-$ as the main charge carrier. Mean open times were less than 5 msec and were independent of voltage in this range. Interestingly, the morphology of many of the openings was reminiscent of "double-barrelled" $Cl^-$ channels from Electrophorus (right; currents filtered at 2 kHz and digitized at 5 kHz; bar is 10 msec and 1 pA).

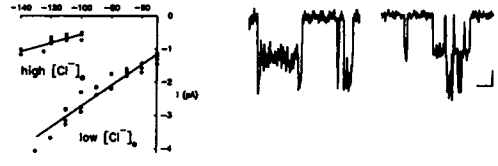


**M-Pos422**

## IS PHOSPHOLEMMAN AN ION CHANNEL, OR DOES IT MODULATE AN ENDOGENOUS HYPERPOLARIZATION-ACTIVATED CHLORIDE CURRENT IN XENOPUS OOCYTES?

((G.C. Kowdley, S.J. Ackerman, J.E. John, L.R. Jones, J.R. Moorman)) University of Virginia, Charlottesville, VA 22908

We have reported that expression of phospholemman (PLM), a 72 amino acid peptide which is the major substrate for protein kinases A and C in ventricular myocytes, induces a hyperpolarization-activated $Cl^-$ current ($I_{Cl(PLM)}$) in Xenopus oocytes (JBC 267:14551). We now find that some batches of uninjected oocytes also have hyperpolarization-activated $Cl^-$ currents. The figure shows current-voltage relations each involving 9 to 21 oocytes. $I_{CL(PLM)}$ was induced after injection of PLM RNA into batches of uninjected (1) oocytes. The uninjected (2) oocytes are from different frogs. The uninjected(2) endogenous currents unlike $I_{CL(PLM)}$ are unaffected by $pH_o$; however, like $I_{CL(PLM)}$, are blocked by $Ba^{+2}$ with $IC_{50}$ 0.18 mM, compared with 0.36 for $I_{CL(PLM)}$, and do not require $[Ca^{+2}]_o$. In fact, currents were 2 to 4 times larger in 0 mM $[Ca^{+2}]_o$ / 5 mM $[Mg^{+2}]_o$ than in 5 mM $[Ca^{+2}]_o$ / 0 mM $[Mg^{+2}]_o$. Further, in two of four batches injected with antisense oligonucleotides to PLM, the endogenous current was attenuated by 50-90%.

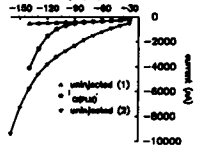


Though there are differences between $I_{CL(PLM)}$ and this endogenous $Cl^-$ current, these data raise the possibility that PLM may modulate an endogenous $Cl^-$ channel in Xenopus oocytes.

**M-Pos423**

## A PUTATIVE CHLORIDE CURRENT IN SYMPATHETIC NEURONS OF CELIAC GANGLION.

((C.A. Lazalde and D.L. Kreulen)) Dept. of Pharmacology, College of Medicine, University of Arizona, Tucson, AZ 85724.(Spon. I.K. Flink)

The celiac ganglion is involved in regulating gastrointestinal activities. Several ionic currents of these neurons have been identified; Na, K, Ca, among them. In this work we show results that suggest the existence of yet another current. Guinea pig neurons in primary culture, less than 80 hours old, were whole cell voltage clamped using low resistance pipettes, ($0.1 < R < 2$, MΩ ). All pipette solutions contained (mM): 11 EGTA, 2 $MgCl_2$ , 1 $CaCl_2$, 10 HEPES. In previous studies of Na currents (Purnyn et al., Abs. Soc. of Neuroscience 17: 955, 1991) a chloride-containing pipette solution was used. To improve recording conditions, we substituted $Cl^-$ with $F^-$ and found a slowly increasing outward current under conditions where $Na^+$ is the major charge carrier. Substitution of all internal Na and K by Cs, and no $K_{out}$, plus 30 mM TEA out, produced an outward-going rectifying current with a reversal potential around -50 mV. To rule out the possibility of having an outward current by way of Cs going out through Ca channels, we substituted Cs with N-methyl glucamine, a large cation, and the current was not affected. 2mM Cd + 2.5 μM nifedipine did not decrease the current (out: 0 Na + 0 Ca + 100 TEA + 10 Mg) which suggests little permeation of NMG or Mg, if any. Because the reversal potential for this current deviates from the expected equilibrium potential for $Cl^-$ (-85 mV), these experiments suggest the existence of a chloride channel that is not perfectly selective. Support: HL27781, DK36289.

**M-Pos424**

BLOCK OF OUTWARDLY RECTIFYING $Cl^-$ CHANNELS BY QUININE.

((Tzyh-Chang Hwang* & William B. Guggino†)) *Laboratory of Cardiac/Membrane Physiology, The Rockefeller University, New York, NY10021 †Department of Physiology, The Johns Hopkins University, School of Medicine. Baltimore, MD21205.

Effects of $K^+$ channel blockers, quinine and its stereoisomer quinidine, on the outwardly rectifying $Cl^-$ channel was studied in excised inside-out membrane patches from a fetal tracheal cell line. Application of quinine (5-50 μM) onto the cytoplasmic side of the channel caused rapid interruptions of the open channel current. This blocking effect was reversible since the channel opening returned to the control after removal of quinine. Quinidine had the same effect as quinine. The open time and close time histograms can be fitted with simple exponential, with the mean open time, $\tau o = 13.57 \pm 2.63$ ms and the mean close time, $\tau c = 0.18 \pm 0.03$ ms (n = 6). In the presence of quinine, the mean open time decreased and the mean close time did not change, for example at 20 μM quinine $\tau o = 0.69 \pm 0.05$ ms and $\tau c = 0.14 \pm 0.01$ ms (n = 6). The block rate ($1/\tau o$) increased linearly with the concentration of quinine, but the unblock rate ($1/\tau c$) did not change with the blocker concentration, suggesting a one-to-one interaction between the channel and the blocker. The calculated Kd was ~50 μM. At 20 μM quinine, the block rate did not change much with the membrane potentials, whereas the unblock rate increased with depolarization. At fixed membrane potential (+50 mV), 20 μM quinine caused more block in acidic solutions (pH = 5.3, $1/\tau o = 1.94 \pm 0.39$ $ms^{-1}$ n = 4) than in alkaline solutions (pH = 8.3, $1/\tau o = 1.13 \pm 0.32$ $ms^{-1}$ n = 4). Since the block rate increased as the pH went down (more acidic), it is proposed that the cationic form of the blocker is more potent in blocking the channel.

*Supported by the NIH and the CF Foundation.*

**M-Pos425**

PROTON BLOCK OF ACUTELY DISSOCIATED RAT CORTICAL NEURONAL FAST CHLORIDE CHANNELS.

((X. Q. Gu and A. L. Blatz)) Department of Physiology, UT Southwestern Medical Center, Dallas, TX 75235.

The effects of low intracellular pH on the conductance properties and gating kinetics of fast $Cl^-$ channels from acutely dissociated rat cortical neurons were studied. Patch-clamp experiments were performed using excised, inside-out membrane patches under the following conditions: (in the pipette (extracellular) (mM): 140 KCl, 5 TES, 1 EGTA, pH 7.0; in the bath (intracellular): 1000 KCl, 10 TES, 10 K biphthalate titrated to different pH values between pH 7.0 and pH 5.0). Slope conductance at pH 7.0 under these conditions is about 130 pS. Reduction of intracellular pH from 7.0 to 5.5 reduces single channel current amplitude of $Cl^-$ channel by about 10-30%. Lowering intracellular pH from 7.0 to 5.5 reversibly reduced the mean open time of the channel and sometimes increased the mean closed time, such that the overall effect was a decrease in the fraction of time that the channel was open (open probability). The kinetic effects of lowered intracellular pH on fast $Cl^-$ channels from rat cortex are similar to those from cultured rat skeletal muscle (Blatz & Magleby, 1985, Biophys. J. 47:119) and also to a $Ca^{2+}$-activated $K^+$ channel from rat skeletal muscle incorporated into planar bilayers (Laurido et al., 1991, J. Gen. Physiol. 98:1025). Supported by AHA, Texas Affiliate (91G-084) and NIH (GM-39731).

**M-Pos426**

Chloride channels with reduced conductance in recessive generalized myotonia

((Ch. Fahlke, E. Zachar. R. Rüdel)) Department of General Physiology, University of Ulm, D-7900 Germany

Recessive generalized myotonia (RGM) is a hereditary muscle disorder characterized by transient muscle stiffness. The electromyogram reveals repetitive firing of the muscle fibers in response to single stimuli. The increased excitability is related to a reduction of the macroscopic $Cl^-$ conductance of muscle fibers to about 50%. We have characterized the $Cl^-$ channels in myoballs from controls and 3 RGM patients using single-channel and whole-cell recordings. In controls, the major $Cl^-$ pathway is a channel showing a pronounced outward rectification, a $P_{Cl}/P_{Na}$ of 9.5, and an open-channel substructure with two equally spaced subconductance levels. The channel can exist in two gating modes that differ in the open probability in the negative potential domain (Fahlke et al, Pflügers Arch *421*:108-116, 1992). Following direct interaction with a G protein the gating mode having higher open probability is highly preferred (Fahlke et al, Pflügers Arch, in press). In RGM myoballs, a channel with similar gating properties, selectivity and response to G proteins, but reduced single-channel conductance was found. For $[Cl^-]_o/[Cl^-]_i$ = 150 mM/150 mM, the conductance in the negative potential domain was 10.5 ± 2 (21.6) pS (means ± S.D., n = 5 patches; controls in parantheses). For $[Cl^-]_o/[Cl^-]_i$ = 150 mM/45 mM, the value was 4.8 ± 1 (6.5) pS. This result may represent the fundamental pathophysiologic defect in RGM. Supported by DFG (Ru-138/17-3).

**M-Pos427**

A CALCIUM-ACTIVATED CHLORIDE CURRENT IN RABBIT CORONARY ARTERY MYOCYTES.

((F.S. Lamb, J.J. Matsuda, K.A. Volk, E.F. Shibata)) Dept. of Physiology and Biophysics, Dept. of Pediatrics, Division of Pediatric Cardiology, University of Iowa, Iowa City, Iowa 52242.

Whole cell patch-clamp techniques were used to study a $Ca^{++}$-activated current in enzymatically dispersed smooth muscle cells from rabbit coronary artery. Depolarizing pulses from -60mV (118 mM cesium, 22 mM TEA, no EGTA pipette solution) produced inward $Ca^{++}$ currents (2.5 mM bath $Ca^{++}$) which were followed by an outward current having slow kinetics (steady-state current at approx. 500 msec). Return to -60 mV elicited inward tail currents having similar slow kinetics. The IV relationship for the tail currents closely paralleled that for the inward $Ca^{++}$ currents. Tail currents reversed at 0 mV in balanced chloride solutions and reversal potential was shifted negatively as intracellular chloride was reduced. Reduction of $[Cl]_i$ also produce larger outward currents at depolarizing pulse potentials. Barium substitution (10 mM) for calcium produced persistent inward currents but no outward currents or tail currents were seen. Tail currents but not calcium currents were blocked by 4,4'-diisothiocyanatostilbene-2,2'-disulfonic acid (DIDS) at 0.1 mM. When intracellular calcium was buffered to fixed levels (330-500 nM), outward currents were elicited only at very positive potentials. We conclude that the rabbit coronary artery contains calcium-activated chloride channels which are weakly voltage-dependent. Supported by NIH HL41031 and NIH T32 HL07413, EI of AHA to EFS.

**M-Pos428**

HYDROGEN ION CURRENTS IN HUMAN NEUTROPHILS

((T. E. DeCoursey)) Dept. of Physiology, Rush Med. Center, Chicago, IL 60612.

A $H^+$ selective conductance, $g_H$, was studied in human neutrophils with whole-cell patch-clamp techniques. Neutrophils were isolated from normal human blood by density gradient centrifugation. Pipette and bath contained TEA methanesulfonate with 20 mM buffer. This $g_H$ resembles a $g_H$ in human neutrophils activated during superoxide ($O_2^{\cdot-}$) generation proposed on the basis of intracellular *pH*, $pH_i$, and membrane potential measurements (Henderson *et al., Biochem. J.* 246:325-329, 1987; 251:563-567, 1988). The $g_H$ is low at negative potentials and activates slowly on depolarization. The maximum whole-cell $H^+$ current with $pH_i$ 6.0 was 21 ± 15 pA/pF (mean ± SD). If mediated by a channel, the unitary conductance estimated by current variance is < 10 fS. The reversal potential of tail currents corresponds with the Nernst potential for $H^+$, after considering $H^+$ depletion during prepulses. The $g_H$ does not inactivate during depolarizations up to 3 minutes. Droop occurs only during large $H^+$ currents, not in cells with a small $g_H$. The $g_H$ is inhibited by 10-100 μM $Cd^{2+}$ or $Zn^{2+}$, concentrations which enhance activation-induced depolarization (*above references*), supporting the idea that the $g_H$, by permitting prolonged $H^+$ efflux, limits depolarization and cytoplasmic acidification. $H^+$ generated during neutrophil activation would be fully dissipated by 16 pA $H^+$ current per cell, within the range observed. In summary, the voltage-gated $g_H$ of human neutrophils appears to be identical with that activated during $O_2^{\cdot-}$ (and $H^+$) production. *Supported by a Grant-in-Aid from the American Heart Association with funds contributed by the A.H.A. of Metropolitan Chicago.*

**M-Pos429**

VOLTAGE AND pH-DEPENDENT $H^+$(EQUIVALENT) CURRENTS IN MACROPHAGES

(( A. Kapus, R.J. Romanek, O.D. Rotstein and S. Grinstein)) The Hospital for Sick Children, Toronto, Ont. Canada, M5G 1X8 (Spon. by S. Grinstein)

The activation of phagocytes is accompanied by a massive burst of $H^+$ generation. The existence of a $H^+$ conductance, which may play a role in maintaining physiological intracellular pH (pHi) was recently suggested. The aim of the present study was to characterize this putative $H^+$ channel in mouse peritoneal macrophages (MPM) using the whole cell patch-clamp technique, while monitoring pHi fluorimetrically in single cells. Upon depolarization of MPM a slowly activating outward current was observed. This current is carried by $H^+$ (equivalents) since: a) it is accompanied by cytoplasmic alkalinization; b) it is essentially insensitive to changes in the concentration of ionic constituents other than $H^+$ and c) the reversal potential is in good agreement with the predicted $H^+$ equilibrium potential. Activation of the conductance is dependent on membrane potential, pHi and external pH (pHo). A decrease in pHi causes an increase in the chord conductance and shortens the half time for activation ($T_{1/2}$) when voltage and pHo are held constant. The threshold voltage for activation is more negative at lower pHi. Conversely, at constant pHi, lowering pHo reduces the conductance, lengthens $T_{1/2}$ and increases the activation threshold. These observations are consistent with the existence of both internal (activating) and extracellular (inhibitory) $H^+$ binding sites. At pHi=6.0 and pHo=8.1 the conductance saturates at ~0.24 nS/pF. Regardless of the intra- and extracellular pH or the applied voltage, the conductance can be activated only when the net $H^+$ electrochemical gradient is outward. On the other hand, once activated the putative $H^+$ channel does not display rectification. The $H^+$ conductance is reversibly inhibited by submillimolar concentrations of $Zn^{2+}$, which shifts the voltage-dependence to more positive values and lengthens $T_{1/2}$. Together, these findings demonstrate the existence of a voltage-gated $H^+$ selective conductance, which could play a role in pHi regulation when MPM depolarize during stimulation.

**M-Pos430**

THE MAGNITUDE AND KINETICS OF VOLTAGE-DEPENDENT $Na^+$ AND $K^+$ PROTEIN CHANNEL CURRENTS ON SKELETAL MUSCLE MEMBRANE AFFECTED BY EXPOSURE TO A HIGH-INTENSITY ELECTRIC FIELD

((W.Chen and R.C.Lee)) Department of Plastic and Reconstructive Surgery, The University of Chicago, Chicago, IL 60637

The magnitudes and the kinetics of voltage-dependent $Na^+$ and $K^+$ protein channel currents on cell membranes of frog skeletal muscle is reduced and then self-restored to the original value by exposure to a high-intensity electric field.

A cut twitch fiber from the frog semitendinosus muscle was voltage-clamped at resting potential in a double-vaseline gap chamber. High-intensity 4 ms-duration pulses of 300 to 900 mV are imposed on the cell membranes provide by the voltage clamp. Transmembrane current was simultaneously monitored during the high-pulse shock, and also measured responded to a 40 mV/20 ms stimulation pulse before and after the shock. There is no apparent reduction in channel currents responding to a shock pulse lower than 400 mV where electroporation has obviously occured. Relatively, large shock pulses were needed to reduce the transient inward and outward protein channel current when compared with the formation of electropores on the phospholipids of cells membrane. The magnitude of transient inward current is reduced to about 60% and the time delay of activation of Na channel has been shorten to less than 50% after exposure to a shock pulse of 800 mV. Then both the kinetics and the magnitude of channel current was restored to the original with a time course of minutes.

The effect of large shock pulses was pulse amplitude dependent. Pulses is 400-500 mV range to induce electropores and large leakage currents. Stronger pulses (~700 mV) were requared to transiently denature ion channel proteins. The change of the dynamics of channel current may result from a shift in the activation threshold of protein channels.

**M-Pos431**

PATHOGENESIS OF FREE RADICAL-INDUCED Ca UPTAKE IN CARDIOMYOCYTES

((Jonathan R. Clague and Glenn A. Langer)) Cardiovascular Research Labs., UCLA School of Medicine, MRL-3645, Los Angeles, CA 90024.
Supported by USPHS grant, the Laubisch and Castera Endowments.

Ca uptake is important in the pathogenesis of ischemia-reperfusion injury. The mechanism is unknown but Na-Ca exchange is a current favorite. We have used a unique, on-line isotopic technique to measure Ca fluxes in cultured neonatal rat cardiomyocytes exposed to 50 μM $H_2O_2$ as a free radical-generating system.

Intracellular high energy phosphate levels were measured by HPLC and were found to be unaffected by the presence of $H_2O_2$ at this concentration. The production of malondialdehyde was used as evidence of lipid peroxidation and was found to be significant after 15 min of $H_2O_2$ exposure. Ca uptake began after 22 min, reaching a maximum of 11.7 nmoles/kg dry cellular weight after 60 min. The uptake was abolished by catalase. I μM nifedipine had no effect but 50 μM augmented the uptake. Na-Ca exchange inhibition with 20 μM 3,4-dichlorobenzamil and 0.5 mM Cd also had no effect. The uptake was inhibited by the cationic amphiphiles polymyxin B and dodecyltrimethyl ammonium bromide and was augmented by the anionic amphiphile sodium dodecyl sulfate. The uptake occurred before the cells had become leaky with respect to large molecules (as indicated by LDH release) and sarcolemmal (SL) phospholipid rearrangements had occurred. At this concentration of $H_2O_2$, the cells did not become leaky with respect to K, as evidenced by the $^{42}K$ washout pattern.

Thus, in this model, Ca uptake did not occur through L-type channels or Na-Ca exchange. Major SL defects were not responsible and small, non-specific cation-permeable defects were also not responsible. The uptake was affected by alterations in SL surface charge. The $H_2O_2$ was acting via its free radical-generating capacity, as indicated by the inhibitory effect of catalase. Lipid peroxidation was an early event, although its significance is unclear.

We conclude, by a process of elimination, that in this model, the uptake occurs through defects *specific* for Ca and that the uptake shares properties in common with Ca leak channels. There are clearly fundamental differences between this model and the in-vivo situation, but we propose that Ca uptake in ischemia-reperfusion occurs through specific Ca leak channels which open in response to free radical exposure and can be modulated by alterations in surface charge. This approach may permit the development of novel cardioprotective agents.

**M-Pos432**

**EFFECTS OF ETOMIDATE AND MIDAZOLAM ON CALCIUM CURRENT IN ISOLATED VENTRICULAR CELLS.** (N. Buljubasic, V. Berczi, D.F. Supan, J P. Kampine and Z.J. Bosnjak) Departments of Anesthesiology and Physiology , Medical College of Wisconsin, Milwaukee, WI 53226 (Spon. by Z. Bosnjak)

Intravenous anesthetics are often used during diagnostic and surgical cardiac procedures. These agents are known to have negative inotropic effect, hence they may play important role in patients with compromised cardiac function. Alteration of transmembrane ionic fluxes by intravenous anesthetics may underlie the myocardial depression by these agents. The purpose of our study was to investigate and compare the effects of etomidate and midazolam on L-type $Ca^{2+}$ current ($I_{Ca}$) in single canine ventricular cells using whole-cell patch-clamp method.

Single myocytes were isolated from the canine ventricle with collagenase. A drop of dispersed cells was placed in the microscopic chamber and superfused with 10 mM $BaCl_2$ at 22°C. Intrapipette solution contained 130 mM $CsCl_2$. $I_{Ca}$ was elicited by stepwise depolarizing pulses from a holding potential of -40 mV to +40 mV. After stable controls, cells were exposed to equimolar concentrations of etomidate and midazolam (5 and 60 μM). These concentrations of etomidate and midazolam decreased the $I_{Ca}$ by 4 ± 2% and 17 ± 4%, and 5 ± 2% and 50 ± 7%, respectively (n = 5 cells in each group). While both etomidate and midazolam (60 μM) significantly depressed inward $I_{Ca}$, midazolam was significantly more potent than etomidate at the higher equimolar concentration used (60 μM). The direct depressant effects of intravenous anesthetics on the cardiac transsarcolemmal L-type $I_{Ca}$ may be, at least in part, responsible for the negative inotropic response produced by these agents.

**M-Pos433**

ALTERATIONS OF ELECTRICAL AND BIOCHEMICAL PARAMETERS OF ISCHEMIC AND REPERFUSED RAT SKELETAL MUSCLE FIBERS.

((D.Tricarico and D. Conte Camerino))Unit of Pharmacology, Dept.of Pharmacobiology, Faculty of Pharmacy, University of Bari, Italy.

Severe muscle ischemia was produced in adult rats by multiple ligations of the right common iliac artery, femoral artery and its branches feeding the Extensor Digitorum Longus (EDL) muscle. In a group of animals the effects of pure ischemia were studied after 4h of irreversible artery occlusion; in another group, the effects of reperfusion were evaluated after declamping the temporary ligatures for 30'-120'. After these surgical procedures the EDL muscles of treated and contralateral limbs were dissected and studied "in vitro" at 30°C for their passive and active electrical parameters by computerized two intracellular microelectrodes technique (Bryant and Conte Camerino, Pflughers Arch 417:605-610, 1991). In some other muscles the ATP levels were detected. The pure ischemia led to a 39% reduction of chloride conductance (GCl), whereas the reperfusion increased it of 18% as compared to contralateral controls. On the other hand either ischemia or reperfusion increased potassium conductance (GK) respectively of 21% and 64%; this increase was reversed by 50μM of glybenclamide. A significative hyperpolarization was observed after ischemia, whereas in contrast, after the reflow period, the fibers were depolarized. Moreover the ischemia led to a slight hyperexcitability of the fibers, decreasing the threshold current (TH) needed to elicit an action potential (AP) and increasing the latency and amplitude of AP. In contrast, the reperfusion caused an increase of TH without altering the other AP parameters. In addition, the levels of ATP in ischemic and reperfused muscles were respectively 18% and 64% lower than the contralateral controls. Our results suggest an involvement of ATP $K^+$ channels that explain the glybenclamide sensitive GK increases observed in ischemic or reperfused muscles. It has been shown that skeletal muscle $Cl^-$ channels undergo an inhibitory control by protein kinase C (PKC) (Tricarico et al., Pflugers Arch 418:500-503, 1991). During ischemia an increase of PKC activity occurs in heart (Meszaros et al., Am J Physiol 258:H931-H938, 1990); if this happen also in skeletal muscle, this could account for the observed reduction of GCl. On the other hand, the increase of GCl recorded after reperfusion could be justified by an unspecific alteration of membrane permeability due to free radical overactivity. (Italian M.U.R.S.T. 91-92).

**M-Pos434**

MEMBRANE IONIC CONDUCTANCES AND EXCITABILITY CHARACTERISTICS OF EXTENSOR DIGITORUM LONGUS MUSCLE FIBER FROM MDX MICE.

((A. DE LUCA, S. PIERNO, F. GIORDANO and D. CONTE CAMERINO)) Dept. of Farmacobiology, Faculty of Pharmacy, University of Bari, ITALY.

Lack of dystrophin and associated glycoprotein complex in muscle sarcolemma may cause ion channel malfunction which in turn could contribute to the degenerative condition occurring in dystrophin related myopathies (Ibraghimov-Beskrovnaya et al. Nature, 355: 696, 1992; Matsumura et al. Nature, 359: 320, 1992). We measured "in vitro" resting membrane conductances to chloride ($G_{Cl}$) and potassium ($G_K$) ions and excitability characteristics of extensor digitorum longus (EDL) muscles from mdx and control mice aged 6-12 weeks, by means of standard microelectrode technique. At 6 weeks of age no significant differences in either $G_{Cl}$, $G_K$ or excitability characteristics between mdx and control EDL muscles were observed. At 8 weeks $G_{Cl}$ was significantly higher in EDL fibers from mdx (3003±241μS/cm²; n=20) than from control mice (2257±164μS/cm²; n=24) whereas $G_K$ was unchanged. Accordingly, in mdx muscle the threshold current ($I_1$) and the current to elicit two action potentials ($I_2$) were significantly increased, the latency of action potential shortened and the firing capability reduced with respect to the controls. Similar changes, although attenuated, were recorded at 10 and 12 weeks of age. Drugs highly specific for muscle chloride channels (De Luca et al. J.Pharmacol.Exp.Ther., 260: 364, 1992) were less potent in modulating membrane $G_{Cl}$ in mdx than in control EDL muscles. The present results suggest that in muscles from mdx mice $G_{Cl}$ and, consequently, membrane excitability change transiently after regenerative process. Such changes may be caused by compensatory mechanisms related to regeneration of mdx phenotype other than to a direct consequence of the lack of dystrophin. Experiments at earlier and later stages of development will help to better elucidate this hypothesis.(Supported by Telethon-Italy, 1991).

**M-Pos435**

**ROLE OF NONSELECTIVE CATION CURRENT IN COLONIC MYOCYTES ACTIVATED BY ACETYLCHOLINE**

((H.K. LEE and K.M. Sanders)) Dept. of Physiology, University of Nevada, Reno, NV 89557, USA. (spon. by S. M. Ward)

The ionic mechanisms of the membrane depolarization induced by ACh was investigated in isolated colonic myocytes using the whole cell voltage clamp technique. With $K^+$ currents blocked by internal replacement with $Cs^+$, ACh ($10^{-4}$ M) slightly reduced voltage-dependent $Ca^{2+}$ current and induced a slowly-developing current. The I-V relationship of this ACh-induced current showed voltage-dependency between -80 and 0 mV and reversed between -10 and 0 mV. At a Hp of -70 mV, ACh induced an inward current which reached an initial peak averaging 33 ± 4.7 pA, and then decayed to a sustained level averaging 9.5 ± 1.7 pA (mean ± SEM, n= 12 cells). The current was not due to the movement of $Cl^-$, because $Cl^-$ equilibrium potential was set at -70 mV. Reduction of external $Na^+$ to 35 mM greatly reduced this current, suggesting that the ACh-induced current was carried predominantly by $Na^+$. The ACh-induced current was potentiated when the membrane was depolarized to 0 mV for 1.5 s prior to the addition of ACh. In the presence of nifedipine ($10^{-6}$ M), a similar depolarization step failed to augment the ACh-induced current, suggesting that $Ca^{2+}$ entry through voltage-dependent $Ca^{2+}$ channels may "facilitate" this current. The ACh-induced inward current was blocked by atropine ($10^{-6}$ M), quinine ($5x10^{-4}$ M), $Ni^{2+}$ ($10^{-4}$ M), and $Cd^{2+}$ (8 x $10^{-5}$ M). These results suggest that ACh activates a non-selective cation current in colonic myocytes and this conductance could be responsible for the depolarization of resting membrane potential in intact muscles. (Supported by DK 41315)

**M-Pos436**

## THE DYNAMICS OF THE AB NEURON

((John Guckenheimer [1], Shay Gueron [2], Ronald M. Harris-Warrick [3]))
[1] Mathematics Department and Center for Applied Mathematics
[2] Center for Applied Mathematics
[3] Section of Neurobiology and Behavioral Biology
Cornell University, Ithaca NY 14853

**Abstract**

The Anterior Burster (AB) neuron of the lobster stomatogastric ganglion displays varied behavior when subjected to application of neuromodulators and toxins. We introduce a new, channel based model for this neuron and investigate the response of this model to changes of its parameters. An efficient computational environment aids in the determination of the bifurcations in the model, separating regions of the parameter space with different types of behavior. The model predictions compare well with a limited set of experimental data.

Different two dimensional slices of the parameter space are mapped. They correspond to the application of specific-channel blockers to an experimental preparation. These mapped regions are used to predict the effects of Dopamine on the AB cell ion channels, and to suggest some experiments to support these conjectures.

**M-Pos437**

## TUMOR NECROSIS FACTOR α ACTIVATES NADPH OXIDOREDUCTASE AND WHOLE-CELL CATIONIC CURRENTS IN HUMAN NEUTROPHILS.

((M. A. Schumann, C. C. Leung, J. Lee, and T. A. Raffin)) Division of Pulmonary and Critical Care Medicine, Stanford University School of Medicine, Stanford, CA 94305.

The mechanism underlying the stimulatory effect of tumor necrosis factor α (TNFα) on respiratory burst activity in polymorphonuclear neutrophil leukocytes is unknown. By determining the enzymatic activity of NADPH oxidoreductase and by means of the whole-cell patch clamp methodology, we studied the effect of recombinant human TNFα (rhTNFα) on superoxide anion production and whole-cell cationic currents in human neutrophils, respectively. Human neutrophils freshly isolated from blood, settled on a plastic surface, and incubated with rhTNFα (500 U/ml) for 30 min exhibited an enhancement in superoxide anion production (activity increased from 163.3±16 to 386.3±23.5 pmoles/min/$10^6$ cells, $n=8$). Increasing extracellular $K^+$ concentration in the assay mixture to 15 mM to induce membrane depolarization resulted in about 50% increase in the activity of NADPH oxidoreductase. The rhTNFα-induced enzymatic activity was blocked by 100 μM 8-(4-chlorophenylthio)-adenosine 3', 5'-cyclic monophosphate (CPT-cAMP), a membrane-permeable cAMP analog added 10 min prior to the application of rhTNFα. Bath application of rhTNFα (500 U/ml) for 1-5 min activated the baseline whole-cell cationic current in 70% of tested cells. Current amplitude increased from 45.5±3.0 to 134.9±12.0 pA, $n=9$); the activation rate of the current also was augmented. The activated current was similarly blocked by 100 μM CPT-cAMP. These results suggest that the depolarization produced by rhTNFα-induced outward cationic currents at least in part plays a role in the mechanism involving the activation of NADPH oxidoreductase in human neutrophils.

**M-Pos438**

## A NOVEL CATION CHANNEL INVOLVED IN NEURITE EXTENSION

((J White, C Lagenaur, Y Yen, G Salama*)) Departments of Neurobiology, Anatomy, and Cell Science; and Physiology; School of Medicine, University of Pittsburgh, Pittsburgh, PA 15261

A 35kD protein called M6 has been identified on the plasma membranes of CNS neurons. In primary cerebellar culture, the M6 is concentrated in nerve growth cones as well as neurite processes. A monoclonal antibody (mAb) against the M6 inhibits neurite extension but does not alter the movement of growth cones. The mAb also identifies an M6-like protein exclusively located on the apical surface of both proximal renal tubule and choroid plexus cells. The function of this M6 protein is unknown.

Immuno-affinity purified M6 was incorporated into planar lipid bilayers to test for its activity as an ion channel. With a single cation present in the medium, reconstituted M6 exhibited single-channel fluctuations revealing the presence of cation-selective ionic pores permeable to $Na^+$, $K^+$, $Cs^+$, and $Ca^{2+}$; chloride currents were never observed. In asymmetrical $K^+$-gluconate solutions with $E_r$=90mV, the M6 displayed voltage-rectification with a greater conductance (and activity) at negative $V_m$. The conductance at -40mV was approximately 35 pS, and 2.5 mM $Ba^{2+}$ inhibited or blocked single-channel fluctuations if applied to the *trans*-side when M6 was added on the *cis*-side. A $K^+$-conductance with similar characteristics has been identified on the apical surface of proximal renal tubules. Partial protein sequencing of M6 indicates that this is a novel cationic channel.

**M-Pos439**

## INOSITOL 1,3,4-TRISPHOSPHATE ACTIVATES A CALCIUM-PERMEABLE INWARD CURRENT IN HUMAN MONOCYTE DERIVED MACROPHAGES.

A. Malayev and D.J. Nelson, University of Chicago, Dept. of Neurology. Chicago, IL 60637

Receptor activation of phosphoinositidase C in phagocytic cells results in a rise in internal calcium ($Ca_i$) appears to be due to both discharge from internal stores and influx across the plasma membrane. The initial phase of calcium release is mediated via inositol 1,4,5-trisphospate ($InsP_3$), its role in mediating calcium entry has yet to be determined in phagocytic cells. We have combined whole-cell voltage clamp techniques with fura-2 microfluorimetry in order to characterize the role of $InsP_3$ in the induction of a calcium-permeable entry pathway. Inward current activation was determined in $K^+$-free pipette and bath solutions. The entry of $InsP_3$ into the voltage clamped cells via the patch pipette was monitored as an increase in the fura-2 fluorescence. The magnitude of the inward current at -160 mV increased by 50% in the presence of internal $InsP_3$ (100 μM). Current activation in the presence of $InsP_3$ in response to repeated step hyperolarizations to -100 mV correlated well with step increases in $Ca_i$ indicating the presence of an $InsP_3$-dependent $Ca^{2+}$ entry pathway. The selectivity of the current was determined in experiments in which external calcium was increased from 1 to 10 mM. Elevation in $Ca_o$ was associated with a depolarizing shift in current reversal potential of 15-20 mV. Removal of external $Ca^{2+}$ resulted in an increase in current magnitude an a shift in reversal potential whic suggested that the current may become permeant to monovalents in the absence of external calcium. An inward current with similar selectivity was observed in the presence of elevated intracellular EGTA in the absence of $InsP_3$, suggesting that current activation could be related the depletion of internal calcium stores. Supported by NIH Grants RO1 GM36823 and PO1 NS24575 (DJN).

**M-Pos440**

## DIVALENT CATION SELECTIVITY OF THE CHANNEL INDUCED BY TWO PROTEINS FROM THE LARVAL HEMOLYMPH OF THE POTATO BEETLE, *LEPTINOTARSA DECEMLINEATA* (SAY).

((A. Bortels, M. Amelinckx, A. De Loof and E. Carmeliet)) Zool. Inst. and Lab. Physiology, University Leuven, 3000 Leuven, Belgium.

Two proteins (67 kDa), isolated from the larval hemolymph of the potato beetle, have been shown to induce a cation selective channel with a single-channel conductance of 400 pS (in isotonic 100 mM KCl solutions), a $P_K/P_{Cl}$ of 12 and the following monovalent cation selectivity sequence: $NH_4^+ > K^+ \approx Rb^+ \approx Cs^+ > Na^+ > Li^+ > Tris^+ >$ choline$^+$ (Bortels A. et al., Biophys. J.61:A114, 1992). In this study the divalent cation selectivity of the channel was investigated using the patch-clamp technique on artificial bilayers. Pipette and bath solutions contained (in mM) 100 KCl, 1 $CaCl_2$, 5 Hepes, pH 7.5 with Tris. Addition of divalent cations, such as $Ca^{2+}$ and $Mg^{2+}$, to the bath solution shifted the reversal potential to positive values indicating permeation of divalent cations, but reduced the channel conductance. Replacing 100 mM bath $K^+$ by 70 mM of a divalent cation gave following selectivity sequence: $Ba^{2+} > Sr^{2+} > Ca^{2+} > Mg^{2+} > Mn^{2+}$. 70 mM $Co^{2+}$, $Cd^{2+}$ and $Ni^{2+}$ blocked the channel. Addition of $Ni^{2+}$ to the $K^+$ bath solution induced a voltage-dependent block with a $K_d$ of 1 mM at -20 mV. While the channel is permeable for $Ca^{2+}$, this ion reduces the permeability for monovalent cations. Therefore, this channel does not obey the independence principle. Supported by IWONL grants (A.B., M.A.).

**M-Pos441**

## ION CHANNELS THAT ARE PERMEABLE TO $K^+$ AND $Ca^{2+}$.

((Yoshio Oosawa)) International Institute for Advanced Research, Matsushita Electric Industrial Co., Ltd., 15 Morimoto-cho, Shimogamo, Sakyo-ku, Kyoto 606 JAPAN.

The cation channel from *Tetrahymena* cilia was permeable to $K^+$ and $Ca^{2+}$. The single channel conductance in mixed solutions of $K^+$ and $Ca^{2+}$ was determined by the Donnan ratio of $K^+$ and $Ca^{2+}$. For explaining this fact, the binding sites of the channel were considered to be always occupied by two potassium ions or by one calcium ion under the experimental conditions: 5-90 mM $K^+$ and 0.5-35 mM $Ca^{2+}$. The values of Michaelis-Menten constants and maximum currents carried by $K^+$ and $Ca^{2+}$ were calculated using a two-barrier model. Single channel current amplitudes and reversal potentials were calculated from these values. The calculated reversal potentials were compared with the resting potentials of *Tetrahymena* measured in various concentrations of extracellular $K^+$ and $Ca^{2+}$.

**M-Pos442**

BLOCK OF CFTR BY DIPHENYLAMINE-2-CARBOXYLATE (DPC) AND FLUFENAMIC ACID (FFA). ((S.McDonough, N.A.McCarty, J.Riordan', N.Davidson, H.A.Lester)) Caltech, Pasadena CA 91125, 'Hosp. for Sick Children, Toronto, CAN

We have characterized the block of CFTR expressed in *Xenopus* oocytes by two V-dep. blockers, DPC and FFA, which differ only by a $CF_3$ group. DPC blocked whole-cell current reversibly over ~7 min at neg. Vm, indicating a binding site ~40% through the electrical distance of the channel as measured from the cytoplasmic side. FFA blocked CFTR more quickly, implying primarily external block, but, surprisingly, with a similar V-dep. Neither blocked at +Vm. Single-channel recording from cell-attached patches confirmed that bath-applied DPC and FFA permeate through the oocyte membrane to block from the cytoplasmic side. Blockers (50 μM) were applied to the external face and to the cytoplasmic surface of inside-out patches excised into 1 mM Mg-ATP and symmetric 150 mM Cl⁻. Unblocked CFTR showed long openings at Vm=+100 mV and flickery openings at Vm=-100 mV; the closed time constant within a burst ($\tau_c$) at -100 was 0.28 ±0.025 ms and $P_o$ within a burst was 0.95 (n=4). Both DPC and FFA gave increased flickery block from either surface of the patch at Vm=-100 and had no effect at Vm=+100, confirming whole-cell data. The kinetics, however, differed greatly; FFA blocked much more strongly than DPC with slightly greater external than internal affinity, while DPC showed greater internal affinity. For external DPC, $\tau_c$=0.46 ±0.10 ms, and $P_o$ decreased to 0.80 (n=3); for cytoplasmic DPC, $\tau_c$=0.62 ±0.15 ms and $P_o$=0.69 (n=4). External FFA block gave two clear closed time constants: $\tau_{c1}$=0.37 ±0.13 ms, $\tau_{c2}$=1.41 ±0.20 ms, with $P_o$=0.70 (n=3). For cytoplasmic FFA, $\tau_{c1}$=0.28 ±0.06 ms, $\tau_{c2}$=1.11 ±0.11 ms, and $P_o$=0.75 (n=4). FFA may be a useful probe for CFTR, since it blocks with high affinity upon external application. Such structurally similar yet kinetically different open-channel blockers combined with site-directed mutagenesis should yield sensitive tools for defining which amino acids line the CFTR permeation pathway. (Support: CFF & GM-29836)

## NEUROEXCITABILITY AND NERVE CELLS

**M-Pos443**

VAGAL STIMULATION CAN PREVENT SEIZURES IN RATS: OPTIMIZING STIMULUS PARAMETERS FOR USE IN HUMAN STUDIES. ((J.W. Woodbury and the late D.M. Woodbury)) Dept. Physiology, Univ. of Utah, Salt Lake City, UT 84108

Clinical trials show that repetitive stimulation of the vagus nerve (VS) reduces seizure frequency and/or intensity in a large fraction of epileptic patients who are refractory to anti-convulsant drugs. This concurrent study on rats shows: (1) The anti-convulsant (AC) effect of VS is mediated solely by small unmyelinated (C) fibers; B fiber stimulation has no AC effect. The size of the effect is directly related to the fraction of C fibers stimulated. (2) Maximal stimulation of C fibers at frequencies greater than 4 Hz shortens or abolishes chemically induced seizures. (3) Maximal AC effect is reached at 20-30 Hz. (4) Stimulus durations of 0.5-1 ms minimize stimulus energy. (5) Maximal C stimulation at 20 Hz abolishes the extensor component of maximal electro-shock seizures, an effect identical to that of the efficacious AC drug phenytoin. Data in the literature indicate that VS acts by initiating widespread release of GABA and glycine in the CNS. Supported in part by a grant from Cyberonics, Inc., Webster, TX

**M-Pos444**

AFFERENT NEURAL OUTPUT OF THE AMPULLARY ELECTRORECEPTOR. I. A RELAXATION OSCILLATOR CIRCUIT MODEL OF THE SPIKE INITIATION ZONE. L. J. Bruner and J. R. Harvey. Dept of Physics, University of California, Riverside, CA 92521.

Passive detection by marine elasmobranch fish of environmental electric fields as weak as 5 nV/cm has been demonstrated in behavioral studies[1]. Steps involved in electroreception are; neurotransmitter release by stimulated receptor cells/ electrotonic spread of EPSP's converging upon a spike ininiation zone (SIZ)/ stimulus-modulated temporal spacing of SIZ output to axon/ neural spike train is transmitted on afferent nerve to CNS. Our circuit model (Fig. 1), utilizing a tunnel diode (TD), is equivalent to an asymmetric multivibrator and outputs a waveform with the neurophysiological interpretation shown in Fig. 2. Stimulus current, $I_s$, simulating dendritic input to the SIZ, modulates oscillator spike frequency, yielding stimulus-response characteristics which can match those reported in the literature for elasmobranch fish.

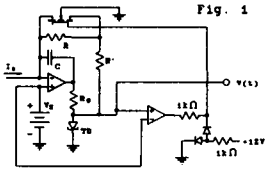


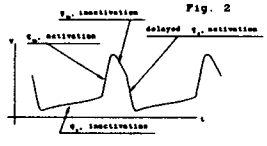


This work is supported by the Office of Naval Research.

1. Kalmijn, A. J. 1982. Science, 218: 916-918.
2. Murray, R. W. 1965. J. Physiol. (Lond.), 180: 592-606.

**M-Pos445**

AFFERENT NEURAL OUTPUT OF THE AMPULLARY ELECTRORECEPTOR. II. SPIKE GENERATOR STABILITY AND THE ELECTRIC FIELD DETECTION THRESHOLD. J. R. Harvey and L. J. Bruner. Dept of Physics, University of California, Riverside, CA 92521.

The low threshold for electroreception noted in Abst. I prompts the question- What minimum stimulus current can be detected by our spike generator model? Detection requires that a resolvable shift in mean oscillator period be produced by this minimum current. The minimum resolvable current will be that which produces a shift of mean period by at least one standard deviation. The mean and standard deviation will be that of a sample of successive interspike intervals acquired in a time which is a) short compared with the time required for adaptation of the tonic electroreceptor (~5s) and b) short enough to be of survival value to the animal. Our chosen sampling time is that required to acquire 20 periods (~0.5s). If a discriminable stimulus (or change of stimulus) must also meet the Weber-Fechner criterion, then a standard deviation / mean period ratio in the range 0.01-0.1 should be seen. Data taken with the spike generator circuit model of Abst. I (Fig. 1) show that stimulus current shifts as small as ~0.1pA can be resolved under the stated conditions. We conclude that spike generator stability does not limit the sensitivity of electroreception.

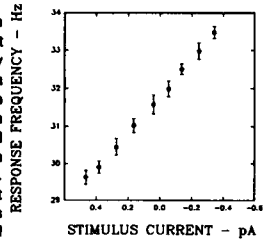


Fig. 1. Mean spike generator frequency is plotted vs. input stimulus current. Error bar height equals two standard deviations, as measured for each sample of 20 consecutive periods.

This work is supported by the Office of Naval Research.

**M-Pos446**

EFFECTS OF CYTOPLASMIC $Ca^{2+}$ AND $Mg^{2+}$ ON THE cAMP-ACTIVATED CONDUCTANCE IN OLFACTORY CILIA. ((Steven J. Kleene)) University of Cincinnati College of Medicine, Cincinnati, OH 45267-0521.

Olfactory receptor neurons depolarize in response to odorants. This depolarization is mediated by an increase in intracellular cAMP, which directly gates channels in the membranes of the neuronal cilia. Previous evidence suggests that a $Ca^{2+}$ influx during the odorant response may ultimately play a role in terminating the response. One way $Ca^{2+}$ inside the cell could terminate the odorant response would be to directly inhibit the cAMP-gated channels. The effects of cytoplasmic $Ca^{2+}$ and $Mg^{2+}$ on the macroscopic cAMP-activated current were measured in single olfactory cilia. At positive membrane potentials, cytoplasmic $Mg^{2+}$ was especially effective, eliminating most of the cAMP-activated current. Near resting potential, however, both divalent cations were very weak inhibitors, even when elevated beyond their physiological concentration ranges. At -50 mV, 1.0 mM cytoplasmic $Ca^{2+}$ inhibited the cAMP-activated current by 20.5 ± 2.8 % (range 2.0 to 35.1 %, $n$ = 14) in the frog and 22.8 ± 2.2 % (range 12.4 to 31.7 %, $n$ = 8) in the salamander. 5.0 mM cytoplasmic $Mg^{2+}$ inhibited the current by 18.0 ± 3.0 % (range 9.0 to 24.4 %, $n$ = 6) in the frog. It is therefore unlikely that an influx of divalent cations terminates the odorant response by a direct effect on the cAMP-gated channels. This work was supported by NIH grants PO1 DC00347 and R55 DC00926.

**M-Pos447**

SODIUM CHANNELS IN CEREBELLAR PURKINJE CELLS.

((W.G. Regehr and C.M. Armstrong)) Dept. of Physiology, Univ. of Pennsylvania, Philadelphia, Pa. 19104-6085.

Purkinje cell dendrites generate action potentials, but there is question regarding their ionic basis, particularly the presence of a sodium component. Using a whole-cell clamp on axotomized Purkinje cells in thin slices, large, TTX-sensitive current spikes are seen in response to voltage clamp steps, extracellular stimulation, or synaptic input. These current spikes are unlikely to arise in the soma, which is voltage-clamped. As a further test of spike origin, we filled cells with Cs to depolarize the poorly clamped dendrite and thus inactivate dendritic Na channels. Holding the soma at -60 mV, spike amplitude fell to about a third as Cs diffused in, but could be restored to full size by hyperpolarizing the soma to -100 mV. This supports the idea that dendrites have Na channels, since somatic Na channels would remain functional at -60 mV. Similar results were obtained when kainate or glutamate was used to depolarize the dendrites. Most current spikes had an inflection on their rise, suggesting two components. In some conditions the first component failed to trigger the second. We think the components arise from two major dendritic branches, or from a distal dendritic spike with variable invasion of the proximal dendrite and (when access resistance is high) the soma. On-cell recordings of soma membrane show a large K current, and a sodium current density too small to account for the whole-cell current spikes. We are further investigating Na channel distribution with on-dendrite patches.

**M-Pos448**

POTASSIUM CHANNEL OPENERS BLOCK SEIZURE ACTIVITY IN AN IN-VITRO MODEL OF EPILEPSY

((R.L. Simon and S.S. Lin)) CV/MD, Wyeth-Ayerst Research, Princeton, NJ 08543

Long-term cultures of rat hippocampal neurons were used to measure the anticonvulsant activity of drugs, such as lemakalim, nicorandil, and pinacidil, that open ATP-sensitive potassium ($K_{ATP}$) channels. Under appropriate conditions, cultured hippocampal neurons can be induced to generate paroxysmal depolarization shifts, or PDSs, that are characteristic of epileptic seizures *in vivo* (Furshpan and Potter, Neuron, 1989). The amplitude, duration, and frequency of PDSs in cultured hippocampal neurons are reduced or blocked by lemakalim and pinacidil, at 10 and 100 μM. Block of PDSs with these drugs does not prevent the firing of spontaneous action potentials by the neurons. These and similar results with cromakalim in guinea pig hippocampal slices (Alzheimer and ten Bruggencate, Archives of Pharmacology, 1989) suggest that $K_{ATP}$ channel openers might be useful anticonvulsants. The concentrations of lemakalim and pinacidil required to block seizure activity, however, are one to two orders of magnitude greater than that needed to open $K_{ATP}$ channels in smooth muscle. It is possible that at these higher drug levels, other ion channels might be affected in hippocampal neurons. Nicorandil at 10 μM does not inhibit PDSs in cultured neurons. In some experiments, it actually increases seizure activity. This increase may be due to nicorandil's indirect effects on intracellular cGMP levels rather than its primary effect on $K_{ATP}$ channels.

**M-Pos449**

SINGLE-CHANNEL CHARACTERIZATION OF MULTIPLE TYPES OF $K^+$ CHANNELS IN THE INTERNODE OF FROG AXONS.

((Jin V. Wu, Chaim T. Rubinstein, and Peter Shrager)) Department of Physiology, University of Rochester, Rochester, NY 14642.

Single-channel currents in internodes of demyelinated *Xenopus* axons were measured with the giga-seal patch-clamp technique. Lysolecithin induced demyelination allows the entire internodal axolemma to be accessible with a patch electrode. We found six types of $K^+$ channels in this region. Type I $Ca^{2+}$-activated $K^+$ channels (190 pS) were usually found in clusters. Type II $Ca^{2+}$-activated $K^+$ channels (240 pS) were also detected, but generally occurred with just one channel per patch. Activation of these large channels by elevated $Ca^{2+}$ could contribute to axonal after-hyperpolarization. An ATP-sensitive $K^+$ channel (125 pS) was inhibited by the internal application of 2 mM ATP, and its activation was voltage-independent. A background $K^+$ channel exhibited outwardly rectifying unitary current (176 pS) in symmetrical solutions but the ensemble-averaged I-V curve was ohmic. A second type of background $K^+$ channel shares characteristics with the first, but has a single channel conductance of about 300 pS. The nearly symmetrical macroscopic I-V curve of these background channels suggests a role in maintaining axonal resting potential. We found also $K^+$ selective channels (24-40 pS) that resemble the classical delayed rectifier.

**M-Pos450**

RESOLVING THREE TYPES OF CHLORIDE CHANNELS IN INTERNODES OF DEMYELINATED FROG AXONS.

((Jin V. Wu and Peter Shrager)) Department of Physiology, University of Rochester, Rochester, NY 14642.

Using the giga-seal patch clamp technique in the inside-out configuration, we have recorded unitary $Cl^-$ currents in internodes of demyelinated *Xenopus* axons. At least three types of $Cl^-$ channels in this region were found. The most frequently seen are inwardly rectifying $Cl^-$ channels with a single channel conductance of 50 pS. The currents of this channel were blocked by both SITS and DIDS. When internal chloride was entirely replaced with gluconate, the reversal potential shifted 60 mV. The second anion channel type is outwardly rectifying, with a conductance ranging from 50 to 75 pS. The open probabilities of both species of channels are largely voltage insensitive. The third type exhibited a very large single channel conductance, 390 pS in KCl and 300 pS in NaCl. In the gluconate substituted internal solution, the reversal potential shifted 15 mV and the current was only 50% of that with NaCl. This channel opens at the resting potential, but shows inactivation at high depolarized voltages. These 3 internodal $Cl^-$ channels may contribute to the regulation of axonal resting potential. Sponsored by the National Multiple Sclerosis Society and the NIH.

## NEUROBIOLOGY

**M-Pos451**

S100 PROTEINS AS AN ACTIVATOR OF CYCLIC NUCLEOTIDE PHOSPHODIESTERASE.

((1H. N. Parikh, 1V. Krishnan, 2P.L. Pingerelli and 1H. Mizukami)). 1Division of Regulatory Biology and Biophysics, Dept. of Biological Sciences, Wayne State University, Detroit, MI 48202. 2Calbiochem Corporation, La Jolla, CA 92037.

S100 proteins are acidic calcium binding proteins, originally isolated from the cytoplasm of the glial cells. Although S100 proteins are found to be ubiquitous, still mammalian brain is the richest source of these proteins. Calmodulin and S100 proteins possess homologous structural properties which are responsible for calcium dependent regulatory activities. Although calmodulin is known to act as activator of cyclic nucleotide phosphodiesterase (PDE), whether or not S100 proteins behave similarly is not known. In order to investigate, if indeed, the activity of S100a and S100b stimulated PDE, an enzyme assay using 2'-(N-methyl)anthraniloyl guanosine-3'-5'cyclic monophosphate (Mant-cGMP), a fluorescent analog of cGMP as a substrate was performed. The fluorescent intensity of Mant-cGMP decreases upon addition of calcium saturated S100a and S100b proteins in the presence of calmodulin free PDE. The estimated $K_m$ values for $Ca^{++}$/S100a and $Ca^{++}$/S100b stimulated PDE are 3.5μM and 2.4μM, respectively. The $V_{max}$ values for these proteins are 0.013 and 0.015μM $sec^{-1}$, respectively.

**M-Pos452**

OUTWARD CURRENT IN THE EMBRYONIC CHICK HEART USING THE PERFORATED PATCH CLAMP.

((T.L. Creazzo and L. Bertollini)) Medical College of Georgia, Augusta GA 30912.

Myocytes were prepared from the ventricles of chick embryos from day 11 of incubation. Using the perforate patch clamp (nystatin) method a time-dependent outward current ($I_{out}$) was observed which was not present when using the standard whole-cell approach. $I_{out}$ was observed at test potentials positive to 0 mV when stepping from a holding potential of -80 mV. $I_{out}$ reached a peak after 500 msec, did not decay and appeared to rectify at +30 mV. At potentials positive to +30 mV a transient component was observed which peaked within 100 msec and decayed to the level of the rectifying component within 500 msec. The transient component appeared to increase linearly with test potentials to +90 mV. The peak magnitude at +90 mV was 67 ± 9 pA (n=6, SEM). Both components of $I_{out}$ were observed despite the presence of $K^+$ channel blockers in the extracellular solution (20 mM CsCl, 85 mM TEA-Cl and 5 mM 4-AP). These results suggested that $I_{out}$ may be a $Cl^-$ current. $I_{out}$ was increased by 30% in the presence of 10 μM isoproterenol. The outward current quickly disappeared if the perforated patch was disrupted to achieve the standard whole-cell clamp. Supported by NIH grants HL39039 and HL36059.

**M-Pos453**

**RAPID, VOLTAGE-DEPENDENT CAPACITANCE INCREASES IN RAT ADRENAL CHROMAFFIN CELLS ARE NOT DUE TO EXOCYTOSIS**

((Frank T. Horrigan & Richard J. Bookman)) Dept. of Mol. & Cell. Pharmacology, Univ. of Miami School of Medicine, Miami, FL 33136

Admittance analysis of rat adrenal chromaffin cells under whole cell patch clamp reveals rapid and maintained increases in cell capacitance following depolarizations. Such capacitance-jumps have previously been observed in several neurosecretory preparations including bovine chromaffin cells and have been attributed to net increases in cell membrane surface area associated with a rapid phase of Ca-dependent exocytosis. These experiments demonstrate that a rapid transient component of this capacitance increase in rat chromaffin cells is Ca-independent and is not associated with exocytosis. Na channel gating charge movement (see following poster) is the likely source of this signal. Brief depolarizations (0.5 to10ms to +20mV, from HP=-80mV, with a pipette solution containing 100μM BAPTA & 2mM Mg-ATP and with 10mM external Ca & 1μM TTX), resulting in little Ca entry, evoke transient capacitance increases ($\Delta C_t$) that decay exponentially with a time constant of ~1s. Upon substituting 10mM $MgCl_2$ for $CaCl_2$, the maintained capacitance increases (as well as $I_{Ca}$) are eliminated while $\Delta C_t$ remains. $\Delta C_t$ can also be isolated in the presence of Ca by depolarizing to $E_{Ca}$ or by using an ATP-free internal pipette solution containing 5 mM EGTA or can be reversibly blocked by dibucaine. The amplitude of $\Delta C_t$ saturates (at ~20-50fF for a 5-8pF cell) for a 10ms pulse to +20mV and is not reduced by pulsing to +80mV. Similarly, at a saturating voltage, $\Delta C_t$ does not increase with longer pulses. The decay time constant is voltage-dependent (decreasing with more negative holding potentials). Capacitance records that have been corrected for $\Delta C_t$ display little or no fast phase increase following a 30-50 ms depolarization (to +20mV) and rise to a steady state over the course of several seconds. These corrected records suggest that a very rapid phase of Ca-dependent exocytosis in rat chromaffin cells is less important than was previously thought. (Supported by NSF, NIH & AHA).

**M-Pos454**

**NA CHANNEL GATING CHARGE MOVEMENT IS RESPONSIBLE FOR THE TRANSIENT CAPACITANCE INCREASE EVOKED BY DEPOLARIZATION IN RAT ADRENAL CHROMAFFIN CELLS**

((Frank T. Horrigan & Richard J. Bookman)) Dept. of Mol. & Cell. Pharmacology, Univ. of Miami School of Medicine, Miami, FL 33136. (Spon. by D.J. Adams)

High resolution admittance measurements of rat adrenal chromaffin cells under whole cell patch clamp reveal transient increases in the capacitance signal ($\Delta C_t$) of 20-50 fF following brief membrane depolarization (5ms @+20mV, HP=-80mV; see previous poster). $\Delta C_t$ is observed under conditions which inhibit exocytosis ($[Ca]_O$=$[ATP]_i$=0, $[EGTA]_i$=5mM) and eliminate ionic currents ($I_{Na}$ ~1nA/pF; $I_{Ca}$ ~ 100pA/pF). Several lines of evidence argue that $\Delta C_t$, measured at-80mV, reflects increased Na channel gating charge movement when Na channels are in the inactivated state. First, initial $\Delta C_t$ amplitude saturates with pulse duration and with amplitude and is not observed following a hyperpolarizing pulse to -180mV. Second, the exponential decay of $\Delta C_t$ is voltage dependent and follows the time course of recovery of Na current from inactivation. Third, the relationships between initial $\Delta C_t$ amplitude and either pulse duration or prepulse amplitude match the kinetics of Na current inactivation and the steady state inactivation relationship respectively. Fourth, dibucaine (250 μM), which has previously been shown to immobilize Na channel gating charge in squid axon, reversibly eliminates both Na Current and $\Delta C_t$. 1 μM TTX also eliminates Na current but has no effect on $\Delta C_t$ amplitude or on the voltage dependence of $\Delta C_t$ decay. TTX does, however, have a dramatic effect on the rate of decay of $\Delta C_t$, slowing it by a factor of 10 relative to controls. This last result suggests that TTX can influence parts of the channel protein involved with inactivation gating. Thus, in cells with sufficiently high channel densities admittance measurements can provide new information about voltage-dependent channel gating that is difficult to obtain by other methods. (Supported in part by NSF, NIH & AHA).

**M-Pos455**

**CHARACTERIZATION AND DIFFERENTIAL EXPRESSION OF A MEMBRANE PUMP BY GLIAL CELLS IN CULTURE.**

((R.E. Petroski and H.M. Geller)) Department of Pharmacology, UMDNJ-Robert Wood Johnson Medical School, Piscataway, NJ 08854.

Glial cells play an important role in regulating the chemical and osmotic balance in the central nervous system. Astrocytes express several membrane transporters and pumps in order to maintain ionic homeostasis; disrupted ionic balance and astrocyte swelling is correlated with neural injury (i.e. ischemia, trauma). Protoplasmic (type 1) astrocytes grown in cell culture provide an excellent model system to investigate the activity of membrane transporters and pumps involved in astrocyte swelling. We have demonstrated that the vital dye 5(6)-carboxyfluorescein diacetate (CFDA) can be used to assay the activity of a membrane pump in cultured astrocytes. CFDA is hydrolyzed by cellular esterases and the negatively charged, fluorescent product is retained in the cytoplasm of viable cells. Protoplasmic astrocytes rapidly expel this dye with a time course of minutes at 37°C. In contrast, neurons retain the dye for several hours. Moreover, glial cells derived from the O2A lineage (type 2 astrocytes and oligodendrocytes) also retain the dye, indicating a functional difference in the membrane transport properties of glial cells. The physiological role of this membrane transporter has been investigated pharmacologically. The efflux of carboxyfluorescein is attenuated by reducing temperature to 22°C and by depleting energy reserves with 20 mM sodium azide and 20 mM 2-deoxyglucose. Efflux is inhibited by organic anions known to prevent astrocyte swelling and which block the $Cl^-/HCO_3^-$ antiporter and the $Na^+/K^+/2Cl^-$ transporters and by reserpine which is known to block vesicular storage of neurotransmitters. Efflux is not affected by the elimination of $Na^+$ and/or $Cl^-$ from the bath. Further characterization and identification of this novel membrane transporter will be presented. Supported by NIH NS 24168.

**M-Pos456**

**REGULATION OF GENE EXPRESSION OF AMYLOID PRECURSOR PROTEIN IN PC12 AND HUMAN LYMPHOID CELLS**

((R. Fukuyama and S.I. Rapoport)) LNS, NIA, NIH, Bethesda, MD, 20892

**Amyloid precursor protein (APP) is a membrane spanning molecule whose fragment is a major component of the senile plaque of Alzheimer Disease (AD). To understand the signal transduction mechanism involved in the regulation of APP, we treated tissue culture cells with growth factors, calcium ionophore, phorbol ester, lectins and β-amyloid polypeptide (βA4) and monitered the levels of APP protein and mRNA by Western blot, immunoprecipitation and Northern blot methods. In PC12 cells, the level of APP protein and mRNA decreased dramatically after 5 days in culture. Addition of NGF induced neuronal differentiation and increased selectively the level of APP695 protein form. However, the overall levels of APP protein and mRNA were not altered. Selective induction of the APP695 form also was observed with A23187 (calcium ionophore) whereas the level of APP mRNA showed a small increase. βA 4 treatment did not alter total level of APP protein and mRNA nor selectively the APP695 form. In human T and non-T cells the levels of APP protein and mRNA were about 10 fold less than that of PC12 cells. However, addition of mitogens increased the level of APP mRNA up to 3 fold. These results indicate that (1) the second messenger involved in the regulation of APP gene expression appears to be likely calcium (2) APP695 form may be related to promotion of neurite outgrowth, (3) APP 751/770 form may have a role in cell-cell adhesion in human lymphocytes and (4) influx of calcium by βA4 may be compensated in PC12 cells.**

**M-Pos457**

**EXOGENOUS β-AMYLOID PEPTIDE INCREASES MEMBRANE LEAKINESS IN CULTURED PC12 CELLS.**

((Z. Galdzicki, R. Fukuyama and S.I. Rapoport)) LNS, NIA, NIH, Bethesda, MD 20892

A hallmark of Alzheimer disease (AD) is senile (neuritic) plaques in the brain. The major constituent of the plaque is βA4 polypeptide (βA4), derived from amyloid precursor protein (APP) by normal and/or abnormal processing. It has been reported that βA4 has a toxic effect on neurons and cultured cell lines. However, little is known about the mechanism of cell toxicity. We analyzed electrophysiological properties of rat pheochromocytoma -derived PC12 cells after application of βA4 in cell culture medium. In PC12 cells exposed to NGF and βA4, the number of cells decreased to half of those exposed to NGF alone for 9 days. Using the whole cell patch-clamp technique, recordings were made from cells between 1 day and 2 weeks in culture. The extracellular solution contained cholineCl (120 mM), $CaCl_2$ (10 mM), $MgCl_2$ (2 mM), HEPES (10 mM), TEACl (10 mM) whereas the intracellular solution included CsCl (130 mM), TEACl (20 mM), BAPTA (10 mM), HEPES (10 mM), $MgCl_2$ (2 mM). Membrane resistance and membrane time constant were reduced 3-fold when NGF plus βA4 were present, whereas in undifferentiated cells, not exposed to NGF, a 5-fold reduction in these parameters was observed with βA4 alone. For differentiated cells βA4 effect was independent of time in culture. These results indicate that βA4 increases cell membrane conductance in PC12 cells, most likely by forming transmembrane ionic pores. An increased conductance may place an excess energy burden on the cells for maintaining ionic gradients, and may alter intracellular ion homeostasis.

**M-Pos458**

**ELECTRIC FIELD-BIASED N1E-115 GROWTH CONE FILOPODIAL PROTRUSIONS ARE INHIBITED BY VERAPAMIL**

((R.S. Bedlack Jr., M.-d Wei, and L.M. Loew)) Neuroscience Program and Physiology Dept., University of Connecticut Health Center, Farmington, CT 06030

We recently showed (Neuron 9, 393-403 (1992)) that 0.1-1.0 mV/μm uniform D.C. electric fields can induce four cathode-localized events in differentiated N1E-115 neuroblastoma cells: membrane depolarizations, calcium influx, growth cone filopodial protrusions, and neurite initiation and elongation. The high degree of temporal and spatial correlation between these events suggests that they are causally related, but we are attempting to gain further proof. We have data indicating that organic calcium channel blockers (100 μM verapamil), inorganic calcium channel blockers (1 mM lanthanum), and removal of calcium from the extracellular fluid all prevent field-induced calcium influx. High resolution DIC microscopy reveals that verapamil also eliminates the ability of electric fields to bias filopodial protrusions. Further, this agent reduces control growth cone filopodial activity. One interpretation of these results is that normal filopodial protrusion occurs as a result of spontaneous foci of calcium influx, and that electric field-biased protrusion is simply a result of synchronized influx along the cathode-facing (depolarized) portion of the growth cone. Unfortunately, as verapamil treated neurites lose increasing numbers of filopodia, they eventually retract, making long-term time-lapse investigation of neurite initiation and elongation impossible. (Supported by USPHS grant ES05973)

**M-Pos459**

STRETCH-DEPENDENT MEMBRANE CAPACITANCE OF THE AUDITORY OUTER HAIR CELL. ((K. H. Iwasa)) NIDCD, NIH Bldg. 9, Rm 1E124, Bethesda, Maryland 20892.

The membrane capacitance of the cochlear outer hair cell during application of mechanical stress was measured in the whole-cell recording configuration with a lock-in amplifier operating at a frequency range between 1 and 2 kHz. A brief external perfusion by a hypo-osmotic medium was used as means of stretching the cell membrane reproducibly without changing access resistance. The capacitance of the cell was about 40 pF. At around the resting potential of the cell (ca.-60 mV), the membrane capacitance decreased about 5 % on stretching of the cell membrane. Stretching a lipid bilayer should increase the surface area and reduce the membrane thickness. Either of these changes results in an increase in the membrane capacitance. Thus we may conclude that the membrane stress does not seriously affect the lipid bilayer in the membrane. In addition, there must be a component in the capacitance that decreases on stretching of the membrane. It has been known that charge movements across the membrane appear as a non-linear capacitance. If membrane stress at the resting potential restricts the movement of the charge associated with force generation, the total capacitance will decrease. This interpretation is consistent with the observed magnitude of the non-linear capacitance, which is about 10 % of the total [Santos-Sacchi, J. Neurosci. (1991)]. Further, this picture predicts that the capacitance reduction by membrane stretching is less when the membrane is already stretched by the (hyperpolarizing) membrane potential. Indeed, it was found that at hyperpolarized potentials (e.g. -100 mV), the reduction of the membrane capacitance due to stretching is less than 1 %. This effect can be described by a model in which a unit can take two states, contracted and stretched, and the free energy difference between the two states has both electrical and mechanical components. This is equivalent to the explanation that a force-producing (motility) element, presumably a protein, has an electro-mechanical coupling.

**M-Pos460**

A MODEL SYSTEM TO DEMONSTRATE CELLULAR EFFECTS FROM POWER-LINE-FREQUENCY MAGNETIC FIELDS. ((C. F. Blackman, and S. G. Benane)) US Environmental Protection Agency (MD-68), Research Triangle Park, NC 27711 USA

Theoretical considerations have been used to claim that low-flux-density magnetic fields can not cause changes in biological processes. We provide experimental evidence for magnetic-field-induced inhibition of neurite outgrowth (NO) in PC-12 cells stimulated with nerve growth factor (NGF). Primed PC-12 cells are plated in collagen-coated, plastic petri dishes with or without 5 ng/ml NGF and exposed to sinusoidal magnetic fields for 22 hours in a $CO_2$ incubator at 37 °C. Sham exposure demonstrates no difference in % of cells with NO between exposed and magnetically shielded locations within the incubator. Helmholtz-configured coils produced a uniform, vertical, 50-Hz sinusoidal magnetic field which causes an intensity dependent reduction in the NGF stimulation of NO in PC-12 cells within the 5 to 10 μTesla (μT) range. Similar results with dishes of different annular radii demonstrate that the results are entirely dependent on the flux density of the magnetic field and are independent of the intensity of the induced electric field over a 12-fold intensity range. The frequency/flux-density dependence of this phenomenon is examined by stacking the dishes on the center axis of a single coil, thereby providing a range of flux densities between 3.5 and 9 μT for any given frequency. Frequencies between 15 and 70 Hz, at 5-Hz intervals, as well as at other selected frequencies are tested. Frequency-dependent reductions in NGF-stimulated NO are observed, with relatively higher sensitivities at 35 Hz and between 40 and 42.5 Hz, whereas 15 to 30 Hz fields produces no detectable reduction within the 3.5 to 9 μT range. Additional research is needed to determine whether there are more subtle differences in sensitivity to flux densities at different frequencies, and to determine the precise exposure parameters responsible for the response. This widely utilized, standard biological preparation is readily available to provide data to guide future theoretical analyses.

Supported by DOE, Office of Energy Management, IAG# DE-AI01-89CE34024. This is the abstract of a proposed presentation and does not necessarily reflect EPA policy.

**M-Pos461**

PROPERTIES OF p21 (NEUROCALCIN), A CENTRAL NERVOUS SYSTEM-SPECIFIC $Ca^{2+}$-BINDING PROTEIN.((E.R. Paul, E.D. Fraser and M.P. Walsh.)) Dept. of Medical Biochemistry, University of Calgary, Calgary, Alberta T2N 4N1, Canada. (Spon. by G.C. Scott-Woo)

We previously isolated a 21 kDa $Ca^{2+}$-binding protein (p21) from bovine brain (McDonald *et al.* (1987) Methods Enzymol. 139, 88). *N*-terminal sequencing of several CNBr and tryptic peptides of p21 revealed identity with the deduced amino acid sequence of neurocalcin (Okazaki *et al.* (1992) Biochem. Biophys. Res. Commun. 185, 147). Western blotting with affinity-purified antibodies to p21 revealed its relative abundance in brain but absence from other chicken tissues: lung, liver, heart, gizzard, kidney, trachea, oesophagus, large intestine, small intestine and skeletal muscle. p21 expression was observed in all regions of the brain: midbrain > pons > cerebellum = hippocampus = cerebral cortex > medulla. Homogenization and centrifugation of brain tissue ± $Ca^{2+}$ indicated $Ca^{2+}$-dependent association of p21 with the particulate fraction. This was confirmed by the $Ca^{2+}$-dependent association of purified p21 with the p21-depleted particulate fraction. At least part of this association of p21 with the particulate fraction appears to be due to interaction between p21 and membrane lipids: p21 bound to phosphatidylserine liposomes in a $Ca^{2+}$-dependent manner. p21 may therefore regulate the activity of a membrane-bound enzyme in a $Ca^{2+}$-dependent manner. Alternatively, p21 may bind to and regulate a cytosolic enzyme at low [$Ca^{2+}$] and dissociate from this target in the presence of $Ca^{2+}$ and bind to the membrane. (Supported by MRC Canada).

**M-Pos462**

SIMULATED EFFECTS OF NEUROMODULATORS ALTER NONLINEAR AND CHAOTIC DYNAMICS IN A MODEL NEURON

C. C. Canavier, D. A. Baxter, J. W. Clark[1], and J. H. Byrne. Dept. of Neurobiology and Anatomy, The University of Texas Medical School, Houston, TX 77030 and [1]Dept. of Electrical and Computer Engineering, Rice University, Houston, TX 77251.

By examining a mathematical model of the bursting neuron R15 in *Aplysia* (Canavier et al, *J. Neurophysiol.* 1991; Canavier et al, *Soc. Neurosci. Abstr.* 1992), we have shown that multiple stable modes of electrical activity can coexist at a given set of fixed parameters. We have extended these observations by investigating the effects on model activity of changes in a model parameter, the anomalous rectifier conductance ($g_R$), that simulate the known actions of the neuromodulatory agent serotonin. We have found that small changes in this parameter can create or annhilate certain coexisting modes of electrical activity, such as periodic beating (tonic firing), periodic bursting (bursts of action potentials separated by quiescent periods), and even chaotic bursting. Examination of the phase space of the model has revealed the appearance of nested attractors at certain values of $g_R$ called bifurcation points. At a high value of $g_R$, only one type of bursting activity can be sustained. As $g_R$ is decreased, either bursting or beating can be observed depending on the history of synaptic stimulation (the equivalent of perturbations in membrane potential). As $g_R$ is decreased still farther, seven distinct oscillatory modes can be observed, some of which appear to be chaotic. Since we have also shown that transient synaptic inputs can induce a shift from one mode to another, changing the value of $g_R$ can potentially provide the neuron a greater repertoire of electrical activity. Conversely, a change that is opposite in direction can limit the modes that the model and, by analogy, the neuron can exhibit. Supported by a grant from the ONR.

**M-Pos463**

POSTSYNAPTIC ACTIVATION AT THE SQUID GIANT SYNAPSE BY FLASH PHOTOLYTIC RELEASE OF GLUTAMATE FROM A 'CAGED' L-GLUTAMATE.

**John E. T. Corrie, Amadeo De Santis, Yoshiki Katayama, Kamran Khodakhah, John Messenger, David Ogden & David R. Trentham.**
***Laboratory of the Marine Biological Association, Plymouth, UK & National Institute for Medical Research, Mill Hill, London NW7 1AA, UK.***

**Indirect evidence suggests that L-glutamate is a neurotransmitter at the squid giant synapse but a direct experimental demonstration of postsynaptic activation by exogenous L-glutamate is lacking, apparently because the complex structure of the synapse prevents a sufficiently rapid change in concentration of exogenously applied neurotransmitter. Flash photolysis of a pharmacologically inert photolabile ('caged') derivative of L-glutamate, *N*-1-(2-nitrophenyl)ethoxycarbonyl-L-glutamate, pre-equilibrated in the synapse caused production of L-glutamate within the synaptic cleft and a postsynaptic depolarisation which generated action potentials. At normal pH, 7.8, the rate of glutamate photo-release is slow and only caused a slow depolarization. The rate of photolysis is proportional to [$H^+$] and at pH 5.5 is 200 fold faster, estimated as 135 $s^{-1}$ at sea water ionic strength. Synaptic transmission in the giant synapse of *Alloteuthis* is unaffected at pH 5.5 and under these conditions photolysis of caged glutamate to release 5-10 mM glutamate resulted in a postsynaptic depolarisation fast enough to fire trains of 2 or more action potentials of the same amplitude as normal transynaptic spikes. Release of ß-alanine from caged ß-alanine with the same photochemistry was without effect. These results provide further strong evidence that L-glutamate is a neurotransmitter in the squid giant synapse.**

**M-Pos464**

**RAPIDLY DESENSITIZING AND SLOWLY DESENSITIZING KAINATE RECEPTORS IN IDENTIFIED NEURONS OF THE VERTEBRATE RETINA.**

((Greg Maguire)) Sensory Sciences Center, Graduate School of Biomedical Sciences, University of Texas, Houston, TX 77030.

Glutamate receptors underlie the excitatory synaptic transmission from photoreceptors to bipolar cells, and from bipolar cells to amacrine and ganglion cells in the vertebrate retina.

I have used the whole cell patch clamp method in retinal slices and isolated retinal neurons, along with Lucifer yellow filling of each recorded cell in the slice, to measure the synaptic and ligand gated currents of physiologically and morphologically identified retinal neurons. Ligand gated currents were recorded in response to the pressure application of glutamate and its analogues from a micropipette (tip lumen less than 1 micrometer) placed onto specific and identified regions of intact (in the slice) or whole neurons (in isolation).

The results suggest that retinal amacrine cells possess a variety of glutamate receptors, including a rapidly desensitizing (less than 100 msec) kainate receptor which may be related to the transient amacrine cell's signature response; namely its transient excitation at light-on and -off. Further, the glutamate receptors are targeted to specific regions of the processes of the amacrine cell and confer upon the cell a unique functional identity related to the cell's ability to be excited at light-on and/or light-off.

M-Pos465
**THE DYNAMIC CLAMP: A NEW APPROACH FOR UNDERSTANDING THE ROLE OF IONIC CONDUCTANCES IN NEURAL NETWORK REGULATION.** ((A.A. Sharp, M.B. O'Neil, L.F. Abbott and E. Marder)) Brandeis Univ., Waltham, MA 02254.

Conventional voltage-clamp techniques provide data describing how the conductances that shape neuronal excitability depend on voltage and time, but do not allow the investigator to determine the participation of individual currents in the dynamic behavior of a neuron. We have devised a method, called a dynamic clamp, that allows us to introduce artificial conductances into neurons during their normal dynamic behavior. To construct the dynamic clamp, an Axoclamp-2A in DCC mode is used to monitor the cellular potential and to inject current. Based on this potential and a computational model describing the dynamics of the conductance under investigation a computer determines the current to be injected.
We use this technique to investigate the role of the peptide proctolin in modulating the pyloric network in *Cancer borealis*. Proctolin has previously been shown to directly modulate several neurons within the network and the biophysical nature of the proctolin mediated conductance has been described. We use the Dynamic Clamp to introduce an artificial proctolin conductance into the individual neurons modulated by proctolin in order to ascertain the role each neuron plays in generating the ensemble network effects of proctolin. Supported by NSF BNS 9009251.

## ELECTRON TRANSFER SYSTEMS

M-Pos466
**BINDING OF NAD(P)H TO COMPLEX I IN BEEF HEART SUBMITOCHONDRIAL PARTICLES.** ((M. GLinn[1], L. Ernster[2] and C.P. Lee[1])) [1]Dept. Biochem., Wayne State Univ. Med. Sch., Detroit, MI and [2]Dept. Biochem., Arrhenius Lab., Stockholm Univ., Stockholm, Sweden.

Submitochondrial particles oxidize both NADH and NADPH in a rotenone-sensitive manner. NADPH is oxidized *via* 2 routes. Ubiquinone [UQ] and cytochromes *b* [$b_{560}$ & $b_{566}$] participate only in one route and bypass the other [see companion abstract, Glinn et al]. Rhein, an inhibitor competitive with NADH, reduced respiration with NADH, but not with NADPH. In the presence of ADP-$Fe^{3+}$, rhein stimulated lipid peroxidation supported by NADH, but not by NADPH. Rhein altered the titration profile of NADH on lipid peroxidation by changing the NADH titration curve from biphasic to hyperbolic; no effects on the hyperbolic NADPH titration curve were seen. In the presence of KCN, NADH and NADPH oxidation occurred at comparable rates. At < 10 $\mu$M NADH, the extents of cytochrome reduction were similar to those with NADPH, i.e. cyt. *b* was partially, but cyts. *c* & *a* were fully, reduced. Complete reduction of cyt. *b* occurred at NADH > 15 $\mu$M. Difference spectra between 300 $\mu$M and 3 $\mu$M NADH were similar to those between 300 $\mu$M NADH and 300 $\mu$M NADPH. Our data indicate that (a) 2 distinct nucleotide binding sites exist on Complex I: a low-affinity site, which binds NADH and rhein, and from which UQ and cyt. *b* are reduced; and a high-affinity site, which binds NAD(P)H, but not rhein, and from which UQ and cyt. *b* are bypassed; and (b) lipid peroxidation may be preferentially induced by NAD(P)H bound to the high-affinity site.

M-Pos467
**EFFECTS OF Q CYCLE INHIBITORS ON NAD(P)H OXIDATION AND LIPID PEROXIDATION IN SUBMITOCHONDRIAL PARTICLES.** ((M. Glinn[1], L. Ernster[2] and C.P. Lee[1])) [1]Dept. Biochem., Wayne State Univ. Med. Sch., Detroit, MI 48201 USA & [2]Dept. Biochem., Arrhenius Lab., Stockholm Univ., S-106 91 Stockholm, Sweden.

In the presence of ADP-$Fe^{3+}$, NADH and NADPH induce lipid peroxidation in beef heart submitochondrial particles [SMP] *via* different enzymatic routes [Glinn et al. *ABB* 290:57, 1991]. The participation of ubiquinone [UQ] and cytochromes *b* [$b_{560}$ & $b_{566}$] in these pathways was studied using the Q cycle inhibitors myxothiazol [MYX] and 5 n-undecyl 6-hydoxy-4,7-dioxobenzoxythiazole [UHDBT]. MYX inhibited respiration with NADH and succinate by > 90%, but much less (< 60%) with NADPH. UHDBT strongly inhibited respiration with NADH and succinate, but had no effect with NADPH. Addition of antimycin [ANT] enhanced all inhibitory effects. Both MYX and UHDBT decreased the amount of malondialdehyde [MDA] formation induced by NADPH + ADP-$Fe^{3+}$ in the absence, but not in the presence, of rotenone. MYX decreased the amount of MDA formed by NADH + ADP-$Fe^{3+}$. In the presence of KCN, MYX increased the amount of cyt. *b* reduced by NAD(P)H and succinate, while MYX + ANT decreased the amounts of cytochromes reduced by all 3 substrates. UHDBT ± ANT had no effects. Our data indicate that (a) 2 routes exist for NADPH oxidation in SMP; (b) UQ and cytochromes *b* [$b_{560}$ & $b_{566}$] participate in only one route of NADPH oxidation, and bypass the other; (c) as expected, reduced UQ inhibits MDA formation.

M-Pos468
**Multiwavelength studies on the kinetics of cytochrome $aa_3$ reduction by cytochrome c.**
R. W. Hendler[a], S. K. Bose[a], and R. I. Shrager[b]. [a]Laboratory of Cell Biology, NHLBI and [b]Laboratory of Applied Studies, DCRT, NIH, Bethesda, MD. 20892.
A new type of ultrarapid spectrometer has been designed and built with W. S. Friauf, J. Cole, and P. D. Smith of BEIP, NCRR, and H. A. Fredrickson, CSL, DCRT, NIH. This instrument has two spectrometers, each covering ~130 nm wavelength and acquires up to 1024 spectra at 10 $\mu$s resolution. Global analyses are performed using singular value decomposition and Gaussian deconvolution. With the resting enzyme, two major (and several minor) kinetic phases are seen. The 1st electron is added with a time constant ($\tau$) of ~4 ms. It is shared equally between heme a and $Cu_A$. At 4 s, heme a is ~67% and heme $a_3$ ~10% reduced. At 120 s, both hemes a and $a_3$ are ~50% reduced. Although reduced cytochrome c is present at a 6/1 ratio to the oxidase, no further reduction occurs during the next 30 min. However, the introduction of a small quantity of $O_2$ at this point results in 100% reduction of both hemes. Experiments starting with the pulsed enzyme show multiphasic behavior, not readily modelled by simple exponentials. The 1st electron binds with $\tau$~6 ms and is shared between heme a and $Cu_A$. During the next 100 s, the two hemes approach 100% reduction.

M-Pos469
**EFFECTS OF SITE-DIRECTED MUTAGENESIS ON VECTORIAL PROTON TRANSLOCATION IN RHODOBACTER SPHAEROIDES CYTOCHROME *C* OXIDASE** (J. Fetter, J.P. Hosler, J.P. Shapleigh*, J.W. Thomas*, M.M.J. Tecklenburg, Y. Kim, R.B. Gennis*, G.T. Babcock and S. Ferguson-Miller) Departments of Biochemistry and Chemistry, Michigan State University, East Lansing, MI 48824 and *School of Chemical Sciences, University of Illinois, Urbana, IL 61801
A three-subunit cytochrome *c* oxidase from *Rb. sphaeroides* translocates protons across a membrane using the driving force of electron transfer through copper and Heme A centers to oxygen. Mutant forms of the oxidase have been reconstituted into bilayer vesicles to measure effects on proton pumping activity. Among the regions investigated is a highly conserved loop between helices IX and X in COXI. We have mutated His411, Asp 412, Thr413, and Tyr414 which could participate in proton channelling because of their ability to reversibly bind protons and their proximity to the binuclear center. All four retain electron transfer activity and three have been shown to be competent in proton pumping: His411Ala, Asp412Asn, and Tyr414Phe. Another region of potential interest is the amphipathic Helix VIII containing conserved residues Thr352, Thr359, and Lys362. Of the mutants constructed so far, only Thr359Ala retains electron transfer activity with a turnover of 25% of the wild type. Studies have also been initiated on the highly conserved loop between helix II and III. Mutation of the totally conserved Asp 132 to Asn causes strong inhibition of electron transfer in the purified enzyme. This indicates the functional importance of this predicted extramembrane region, possibly as a proton loading site.

**M-Pos470**
REDOX-ASSOCIATED CONFORMATIONAL CHANGES IN CYTOCHROME *C* OXIDASE PROBED BY ABSORPTION, CIRCULAR DICHROIC, AND FLUORESCENCE SPECTROSCOPIES. ((Paul N. Goudreau and Robert A. Copeland)) Department of Biochemistry and Molecular Biology, University of Chicago, Chicago, IL 60637

Cytochrome *c* oxidase functions as a redox-linked proton-translocating enzyme. It has been postulated that in order for the enzyme to work in a proton-pumping role, it must exist in at least 2 distinct conformations; one state corresponding to proton uptake from one side of the membrane and another corresponding to proton release from the other side. We have used the oxidase obtained from the bacterium *Paracoccus denitrificans* to probe for the existence of global conformational changes associated with various redox and liganded states of the enzyme. We report spectra of resting, reduced, and mixed valence forms of the enzyme in the unliganded, CN-bound, and CO-bound states and compare these to spectra of the enzyme obtained in the presence of the structural perturbant guanidine hydrochloride.

**M-Pos471**
PROTEIN-CHROMOPHORE INTERACTIONS IN CYTOCHROME C OXIDASE: HEME A MODEL COMPLEXES.
((J. S. Felsch, M. Ikeda-Saito, W. Morgan, and R. A. Copeland)) Department of Biochemistry and Molecular Biology, University of Chicago, Chicago, IL 60637.

Cytochrome c oxidase is a terminal oxidase in the electron transport chain crucial to the support of respiratory oxidative phosphorylation in eukaryotes and in many prokaryotes. To study the structural changes that attend the catalytic activites of the enzyme, we have studied an anomalous redshift seen in the second derivative absorption spectra of reduced, liganded conformers of the oxidase. Comparisons of these spectra to spectra of heme A in complex with the heme-binding proteins histidine and proline rich glycoprotein, hemopexin, myoglobin, and a site-specified mutagen of myoglobin are reported. The findings are discussed in terms of possible implications for the structure of the oxidase's heme-binding pockets.

**M-Pos472**
STRUCTURAL INFORMATION ON THE PLANT CYTOCHROME OXIDASE REVEALED BY SECOND-DERIVATIVE ABSORPTION SPECTROSCOPY ((W. Peiffer, J. Hosler, and S. Ferguson-Miller)) Dept. of Biochemistry, Michigan State University, East Lansing, MI 48824

Among the unusual properties of plant cytochrome oxidases is their visible spectrum: the α and Soret peaks are blue shifted and the reduced heme *a* Soret is broadened and slightly split. Using second derivative analysis of room temperature spectra of CN, $N_3$, and CO-bound wheat oxidase, we can observe two distinct absorption bands attributable to heme *a* at 438 and 448 nm. These values correspond well to the two maxima reported for heme *a* in CN and $N_3$-inhibited plant oxidase, detected by low temperature difference spectroscopy of whole mitochondria. However, the wheat values are considerably blue-shifted relative to the values for beef heart, 443 and 451 nm, measured under similar conditions. The two Soret transitions can be explained by the inherent asymmetry of the heme A prosthetic group, with relative intensities and positions of the maxima being determined by the protein environment. We have already demonstrated a difference in the protein environment of heme *a* between plant and mammalian oxidase by resonance Raman spectroscopy. Soret splitting is also observable in partially and fully reduced wheat oxidase in the unliganded form. The partially reduced (20%) enzyme displays equal contributions of the 438 and 448 nm absorption bands. The two transitions can also be resolved in fully reduced oxidase because of their shifted positions with respect to heme $a_3$. The heme *a* Soret split therefore appears not to be limited to the ligand-bound form of the enzyme. However, the structural significance of the position and relative intensities of the two transitions, as monitors of the heme *a* environment, remains to be explored.

**M-Pos473**
PURIFICATION AND CHARACTERIZATION OF CYTOCHROME *C* 552 AND CYTOCHROME *C* 550 FROM *PARACOCCUS DENITRIFICANS* . ((Stephen R. Lynch and Robert A. Copeland)) Department of Biochemistry and Molecular Biology, University of Chicago, Chicago, Illinois 60637.

Two different cytochrome *c* 's transfer electrons to cytochrome *c* oxidase in the bacterium *Paracoccus denitrificans* : cytochrome *c* 550, a soluble protein homologous to eukaryotic cytochrome *c* and cytochrome *c* 552, a membrane bound protein with little homology to the eukaryotic protein. Both proteins have been purified through chromatography. The soluble protein has an approximate molecular weight of 14.5 kdal, while the membrane bound protein has a molecular weight of approximately 22 kdal. Absorption spectroscopy, resonance Raman spectroscopy, and circular dichroism have been utilized to characterize and compare the two proteins. The two proteins have the same apparent function, the ability to transfer electrons to cytochrome *c* oxidase. We have studied their activity with cytochrome *c* oxidases isolated from different species to determine the importance of the two proteins in the bacterium and why both do not exist in eukaryotes.

**M-Pos474**
ELECTRIC FIELD INDUCED REVERSE ELECTRON TRANSFER FROM HEME CYT $bH$ TO CYT $b_L$ IN THE CYT $bc_1$ COMPLEX OF *R. CAPSULATUS* ((H. Ding, C.C. Moser and P. L. Dutton)) Johnson Research Foundation, University of Pennsylvania, Philadelphia, PA 19104. (Sponsored by J. M. Keske)

Cytochrome $bc_1$ complex catalyses electron transfer-mediated charge separation and proton translocation across membranes of mitochondria and bacteria. Electron transfer between the two b-type hemes (from cyt $b_L$ to cyt $b_H$) takes place across 70% of the membrane dielectric and dominates membrane potential generation by this complex. In this work, we induce reverse electron transfer from ferro-cyt $b_H$ to ferri-cyt $b_L$ in the cyt $bc_1$ complex of *R. capsulatus* by application of a large electric field across an oriented multilayer inserted between insulated electrodes. Native chromatophore membranes containing reaction center and cyt $bc_1$ complex were deposited by Langmuir Blodgett film method onto glass support coated with a transparent electrode. The multilayer capacitor was completed with evaporation of polyethylene and platinum. The activity of cyt $bc_1$ complex in LB films are sensitive to humidity. Flash activation of reaction center in films at 60% humidity leads to ubihydroquinone oxidation in the $Q_o$ site and the stable formation of reduced cyt $b_H$ via cyt $b_L$. Voltage pulse application drives reversed electron transfer back to cyt $b_L$. The determination of the electron transfer rate of this reaction is in progress. Supported by NIH Grant GM 27309.

**M-Pos475**
OXOCARBOCYANINE DYES REPRESENT A THIRD CLASS OF ROTENONE-TYPE CARBOCYANINE INHIBITORS OF MITOCHONDRIAL AND PARACOCCUS DENITRIFICANS NADH-UBUQUINONE REDUCTASE ((W.M. Anderson, J.M. Wood, and A.C. Anderson)) Ind. Univ. Sch. Med., N.W. Cent. Med. Ed., 3400 Broadway, Gary, IN 46408

Three structurally related oxocarbocyanine dyes (DiOC2(3), DiOC5(3), and DiOC6(3)) and one oxodicarbocyanine dye (DiOC2(4)) also inhibit mitochondrial NADH oxidase activity, and DiOC6(3) inhibits P. denitrificans NADH oxidase activity, with succinate and cytochrome oxidase activity substantially unaffected in either system. Using submitochondrial particles (SMP), all four compounds inhibited NADH-dependent duroquinone and coenzyme Q reduction, while NADH-dependent menadione reduction was inhibited by DiOC5(3). Using purified complex I, all four dyes inhibited NADH-dependent reduction of coenzyme Q. Using P. denitrificans membrane vesicles, DiOC6(3) inhibited NADH-depen-dent reduction of coenzyme Q. The oxocarbocyanines mechanism of inhibition appears similar to rotenone since (a) essentially only rotenone-sensitive electron acceptors are affected by these dyes, (b) inhibition of menadione reduction was greatly diminished with rotenone-saturated SMP, and (c) inhibition of coenzyme Q reduction was largely eliminated with rotenone-insensitive complex I and P. denitrificans membrane vesicles. Supported by Ind. Heart Assoc.

**M-Pos476**

THE EFFECTS OF PH AND SALTS ON THE NADH DEHYDROGENASE COMPLEX OF RHODOBACTER CAPSULATUS.

((Steven W. Meinhardt and Adela Cruz de la Rosa)) Department of Biochemistry, North Dakota State University, Fargo, ND 58105

The effects of pH and salts on the NADH Dehydrogenase activity of aerobically grown Rhodobacter capsulatus membrane particles has been investigated. This activity is strongly pH dependent with a maximal activity at pH 7.2 and decreasing to less than 10% of the maximal activity at both pH 4.7 and pH 9.7. Determination of the Michaelis-Menton parameters, $K_m$ and $V_{max}$, at several pH values indicate that at acid pH values there is a decrease in both the turnover of the enzyme and in the binding of NADH. At basic pH values the NADH binding is unaffected and the turnover of the enzyme is decreased. The activity of the enzyme is affected at all pH values by the addition of salts. At basic pH values the pK associated with the $V_{max}$ shifts from approximately 9.2 in the absence of salts to approximately 8.5 in the presence of 50 mM KCl. Increasing the salt concentration results in further shifts in the pK. The addition of 100 mM KCl or 50 mM $K_2SO_4$ results in similar shifts indicating this is a cation effect. Divalent cations are nearly 10 times more effective in shifting the pK. The addition of 5 mM $CaCl_2$ results in a shift similar to the addition of 50 mM KCl.

**M-Pos477**

THERMODYNAMIC ANALYSIS OF FMN IN MITOCHONDRIAL NADH:UBIQUINONE OXIDOREDUCTASE (COMPLEX I)

((V. Sled', N. Rudnitzky, Y. Hatefi+, and T. Ohnishi)) Univ. of Pennsylvania, Philadelphia PA 19104; +Dept. of Molec. and Exptl. Med., The Scripps Clinic, La Jolla, CA 92037.

In contrast to iron-sulfur clusters and bound ubiquinones, there is no hard information about the kinetic and thermodynamic properties of the other intrinsic redox component of complex I, non-covalently bound FMN. We have undertaken detailed redox titration analyses of the FMN free radical EPR signal in isolated bovine heart complex I at different pHs. Spin relaxation of this semiquinone is much faster than that of flavodoxin. It is not saturated at microwave power up to 100 mW at -95°C due to spin coupling to the N-3 cluster. It is evident from titration curves and from the g=2.00 signal line shape that flavosemiquinone is protonated at pH values from 7 to 9. On the other hand, the pH dependance of the free radical's stability constant demonstrates a pronounced minimum at pH=8. Possible redox transitions of bound FMN and their role in electron transfer and energy coupling in complex I will be discussed.

(Supported by NIH Grant GM-30736 and NSF Grant MCB-9119300 (T.O.) and by NIH Grant DK-08126 (Y.H.))

**M-Pos478**

MUTATIONS AT CONSERVED RESIDUES IN CYTOCHROME b SUBUNIT OF Rb. SHPAEROIDES AFFECT QUINONE REDUCTASE SITE.

((B. Hacker, B. Barquera, A. R. Crofts and R. B. Gennis)) School of Chemical Sciences, University of Illinois, Urbana, IL 61801 and School of Life Sciences, University of Illinois, Urbana, IL 61801.

The quinone reductase site ($Q_i$) of the $bc_1$ complex is the binding site for inhibitors such as antimycin A and HQNO. Four highly conserved residues in the cytochrome b subunit of Rb. Sphaeroides (A52, H217, K251 and D252) were targeted for mutagenesis. These residues are near the $Q_i$ site based on inhibitor resistant mutations found in yeast. Each of the mutants is impaired in the rate of reoxidation of cytochrome $b_H$. H217A and D252A are unable to grow photosynthetically indicating a severe defect in the $bc_1$ complex. These mutants are the first to selectively impair electron transfer from cytochrome $b_H$ to the $Q_i$-site.

**M-Pos479**

HALOCYANIN: A CUPREDOXIN FROM ARCHAEBACTERIA

((I. Sagi, D.E. Sidelinger, M.R. Chance, M.D. Wirt, *M. Engelhard)) Albert Einstein Col of Med., Bronx, NY 10461 and *Max-Planck Institute fur Ernahrungsphysiologie, Dortmund, Germany.

Type I copper proteins have a blue color due to an absorption maximum at 600 nm. Typical examples (like azurin and plastocyanin) have only one copper, are single domain proteins of 20 kD or less, and mediate important electron transfer reactions. The copper environment of all the cupredoxins is similar, ß-barrel secondary structure with variations in the loop regions. The tertiary structure is well preserved while the primary sequences are only homologous in the copper binding regions. Strikingly, a C-terminal sequence with the general feature CYS-$aa_n$-HIS-$aa_m$-MET has been observed in all documented cases except stellacyanin (lacking met). The tertiary structure homology along with the partial sequence homology of cupredoxins poses questions of convergent versus divergent evolution for this protein class. A proposed common precursor is an ancestral purple photosynthetic Chlorobium-like bacterium. An answer to the problem of evolution can be addressed by identifying new cupredoxin like molecules from other species. We report the first identification of a blue copper protein from archaebacteria (*Natronobacterium pharaonis*) and its analysis by UV, epr, CD, and EXAFS techniques. The epr spectrum of oxidized halocyanin shows a profile typical for unpaired electrons with g = 2.024 and 2.209. The epr signal and the blue color disappear upon reduction. CD spectra of the protein are consistent with the presence of individual copper to histidine, cysteine, and methionine transitions. EXAFS analysis of the reduced protein has been completed and demonstrates reasonable solutions for both 2Cu-N:3Cu-S and 3Cu-N:2Cu-S arrangements. This work has been supported by a grant from the PRF.

**M-Pos480**

HEME O BIOSYNTHESIS IN E. COLI: THE CYOE GENE IN THE CYTOCHROME BO OPERON ENCODES A PROTOHEME IX FARNESYL TRANSFERASE.

T. Mogi, K. Saiki, and Y. Anraku Dep. of Biology, Fac. of Science, Univ. of Tokyo, Hongo, Bunkyo-ku, Tokyo 113, JAPAN

The cytochrome bo complex in the aerobic respiratory chain of E.coli belongs to the heme-copper terminal oxidases and contains protoheme IX (heme B), heme O and CuB as the redox metal centers in subunit I. It catalyzes the reduction of ubiquinol-8 and the oxidation of molecular oxygen and functions as a redox-coupled proton pump. We have carried out the structure-function studies on the last ORF in the cytochorme bo operon, the cyoE gene, via site-directed mutagenesis approach and found that it encodes a protoheme IX farnesyltransferase (heme O synthase) essential for functonal expression of the oxidase activity. We have introduced 7 deletions and 40 Ala substitutions in the CyoE protein and examined their effects on the metal centers by the spectroscopic methods and the oxidase activity by the in vivo complementation test and the quinol oxidase assay. We found that the cyoE mutations eliminated the catalytic activity and specifically reduced the CO-binding activity accompanied by a 3nm red-shift of the Soret peak of the high spin heme. Heme analysis by reverse phase HPLC revealed that heme O present in the high spin heme binding site was substituted by heme B. Since the CyoE homologs contain the putative allylic polyprenyl-PPi binding domain and the expression of the cyoE gene alone could convert heme B to heme O, we postulate that the cyoE gene encodes a novel enzyme, a protoheme IX farnesyltransferase (heme O synthase).

**M-Pos481**

HISTIDINE 217 OF THE CYTOCHROME *B* POLYPEPTIDE IS IMPORTANT FOR EFFICIENT OXIDATION OF CYTOCHROME $B_H$ BY QUINONE AT $Q_i$.

((Kevin A. Gray and Fevzi Daldal)) Plant Science Insitute, Department of Biology, University of Pennsylvania, Philadelphia, PA. 19104-6018

Histidine 217 (H217 in the numbering of *Rhodobacter capsulatus*) is completely conserved in the several hundred sequences available of cytochrome *b* from the cytochrome $bc_1$ complex. H217 is distinct from the four invariant histidines which ligate the Fe atoms of the two *b*-hemes (cyt $b_L$ and $b_H$). Structural models predict that H217 is located at the end of the putative transmembrane helix D which faces the negative side of the membrane (cytoplasm in bacteria) near the presumed $Q_i$ site. It could thus be possible that H217 is involved in the reduction of quinone by cytochrome $b_H$. This residue was changed using site directed mutagenesis on the protein from the Gram-negative photosynthetic bacterium *R. capsulatus*. The substitutions H217D, H217R and H217L were constructed. All strains assemble a $bc_1$ complex however only H217D and R are photosynthetically competent and have active, albeit dysfunctional, enzymes. Flash kinetic analysis has shown that cytochrome *b* is oxidized much slower in H217D and R as compared to wildtype while cytochrome *b* in H217L remains reduced after a flash. In these mutants while the redox properties of cytochrome $b_H$ have not been affected, EPR experiments have shown that a stable, antimycin sensitive semiquinone is formed. Future studies should better define the role of this histidine. This work was supported by the American Heart Association, Southeastern Pennsylvania affiliate (to K.A.G.) and the NIH (GM 38237, to F.D.).

**M-Pos482**

REDUCTION KINETICS OF THE CYTOCHROME P-450 REDUCTASE:CYTOCHROME $b_5$ COMPLEX. ((A.K. Bhattacharyya, J.K. Hurley, L. Waskell and G. Tollin)) Dept. of Biochemistry, University of Arizona, Tucson, Az 85721, Dept. of OB/GYN, University of Kentucky, Lexington, Ky 40536, and Dept. of Anesthesia, UCSF and VAMC, San Francisco, CA 94121. (Sponsor Henry R. Hirsch).

The reduction kinetics of the one-electron reduced P-450 reductase:cytochrome $b_5$ ($P450R_{1e}$:$b_5$) complex has been investigated by the laser flash-photolysis technique. $P450R_{1e}$ and cyt $b_5$ were seperately reduced by laser-generated 5-deazaflavin semiquinone (5-dRfH·) via 2nd order kinetics and rate constants of $8.1 \times 10^7$ and $4.2 \times 10^8$ $M^{-1}s^{-1}$ were obtained. Intramolecular electron transfer between laser generated FADH· and FMNH· in $P450R_{1e}$ was observed at 585 nm, and a 1st order rate constant of 40 $s^{-1}$ was obtained. Reduction of $P450R_{1e}$:$b_5$ by 5-dRfH· was biphasic and 2nd order rate constants of $5.4 \times 10^8$ and $7.5 \times 10^7$ $M^{-1}s^{-1}$ were obtained for the fast and slow phases of reduction. The time-resolved flash-induced difference spectrum was consistent with rapid direct reduction of the protein-bound flavin and heme, followed by a slower 1st order ($k_{lim}$ = 38 $s^{-1}$) intracomplex electron transfer from FADH· to heme. The results indicate that the (laser generated) two-electron reduced form of P450R is catalytically competent in the transfer of reducing equivalents to cyt $b_5$ and that internal electron transfer within P450R is the rate limiting step.

Supported by NIH grants GM 35533 and DK 15057

**M-Pos483**

TRANSMEMBRANE ELECTRON TRANSPORT MEDIATED BY $C_{60}$ AND $C_{70}$. ((K.C. Hwang and D. Mauzerall)) Rockefeller Univ., 1230 York Avenue, New York, NY 10021. (Spon. by T. Marinetti)

Transmembrane electron transport is central to photosynthesis, to mitochondrial respiration, and to the design of molecular systems for solar energy conversion. Herein we report that $C_{70}$ efficiently transports electrons across a lipid bilayer with a quantum yield of ∿ 0.04. This is a minimum yield and the donor, 70 mM ascorbate, is not saturating. 72% of the Nernst potential was measured across a $C_{70}$-containing lipid bilayer separating a concentration gradient of ascorbate, unambiguously indicating that the $C_{70}$-containing bilayer is permeable to electrons. Similar transmembrane electron transport behavior was also observed with a $C_{60}$-containing bilayer. Other experiments indicate the membrane crossing time of the $C_{60}$ anion is ≤10 μs. This study was supported by a NIH grant, GM25693.

**M-Pos484**

THE PHOTOREDUCTION PROCESS OF DNA PHOTOLYASE: FIRST OBSERVATION OF CORRELATED TRIPLET-DOUBLET RADICAL PAIR POLARIZATION

((Craig Essenmacher, Sang-Tae Kim#, Aziz Sancar#, and G.T. Babcock)) Department of Chemistry, Michigan State Univ., East Lansing, MI 48824 and #Department of Biochemistry and Biophysics, Univ. of N. Carolina School of Medicine, Chapel Hill, NC 27599

DNA photolyase utilizes visible light to repair pyrimidine dimers. Isolation of the enzyme produces an inactive form that contains a flavosemiquinone radical (FADH·). Inactive photolyase can be activated in a light-driven reaction that produces the reduced flavin ($FADH^-$). We present here a time-resolved EPR study of the photoreduction process. Photoexcitation of the FADH· form of the enzyme oxidizes an amino acid that we have identified using specific deuteration, $^{15}N$ labeling, and site directed mutagenesis as tryptophan-306 in its cation radical form. The transient tryptophan radical is spin polarized. This polarization arises from interactions between a triplet flavin and a doublet tryptophan radical pair following the electron transfer reaction. The polarization pattern is consistent with a correlated radical pair mechanism as applied to the triplet-doublet case.

Supported by: NIH GM31082 (A.S.) and GM37300 (G.T.B.)

**M-Pos485**

EFFECTIVE TWO-STATE SYSTEMS FOR BRIDGE-MEDIATED ELECTRON TRANSFER: A GREEN'S FUNCTION ANALYSIS. (S. S. Skourtis and J. N. Onuchic) Department of Physics, University of California San Diego, La Jolla CA 92093-0319. (Supported by NSF, Grant No. MCB-9018768)

A Green's function analysis of bridge-mediated electron transfer reactions is given. Possible uses of the Green's function formalism in the study of such reactions are discussed for one-electron and many-electron systems. As an application, the criteria for the validity of the effective two-state picture of long-distance electron transfer are derived. According to this picture, the transfer of an electron from a donor to an acceptor through an intermediate bridge, may be described by a two-state Hamiltonian. This Hamiltonian involves effective donor and acceptor states that have some bridge character. The effective two-state limit is studied for several one-electron and many-electron model systems.

## OXIDATIVE PROCESSES AND PHOSPHORYLATION

**M-Pos486**

MITOCHONDRIAL AND CYTOSOLIC $Ca^{2+}$ TRANSIENTS DURING THE CONTRACTILE CYCLE OF CULTURED CARDIAC MYOCYTES: A LASER SCANNING CONFOCAL MICROSCOPIC STUDY. ((Enrique Chacon, Ian S. Harper, Jeffrey M. Reece, Brian Herman, and John J. Lemasters)) Dept of Cell Biology & Anatomy and Curriculum in Toxicology, University of North Carolina, Chapel Hill, NC 27599.

Cardiac myocytes appear to regulate mitochondrial respiration and ATP synthesis on a beat to beat basis. The mechanisms regulating mitochondrial metabolism are poorly understood, but regulation by changes of mitochondrial free $Ca^{2+}$ has been proposed. However, it is not known whether mitochondrial free $Ca^{2+}$ increases during normal excitation-contraction coupling, conditions when ATP demand is high. In the present study, we report measurements of cytosolic and mitochondrial $Ca^{2+}$ in electrically stimulated rabbit cardiac myocytes using laser scanning confocal microscopy. Cells were co-loaded with Fluo-3 and tetramethylrhodamine methylester (TMRM). Fluo-3 distributed into both cytosol and mitochondria, whereas TMRM concentrated into mitochondria. From line scan images acquired simultaneously for each fluorophore, changes of Fluo-3 fluorescence during the contractile cycle were determined for the cytosol and mitochondria. Resting $Ca^{2+}$ in cytosol and mitochondria were essentially identical. During electrical pacing, parallel transients of $Ca^{2+}$ were recorded in cytosol and mitochondria that were enhanced upon addition of isoproterenol. In conclusion, laser scanning confocal microscopy can measure $Ca^{2+}$ transients in subcellular compartments of living cells. Changes of mitochondrial $Ca^{2+}$ during the contractile cycle may be the mechanism for beat to beat regulation of mitochondrial ATP supply.

**M-Pos487**

CONFOCAL IMAGING OF SARCOLEMMAL AND MITOCHONDRIAL $\Delta\Psi$, CYTOSOLIC AND MITOCHONDRIAL $Ca^{2+}$, AND MITOCHONDRIAL $\Delta$pH IN CARDIAC MYOCYTES DURING ATP DEPLETION. ((John J. Lemasters, Enrique Chacon, Ian Harper, Jeffrey M. Reece, and Brian Herman)), Dept of Cell Biology & Anatomy and Curriculum in Toxicology, Univ of North Carolina, Chapel Hill, NC 27599.

Using laser scanning confocal microscopy, we measured electrical potentials ($\Psi$), free $Ca^{2+}$, and pH in single 1-day-cultured adult rabbit cardiac myocytes. $\Psi$ was measured from the Nernstian distribution of tetra-methylrhodamine methylester, a cationic fluorophore that accumulates electrophoretically into negatively charged compartments. In resting cells, sarcolemmal $-\Delta\Psi$ was 70-90 mV, and mitochondrial $-\Delta\Psi$ was 100-140 mV. pH of cytosol and mitochondria measured by ratio imaging of SNARF-1 fluorescence was 7.0-7.2 and 8.0, respectively. Thus, mitochondrial $\Delta$pH was 0.9 units, and the protonmotive force ($\Delta p = \Delta\Psi + 61\Delta pH$) was 155-195 mV. $Ca^{2+}$ was measured by Fluo-3 fluorescence. In resting myocytes, cytosolic and mitochondrial free $Ca^{2+}$ were similar. To mimic the ATP depletion of anoxia, myocytes were exposed to 2.5 mM NaCN and 20 mM 2-deoxyglucose ('chemical hypoxia'). After 40 min, $\Delta$pH collapsed entirely, but mitochondrial $\Delta\Psi$ was unchanged. Cytosolic $Ca^{2+}$ increased slowly until the cells shortened and hypercontracted after about 50 min. After hypercontraction, mitochondria loaded with $Ca^{2+}$ and subsequently depolarized. Mitochondrial $Ca^{2+}$ was then released, and cells lost viability after several more minutes. The new methods described here allow measurement of the individual components of $\Delta p$ of single mitochondria in living myocytes and demonstrate a distinctive pattern of ionic and electrical changes in mitochondria during the progression of ATP depletion injury.

**M-Pos488**

ISCHEMIA/REPERFUSION-INDUCED INJURY OF THE ENERGY-TRANSDUCING PROCESSES OF FOREBRAIN MITOCHONDRIA AND PROTECTION BY ASCORBATE ((M. Sciamanna and C. P. Lee)) Dept. Biochem., Wayne State Univ. Med. Sch., Detroit. MI 48201.

We have recently shown that rat brain mitochondria [RBM] from ischemic brains (12-30 min ischemia) exhibited impaired State 3 respiratory rates and respiratory control [RC] with both succinate and NAD-linked substrates. The respiratory rates and RC for RBM derived from forebrains which underwent up to 20 min of ischemia [ISC] could be restored to control levels when the assay mixture was supplemented with ED(G)TA or ruthenium red. Only partial restoration (≈ 70%) was seen when ISC was extended to 30 min. An excessive amount of $Ca^{2+}$ was associated with RBM-ISC, and energy-linked $Ca^{2+}$ uptake was greatly decreased. (Sciamanna et al, *BBA* 1134: 223, 1992). Reperfusion [REP] of 5 hrs after 30 min of ISC caused a further decrease in the respiratory rates with both succinate and NAD-linked substrates. Injection of 1 μmole ascorbate/rat prior to (<-10 min) or post (< +60 min) REP restored the respiratory rates of RBM-ISC/REP to 65-80% of control (non-ischemic) levels, with both succinate and NAD-linked substrates; when ED(G)TA was also present, the respiratory rates were near control levels. The energy-linked $Ca^{2+}$ uptake was partially restored (≈60% of control levels). Excess ascorbate (> 2 μmole/rat) showed little or no beneficial effects. Our data indicate that REP induced additional damage, which can be alleviated with low concentrations of ascorbate administered within a reasonable time frame (-5 to +60 min) during reperfusion.

**M-Pos489**

MITOCHONDRIAL EFFICIENCIES UNDER MICROXIC AND NORMOXIC CONDITIONS. ((E. Gnaiger[*], G. Mendez[*] and S.C. Hand[§]))
[*]Department of Zoology, University of Innsbruck, Austria, and
[§]Department of EPO Biology, University of Colorado, Boulder, 80309.

Oxygen levels at mitochondria in cells are often much lower than those selected for studying P:O ratios and phosphorylation efficiencies in isolated mitochondria. To measure thermodynamic efficiencies of isolated mitochondria at microxic conditions (below the critical $pO_2$, i.e., <0.1% air saturation), we have developed the approach of oxygen injection calorespirometry. With this approach, the internal mitochondrial oxygen flux at steady state equals the external oxygen supply set by an electronically controlled microinjection pump. Simultaneously, heat flux was measured directly by titration microcalorimetry. The ratio of externally controlled oxygen flux and measured heat flux yields a direct measure of thermodynamic efficiency when compared in the coupled and uncoupled (2,4-dinitrophenol) states. Oxygen levels during steady state oxygen injection were less than 0.01% air saturation. Thermodynamic efficiency of microxic phosphorylation by mitochondria isolated from embryos of the brine shrimp Artemia franciscana was 0.36 ± 0.1 (S.D., n = 4), while the value for rat liver mitochondria was 0.29. At a molar enthalpy of phosphorylation of 44 kJ.mol$^{-1}$ ATP produced, the efficiency of Artemia mitochondria is equivalent to a microxic ATP/$O_2$ ratio of 2.6, or about 2.6 times higher than under normoxia. Efficiency values at low oxygen and low respiratory activation may be particularly relevant for mitochondria in vivo. [Supported by FWF project P7162-BIO, FFF projects 2/270 and 2/286, Anton Paar KG (Graz, Austria); NSF grant DCB-9018579]

**M-Pos490**

$^{31}$P-NMRS AND FATIGUE IN RABBIT MUSCLE IN VIVO. ((T.W. Ryschon, and R.S. Balaban)) Laboratory of Cardiac Energetics, NHLBI, NIH, Bethesda, MD 20892.

Tibialis anterior (TA) - extensor digitorum longus (EDL) muscles of the rabbit were used to study energy metabolism ($^{31}$P-NMR) and muscle tension in response to acute stimulation of the common peroneal nerve, in vivo. Distal tendons of the TA/EDL in anesthetized rabbits were clamped to an isometric load cell and muscle length was adjusted to optimize twitch tension. NMR (4.7 T) was performed with a 31x8 mm surface coil positioned over the TA/EDL as guided by $^1$H imaging. Continuous 1 min. NMR scans were obtained during sequential contraction (15 min.) - recovery (15 min.) cycles. Using a duty cycle of 0.7%, PCr/β-ATP decreased to steady levels with a half-time of 4.9 min. but recovered to control following each of 6 cycles, while muscle tension declined continuously. When duty cycle was increased to 2.5%, PCr/β-ATP and muscle tension both decreased continuously without reaching steady-state and neither recovered from a single contraction cycle. These findings demonstrate: 1) the dependence of steady-state energy metabolism on duty cycle; and 2) the dissociation of energy state from tension production in skeletal muscle, in vivo.

**M-Pos491**

STUDYING THE NUCLEOTIDE BINDING SITES ON $F_1$-ATPASES USING ESR-SPECTROSCOPY: IS A CLOSE PROXIMITY OF THE SITES REQUIRED FOR HIGH ACTIVITY? ((P.D. Vogel, J.H. Nett, R.M. Lösel, S. Burgard, A. Erbse, and W.E. Trommer)) Universität, 6750 Kaiserslautern, Germany.

We employed spin-labeled (SL) and photoaffinity spin-labeled ATP-derivatives in investigating the relative orientation of catalytic and noncatalytic nucleotide binding sites of various $F_1$-ATPases. Dipolar spin-interactions were observed earlier using beef heart mitochondrial enzyme, indicating that a catalytic and a noncatalytic binding site are about 15-20 Å apart from each other in the presence of $Mg^{2+}$ ions. The absence of $Mg^{2+}$ results in ESR-spectra that indicate at least two different environments for the spin-label with no or very little dipolar interactions. We conclude that binding of $Mg^{2+}$ to the enzyme results in a conformational change to bring the two types of sites in close vicinity. An alternative explanation is that SL-ANP does not bind to at least one of the neighboring sites in the absence of $Mg^{2+}$.

Non-activated $F_1$-ATPase from chloroplasts in complex with SL-ATP exhibits ESR-spectra with at least two bound components. Heat-activation of the enzyme in the presence of nucleotide triphosphates (ATP, GTP) results in very unusual lines in the ESR-spectra that may be caused by Heisenberg spin-exchange of two radicals, indicating that the bound SL-ANP are less than 10 Å apart from each other. In addition, ATP-heat-activated $CF_1$ is partially inhibited by $AP_3A$ but not by $AP_5A$, whereas non-activated enzyme is inhibited by $AP_5A$ and activated by $AP_3A$. The latter observation supports the idea that heat-activation brings the sites closer together.

**M-Pos492**

THE AMPHIPHILIC TETRADECAPEPTIDE MASTOPARAN OPENS THE PERMEABILITY TRANSITION PORE OF THE INNER MITOCHONDRIAL MEMBRANE. ((S.A. Novgorodov, T.I. Gudz and D.R. Pfeiffer)) Department of Medical Biochemistry, Ohio State University, Columbus OH 43210. (Sponsored by G.P. Brierley).

Mastoparan, in concentrations of < 2 μM increases the permeability of the inner membrane to low-$M_r$ solutes (present as an osmotic support), and induces the dissipation of $\Delta\psi$. These effects of mastoparan are prevented by cyclosporin A, a potent permeability transition pore (PTP) inhibitor. Higher concentrations of mastoparan change the permeability of the inner membrane in a cyclosporin A - insensitive manner. This later effect may arise from the formation of the solute conducting channels by the mastoparan molecules themselves. The increase in permeability of the inner membrane induced by low concentrations of mastoparan, can also be inhibited by $Ca^{2+}$ chelators, and by other permeability transistion effectors (i.e. oligomycin). The similarity in the actions of oligomycin, cyclosporin A and EGTA, on PTP and mastoparan activated solute fluxes indicates that the target for mastoparan is PTP. This is the first indication of PTP regulation by a protein/peptide. The ability of mastoparan to form an amphipathic α-helix, which is analogous to the presequences of mitochondrial precursor proteins, raises the possibility that PTP is a part of the inner membrane pathway for the protein import. (Supported by NIH grant HL49182).

**M-Pos493**

*IN VIVO* CONFOCAL MICROSCOPY OF THE HUMAN CORNEA.

(( B.R. MASTERS AND A. THAER*)) Anatomy & Cell Biology, USUHS, Bethesda, MD 20814, *Institute for Medical Vision Aid, & Helmut Hund GmbH, Wetzlar, F.R.G.

*In-vivo* confocal microscopy of the living cornea provides *en face* images of high contrast and resolution. We describe a new flying slit confocal microscope, that has unique features and imaging characteristics for *in vivo* human ocular confocal microscopy. The light source is a halogen lamp. The microscope uses standard microscope objectives which are readily interchangeable. We use a Leitz 50X, NA 1.0 water objective or a Leitz 25X, NA 0.6, water objective. The confocal microscope is based on two sets of adjustable conjugate slits. Slits have the possibility of continually adjusting the depth of focus in the z-axis. A slit confocal system passes many-fold more light from the eye to the detector than pinhole type confocal systems. A rotating mirror scans the image of the slit over the plane of the cornea. The detection system consists of an intensified video camera. The tip of the microscope objective never touches or flattens the corneal surface; a gel layer is between the objective and the eye. The instrument can image the full 500 micron thickness of the cornea. Superficial cells, wing cells, nerves, basal cells, in the normal epithelium are easily imaged. There is no need for video frame averaging or digital image processing techniques to enhance the contrast of single video frames. This instrument is currently used to investigate the tear film, renewal of the ocular surface, the role of epithelial innervation in epithelial cell proliferation, the effects of laser refractive surgery on the keratocyte distribution in the stroma, and the nature of endothelial defects. It can also be used to investigate the fine structure of the lens capsule, lens epithelium, and lens lenticular fibers. Support from NIH EY-06958, The Institute for Medical Vision Aid and Helmut Hund GmbH.

**M-Pos494**

**OPTICAL MEASUREMENTS OF $Mg^{2+}$ USING FLUORESCENCE LIFETIMES AND PHASE-MODULATION FLUOROMETRY.**

((H. Szmacinski and J.R. Lakowicz)) University of Maryland, Center for Fluorescence Spectroscopy, School of Medicine, Dept. Biological Chemistry, Baltimore, MD 21201. (Sponsored by M.L. Johnson).

We measured the $Mg^{2+}$-dependent fluorescence decay times of Mag-fura-2, Mag-indo-1 and Magnesium Green using phase-modulation fluorometry. The phase and modulation values were found to be strongly $Mg^{2+}$-dependent for Magnesium Green. The lifetimes of Mag-fura-2 and Mag-indo-1 increase only ~10% upon $Mg^{2+}$ binding. Binding of $Mg^{2+}$ produces a 13-fold increase in Magnesium Green's fluorescence intensity without a spectral shift and a 4-fold increase in mean lifetime (from 0.9 to 3.7 ns). This increase in lifetime produces a 44 degree and 43% change in phase and modulation, respectively (at f = 151.8 MHz, $\lambda_{exc}$ = 514.5 nm, $\lambda_{em}$ > 530 nm, T = 20°C). The apparent $K_d$ values for $Mg^{2+}$ from phase and modulation measurements are 0.45 and 0.12 mM, respectively. These values make this probe as a valuable for measuring intracellular $Mg^{2+}$ concentrations. The lifetime-based method is desirable because Magnesium Green is not a wavelength-ratiometric probe and intensity measurements are sensitive to other factors (photobleaching, probe concentration, etc.). Another advantage of Magnesium Green over the other two $Mg^{2+}$ probes is visible range of excitation (e.g. argon ion laser). We estimated also $K_d$ for $Ca^{2+}$ (at the same conditions as for $Mg^{2+}$), 350 and 1500 nM from modulation and phase, respectively. Magnesium Green can be used for lifetime imaging of intracellular $Mg^{2+}$.

**M-Pos495**

AN INDIRECT IMMUNOFLUORESCENCE PROCEDURE FOR STAINING THE SAME CRYOSECTION WITH TWO DIFFERENT MOUSE MONOCLONAL PRIMARY ANTIBODIES.

((Stephanie A. Lewis Carl*, Ilona Gillette-Ferguson§, Kelly Felix* and Donald G. Ferguson*.)) Depts. of Physiology and Biophysics*, Molecular Genetics, Biochemistry and Microbiology§, University of Cincinnati, College of Medicine.

Indirect immunofluorescence procedures are generally not effective for co-localization of two antigens when both primary antibodies are raised in the same host species. This is due to the inability of the secondary antibodies to distinguish between the two primary antibodies. We report here a modification of a previously reported protocol (Biophys.J. 61:A158,#907) which circumvents this problem. Monoclonal antibodies specific for myosin and actin were used sequentially to stain the same frozen section of guinea pig skeletal muscle. The myosin antibody was applied first and was localized using a rabbit anti mouse IgG-TRITC secondary antibody. The sections were then 'blocked' to prevent cross reactions by incubating in a non-binding mouse monoclonal antibody followed by treatment with unconjugated goat anti mouse IgG Fab fragments. Finally, the actin antibody was applied and localized using a rabbit anti mouse IgG-FITC secondary antibody. Laser scanning confocal microscopy and image analysis demonstrated that the I-bands, the A-bands and the H-bands of each sarcomere were clearly identifiable using this approach. This protocol can be easily modified to permit indirect immunolocalization of two antigens in the same sample using polyclonal primary antibodies.

Supported by NIH HL34779 and AHA Ohio Affiliate SW 91-08.

**M-Pos496**

THEORY FOR MEASURING BIVALENT SURFACE BINDING KINETICS USING TOTAL INTERNAL REFLECTION WITH FLUORESCENCE PHOTOBLEACHING RECOVERY

((H. V. Hsieh and N. L. Thompson)) Dept. Chemistry, University of North Carolina, Chapel Hill, NC 27599-3290

One method for experimentally examining coupled diffusion and reaction kinetics at planar models of cell membrane surfaces is to use total internal reflection with fluorescence photobleaching recovery (TIR-FPR). In a previous work (Thompson et al., 1981, *Biophys. J. 33*, 435), a theoretical basis for interpreting TIR-FPR data was described for monovalent ligands that undergo a reversible reaction with monovalent surface sites in a single step. However, in the majority of experimental systems that have been examined with TIR-FPR, the fluorescence recovery curves are biphasic or triphasic and cannot be described adequately with the previously developed theoretical framework. Therefore, the theory for TIR-FPR has been extended to two different surface binding mechanisms that involve sequential, bivalent surface attachment. Methods for obtaining the intrinsic surface association and dissociation kinetic rates from measured fluorescence photobleaching recovery curves are described. The new theory should be applicable to the association of multivalent protein ligands, such as antibodies or fibrinogen, with supported planar membrane surfaces. This work was supported by NIH grant GM-37145.

**M-Pos497**

MULTICOLOR FLUORESCENCE SPECTROSCOPIC IMAGING WITH AN ACOUSTO-OPTIC TUNABLE FILTER (AOTF).

((Patrick J. Treado)) Department of Chemistry, University of Pittsburgh, Pittsburgh, Pennsylvania 15260

((E. Neil Lewis and Ira W. Levin)) Laboratory of Chemical Physics, National Institute of Diabetes and Digestive and Kidney Diseases, National Institutes of Health, Bethesda, Maryland 20892

((Martin W. Wessendorf)) Department of Cell Biology and Neuroanatomy, University of Minnesota, Minneapolis, Minnesota 55455

Acousto-optic filters have several features that make them well suited for use as wavelength tuning elements in spectroscopic imaging instruments. AOTFs have rapid optical switching capability, wide spectral coverage, high spectral resolution, good image transmission with minimal optical aberrations, physical compactness, digital tunability and no-moving-parts. We have pioneered the use of AOTFs for vibrational spectroscopic microscopy. Specifically, we have employed AOTFs in microscopes for Raman image filtering and near-infrared source tuning. The instrumentation employed for emission imaging involves the placement of the spectral filter between the emitting sample and the CCD detector. The AOTF simultaneously provides spectral filtering while transmitting the image at high fidelity. Spatial resolution on the order of 1μm has been demonstrated. The instrument is also well suited to fluorescence imaging microscopy, as well as the rapid collection of complete fluorescence emission spectra. For systems employing multiple fluorescent tags, the ability to rapidly collect entire emission spectral profiles at each spatial position is particularly powerful and is not easily accomplished with current technology (filter wheels, prisms and gratings). We will present both design details describing this novel instrumentation and recent applications to biological samples stained with multiple fluorophores.

**M-Pos498**

RAMAN AND NEAR-INFRARED (NIR) MICROSCOPY OF BIOLOGICAL MATERIALS USING A NOVEL ACOUSTO-OPTIC TUNABLE FILTER (AOTF) IMAGING SPECTROMETER:

((E. Neil Lewis and Ira W. Levin)) Laboratory of Chemical Physics, National Institute of Diabetes, Digestive and Kidney Diseases, National Institutes of Health Bethesda, Maryland 20892

Biophysical research methods employing both Raman and infrared spectroscopies have traditionally emphasized their ability to provide extremely sensitive and non-invasive probes for examining molecular reorganizations of biological materials by monitoring the structural and dynamic properties of both lipids and proteins. Recent advances in detector, laser, filter and computer technology have provided a base from which increasingly more sensitive measurements have been made, while contemporary developments, particularly in imaging microscopy, have provided a new and even more effective technique for the study of biological materials at both the cellular and molecular level. We have recently described a novel approach for carrying out both Raman and near-infrared spectroscopic imaging microscopy which is faster and provides significantly higher image fidelity than that previously achievable. Since the method can readily record images with 65,536 (256x256) pixels and since for each pixel there is a measured Raman or near-infrared spectrum,any of the experimentally observed vibrational parameters can be used to construct new image presentations which emphasize different domains of chemically and/or structurally distinct species. We have used this technique to image numerous biological materials and in the future we will be refining the methodology. Data will be presented derived from both model and intact biological systems which highlight the additional power this new tool brings to our current biophysical studies. A description of the acquisition and analysis of these images using new analytical strategies which integrate conventional digital enhancement techniques with spectroscopic methods will be discussed.

**M-Pos499**

COMBINED FURA-2 RATIO AND TMRE 3D IMAGING: MITOCHONDRIAL DEPOLARIZATION FOLLOWING CYTOSOLIC CALCIUM INCREASES. ((L. M. Loew,† W. Carrington,‡ R. A. Tuft,‡ and F. S. Fay‡)) †Physiology, U. Conn. Health Ctr., Farmington, CT 06030, ‡Physiology, U. Mass. Med., Worcester, MA 01605.

Several dehydrogenases involved in mitochondrial respiration are potentiated by $Ca^{2+}$; it has been suggested that this may be a regulatory signal to allow the mitochondrion to respond to increased energy demands during stimulation by an extracellular signal. When challenged with high $Ca^{2+}$, the mitochondrion is also known to be capable of calcium uptake driven by its large membrane potential. Knowledge of the *in situ* response of mitochondrial membrane potential to cytosolic $Ca^{2+}$ changes would be critical to an elucidation of the cell physiological consequences of these phenomena. We have combined several new technologies to make such measurements possible for the first time: 1) The fluorescent potentiometric probe TMRE distributes across membranes according to the Nernst equation. 2) An ultra-fast 3-D microscope collects Z-series data fast enough to freeze mitochondrial motion. 3) Computerized image deconvolution algorithms and calibrations accurately quantitate fluorescence in 3 dimensions from objects as small as mitochondria. In addition, the microscope was modified to permit acquisition of 340/380nm fura-2 image pairs within 6 second after the collection of the 3D TMRE dataset. N1E-115 neuroblastoma cells were stimulated with 100 nM bradykinin or high extracellular $[K^+]$ to produce transient intracellular $[Ca^{2+}]$ increases. A sustained $[Ca^{2+}]$ rise was effected by 2 $\mu$M ionomycin. In all cases, individual mitochondria were significantly depolarized. Very high intracellular calcium levels produced complete and irreversible depolarization. (supported by USPHS grants GM35063 and NSF grant DIR-8720188)

**M-Pos500**

**RESOLUTION ENHANCEMENT IN FLUORESCENCE IMAGES BY DECONVOLUTION WITH AXIALLY ASYMMETRIC POINT SPREAD FUNCTIONS.** ((B. A. Scalettar, J. R. Swedlow, J. W. Sedat & D. A. Agard)), HHMI and Dept. of Biochem. & Biophys., UCSF, San Francisco, CA 94143.

The point spread function (PSF) describes the blurring of a diffraction-limited spot by a microscope objective lens and is used in deconvolution algorithms to deblur images. Although standard analytical expressions for the PSF possess radial and axial symmetry, experimentally derived PSF's often possess a high degree of axial asymmetry that probably arises from spherical aberration. When a sample is illuminated with a fixed wavelength of light, this axial asymmetry can largely be eliminated through choice of objective immersion oil with an appropriate refractive index, and asymmetry can then be neglected during deconvolution. However, for multi-wavelength data sets, wavelength- dependent variations in refractive index make it impossible to neglect axial asymmetry in the PSF. Motivated by our interest in multi-wavelength imaging, we have made a careful study of the improvement in z resolution of a deconvolved image achieved by taking the axial asymmetry of the PSF into account. PSF's that differ in their degree of axial asymmetry were obtained from images of 0.12 µm diameter fluorescent beads, using high numerical aperture objectives and immersion oils with different refractive indices. Multi-wavelength PSF data sets were generated by placing beads of different color on a given slide and using a single immersion oil. These PSF's were then deconvolved using algorithms that either neglect, or account for, axial asymmetry. Comparison of full-width at half maximum intensity falloff for the resulting deconvolved images showed that the algorithm that accounted for asymmetry produced as much as a two-fold enhancement in z resolution for highly asymmetric images, as well as some enhancement in x-y resolution.

**M-Pos501**

FLUORESCENCE PHOTOACTIVATION BY TWO-PHOTON EXCITATION : KINETICS OF UNCAGING AND THREE-DIMENSIONAL POINT DIFFUSION MEASUREMENTS (( I. Cauchetteux-Silberzan, R.M. Williams* and W.W. Webb))
School of Applied and Engineering Physics and *Department of Physics, Clark Hall , Cornell University, Ithaca, NY14853.

The localization of UV two-photon excitation by a focused femtosecond laser beam, as demonstrated in three-dimensional FPR experiments (Piston et al., *Biophys.. J.*, **61**, A34 (1992)), also allows the photorelease of UV photoactivable or "caged" compounds in very small volumes ($0.1\mu m^3$). We apply two-photon excitation for short periods of time (microseconds to milliseconds) to trigger the photorelease of caged fluorophores and a continuous co-focused "one-photon" (488 or 514nm) laser beam and confocal detection to monitor the presence of the freshly uncaged fluorophores. As the uncaged dyes diffuse away from the focal spot after photorelease, the fluorescence intensity decreases. The diffusion constant is extracted from this decay curve in a manner analogous to three-dimensional FPR. We call this technique "FAR", Fluorescence Activation Redistribution. We can also extract from FAR data the kinetics of fluorescence photoactivation in the microsecond to second time scale. We can slow the diffusion of the freshly uncaged fluorophores out of our observation spot by attaching the caged fluorophores to high molecular weight dextrans, increasing the solvent's viscosity or by immobilization. Data are presented for symmetrically caged fluorescein and caged resorufin.

Supported by the Developmental Resource for Biophysical Imaging and Opto-Electronics funded by NSF(DIR8800278) and NIH(RR04224).

**M-Pos502**

INTERACTIONS OF IGE RECEPTORS WITH CELL SURFACE RUFFLES BY SIMULTANEOUS DIC AND CONFOCAL MICROSCOPY. ((D.R. Sandison, T.A. Ryan**, and W.W. Webb*)) Molecular and Cellular Physiology, Stanford University**, Physics and School of Applied and Engineering Physics*, Cornell University, Ithaca, NY 14853.

Rat basophilic leukemia (RBL) cells undergo large scale morphological changes upon crosslinking of cell surface IgE receptors or upon treatment with phorbol ester. Changes include an increase in membrane associated F-actin, formation and motion of large cell membrane ruffles over the entire cell surface, and exclusion of crosslinked receptors patches from the ruffles. To study receptor-ruffle interactions, we use simultaneous laser scanning differential interference contrast (DIC) and fluorescence laser scanning confocal microscopy (LSCM) (Ryan et al., Biophys. J.,**57**, 374a, 1990). The DIC image, with its inherent 3-d resolution, locates the cell surface, and the confocal fluorescence image measures the local concentrations of fluorescent probes. Using LSCM to three-dimensionally map fluorescently labelled F-actin and coanalyzing the DIC an LSCM images, we measure the amount of F-actin associated with the cell surface. Preliminary results show this amount to be within a factor of 3 on and off the ruffles. Laser scanning DIC images yield vertical profiles of cell surface ruffles and are used to study their formation and motion. We combine DIC and nonconfocal fluorescence to simultaneously measure the motions of the membrane ruffles and fluorescently labelled clusters of IgE receptors. This technique shows that monomeric IgE uniformly decorates the cell surface, and that patches of IgE are excluded from ruffles, in agreement with data from electron microscopy. Supported by the Developmental Resource for Biophysical Imaging and Opto-electronics funded by the NIH (5P41-RRO-4224).

**M-Pos503**

FORCE AND MEMBRANE COMPLIANCE MEASUREMENTS USING AN OPTICAL TRAP AND LASER INTERFEROMETRY. (( L.P. Ghislain, I. Brust-Mascher†, and W.W. Webb†)) Dept. of Applied & Eng. Physics, Cornell University, Ithaca, NY 14853.

The use of a single beam gradient force optical trap with a laser interferometer to measure small forces is reported. A micron-diameter dielectric probe in liquid is trapped in a stable, 3-dimensional potential well close to the focus of a near-infrared Nd:YAG laser beam having a gaussian intensity profile. Probe displacement is detected with nanometer sensitivity by a superposed beam from a He:Ne laser two-beam interferometer. Force is proportional to small probe displacements. The spring constant of the optical trap obtained from the corner frequency(kilohertz) of the lorentzian spectrum of probe position fluctuations is significantly smaller than the spring constant of typical cantilevers used in atomic force microscopy, thus the optical trap provides improved detection of small forces. For an incident 500mW beam focussed by a 1.3NA lens to trap a micron-diameter particle the spring constant is ~0.1pN/nm(axial) and ~0.4pN/nm(lateral), the typical AFM cantilever spring constant is 100-1000pN/nm. It is important to minimize the applied force when working with soft samples such as proteins and membranes. The AFM cantilever measures forces that are usually greater than 10pN, near the deformation threshold for globular proteins, while the optical trap provides force sensitivity of about 1 pN. We demonstrate the sensitivity of the technique by probing the membrane of fish keratocytes.

Supported by the Developmental Resource for Biological Imaging and Optoelectronics funded by the NIH (5P41-RRO-4224).

**M-Pos504**

**THE VIABILITY OF CULTURED CELLS UNDER TWO-PHOTON LASER SCANNING MICROSCOPY.** ((J.A. Ridsdale and W.W. Webb)) Applied and Engineering Physics. Clark Hall, Cornell University, Ithaca NY 14853.

The effects of on the viability of tissue culture cells of the red pulsed-laser irradiation, that is focused into the cells for fluorescence excitation, could be an important constraint on the potential usefulness of non-linear microscopy. Cells irradiated with ultrashort-pulsed laser light were tested for membrane permeability with the polar DNA binding dye ethidium bromide. RBL (rat basophilic leukemia) cells were loaded with the calcium indicator Indo 1 and scanned for various times at various laser powers. The fraction of leaky cells increases sharply around 75mW, but laser power of 50mW or less does not detectably kill cells with exposures of up to seven minutes of continuous scanning. This level of laser irradiation is more than adequate for calcium measurements using two channel imaging of Indo 1. RBL cells which have not been loaded with dye show a similar sensitivity to laser irradiation, suggesting that this dye is not potentiating the damaging effects of this irradiation. Indo 1 loaded Pk1 (porcine kidney epithelium derived) cells show similar sensitivity. Similar tests were also carried out using the DNA binding dye Hoescht 33342. Good signals were obtained at laser intensities around 20 mW. At this power level the cells are not killed after several minutes of irradiation. A steep transition to lethality occurs around 40 - 50 mW of laser power when most cells are killed within two minutes. Again, there is a sharp threshold in the number of killed cells as function of laser light power. Our findings to date indicate that cell viability can be significantly compromised during observation with a too high power of two-photon laser scanning excitation by an unknown mechanism Conversely, careful selection of irradiation power allows data collection regimes that do not lead to observable damage to cells .

Supported by grants from NIH and NSF to the Developmental Resource for Biophysical Imaging and Opto-Electronics and by MRC Canada (To JAR)

**M-Pos505**

FLUORESCENCE LIFETIME IMAGING OF RAT BASOPHILIC LEUKEMIA CELLS AND RAT CARDIAC MYOCYTES USING TWO-PHOTON EXCITATION. ((J.B. Guild, D.W. Piston, D.R.Sandison*, and W.W. Webb)) School of Applied and Engineering Physics and *Department of Physics, Cornell University, Ithaca, NY 14853.

The inherent background rejection properties of two-photon fluorescence excitation microscopy enable the determination of fluorescence decay lifetimes within three dimensionally resolved diffraction limited sample volumes [Piston, et al., *Proc. SPIE* **1640**:379 (1992)]. The simultaneous non-linear absorption of two red photons to excite an ultraviolet transition depends on the incident intensity squared and, hence localizes the resulting fluorescence within the focal region. This illumination scheme coupled with an apparatus to measure lifetimes using a frequency domain technique provides a probe of the local fluorophore environment at a specific location within an extended sample. Thus, intracellular parameters and events occuring on a nanosecond time scale are measured with imaging properties identical to an ideal confocal fluorescence microscope using the same optical wavelength. The accuracy of a measured lifetime is limited by photon shot noise and the temporal image pixel width compared to the cross-correlation frequency. The trade-off between these components were explored for cross-correlation frequencies between 10 Hz and 1000 Hz using several fluorphores both in homogenous samples and in living cells. The decay times of 4'-6-Diamidino-2-phenylindole (DAPI) and Indo-1 have been imaged within living RBL cells as determined from phase shift and amplitude demodulation data. Similarly the decay lifetime of NADH and Indo-1 in living rat cardiac myocytes have been imaged.
Supported by the Developmental Resource for Biophysical Imaging and Opto-electronics funded by NSF(DIR8800278) and NIH(RR04224).

**M-Pos506**

THREE DIMENSIONAL IMAGING OF NUCLEAR DIVISION IN LIVING SEA URCHIN EMBRYO BY TWO-PHOTON EXCITATION FLUORESCENCE MICROSCOPY. ((David W. Piston, Robert G. Summers* and Watt W. Webb)) Applied & Engineering Physics, Cornell Univ, Ithaca, NY and *Dept of Anatomy, SUNY Medical School, Buffalo, NY

The manner in which embryonic determinants are distributed by the cleavage process may yield important early clues about cell differentiation. While we have obtained useful information from fixed embryos with confocal microscopy [Summers et al 1992 *Dev Growth Diff* In Press], a more dynamic view is required. The only available fluorophores that stain DNA and are non-toxic to the embryos are excited with ultraviolet (UV) light, which damages the embryos. To successfully image nuclei in living embryos, we have used two-photon excitation of Hoechst 33342 with a laser scanning microscope and water immersion optics. In the two-photon technique, simultaneous absorption of two red photons from a subpicosecond mode-locked laser is used instead of conventional UV excitation [Denk et al 1990 *Science* **248**:73]. Unstained living embryos are not damaged by exposure to the red light, even over several division cycles (~4 hours). With H33342 stained embryos, we typically acquire 10-20 optical sections (spaced 3$\mu$m apart, 3 sec/section) every 10 minutes throughout a single division cycle (45 min.) with excellent embryo viability. These images achieve diffraction limited resolution and single chromosomes within the condensed nuclei are easily visible with no computer image enhancement. In this manner, we have imaged living embryos through either 2nd, 3rd or 4th cleavage, and have obtained good signal levels through the entire 100$\mu$m thickness of the embryo.
Supported by the Developmental Resource for Biophysical Imaging Opto-electronics [NSF(DIR8800278), NIH(RR04224)] and NIH(RR06993).

**M-Pos507**

A TIME-RESOLVED FLUORESCENCE MICROSCOPE.
((T. French, P. So, K. Berland and E. Gratton)) University of Illinois at Urbana-Champaign, Laboratory for Fluorescence Dynamics, Department of Physics, 1110 W. Green St., Urbana, IL 61801.

We have constructed a time-resolved fluorescence microscope system that can collect images which show differences in fluorescence decay times. The microscope system has the abilities of the more common steady-state fluorescence imaging microscope and, additionally, can determine fluorescence intensity as a function of time. A modulated laser beam is the light source and a modulated microchannel plate coupled to a CCD camera serves as the detector. Data arrives at the detector at a chosen frequency (DC–150 MHz) and is heterodyned by the microchannel plate to a frequency slower than the camera's sampling rate (frame rate). Alternatively, the microchannel plate can be set to homodyne the incoming signal at which point the system becomes capable of real time analysis. The homodyning or heterodyning process maintains the spatial coherence of the images, which may have a resolution of 0.5 microns. The frequency domain images (DC intensity, AC intensity, phase shift and demodulation) can be interpreted directly or new combinations can be created for further analysis (e.g., lifetime images or phase-resolved images). Lifetimes as short as about 2 ns can be resolved with a resolution of about 50 ps. Using phase resolved techniques, fractional components of lifetimes at each pixel can be distinguished, potentially with only a single frequency data run. Supported by NIH RR03155.

**M-Pos508**

PREPARATION OF THIN 3-D CRYSTALS FOR ELECTRON CRYSTALLOGRAPHY
((Dan Shi and David L. Stokes)) Department of Physiology, University of Virginia Health Sciences Center, Charlottesville, VA 22908

Three dimensional reconstruction of either 2-D crystals or thin, 3-D crystals requires tilting them to high angles; collection of data at high angles usually represents the rate limiting step of the analysis. In particular, diffraction spots away from the tilt axis are generally blurred either due to a lack of specimen flatness or, in the case of thin 3-D crystals, due to crystal disorder normal to the substrate plane. We are studying thin, 3-D crystals of CaATPase and have used thin, 3-D catalase crystals as a model for developing specimen preparation methods. Catalase crystals were adsorbed to 400-mesh copper grids coated with carbon film with minimal surface roughness made by multiple evaporation of carbon onto mica. Crystal flatness was judged by comparing electron diffraction patterns of untilted crystals with those tilted at 60°. When catalase crystals were dried in 1% glucose, very poor diffraction was obtained from tilted crystals even though untilted crystals diffracted to ~3Å. In contrast, frozen-hydrated catalase crystals produced high resolution, though blurred, spots off the tilt axis, indicating that crystal curvature was limited to ~1°. This suggests that dried crystals suffer from disordering normal to the substrate. To try to improve flatness of frozen- hydrated crystals, they were centrifuged at 300 rpm, prior to freezing. Indeed, most high resolution diffraction spots remained sharp at 60° tilt, suggesting that crystals pushed onto the carbon film by centrifugal force are flatter than those simply adsorbed to the film. We infer that with suitable centrifugal force the flatness of frozen-hydrated crystals will only depend on the roughness of the film.(Supported by NIH grant AR40997)

**M-Pos509**

AFM STUDIES OF JUNCTIONAL FACING MEMBRANE AND PURIFIED RYANODINE RECEPTOR.
(M. Ronjat[$], J.-J. Lacapère° and D. Chatenay*) (*)URA CNRS 1379, Institut Curie, Paris, FRANCE; (°)URA CNRS 1290, CEN Saclay, Gif/Yvette, FRANCE; ($)URA 520 CNRS, CEN Grenoble, FRANCE, (Spon. by M. MICHELVILLAZ)

The Ryanodin Receptor (RR) is one of the biggest proteins complex and is therefore a good candidate for Atomic Force Microscopy (AFM) studies. AFM images of RR either in Junctional Facing Membranes (JFM) or in a purified form have been obtained both with dried and hydrated samples. Monomeric form obtained from purified RR in the presence of Zwittergent 3-14 has also been studied. Though no intramolecular resolution is achieved the overall shape and size of the observed hydrated objects are in agreement with previous electron microscopy studies. Furthemore using various substrates such as mica or polylysin coated mica, we have been able to determine which part of the protein (both in JFM or purified form) is in contact with the substrates. Interactions between functionnalized tips and adsorbed proteins have also been investigated by AFM.

**M-Pos510**

NEAR-FIELD SCANNING FLUORESCENCE MICROSCOPE FOR STUDYING MUSCLE PROTEIN FILAMENTS AT SUPER RESOLUTION. ((E.J. Seibel and G.H. Pollack)) Center for Bioengineering WD-12, University of Washington, Seattle, WA 98195.

Near-field scanning optical microscopy (NSOM) is a new method of attaining super resolution ($\lambda$/43) with visible light, thus breaking the diffraction limit (Betzig *et al. Science* 251:1468,1991). NSOM is a scanning-probe microscopy that uses light guided down the probe and through an aperture smaller than its own wavelength, emerging collimated for a limited range (near-field). By scanning the probe in the near-field across the surface of a protein and collecting the extrinsic or intrinsic fluorescence, an image of that surface can be generated with resolution comparable to the tip aperture. For imaging protein structures in their native state, NSOM has several advantages over other scanning probe microscopies: it capitalizes on the noninvasiveness of light, it has direct correlation with images from conventional microscopy, and it can exploit the many available fluorescent labels that enhance signal-to-noise. In our novel design, NSOM is used in an epi-illumination mode, specifically designed to detect fluorescence from thick specimens in physiological buffer. It is coupled to a conventional optical microscope so the user can locate and position the labeled structure under the probe, then zoom up to NSOM super-resolution. Aluminum-coated, tapered quartz probes have been made with 50-100 nm tip apertures. The feasibility of epi-illumination and other aspects of microscope testing are nearing completion. To our knowledge, NSOM has never been applied in a biological experiment. We plan to measure the length of actin and myosin filaments in a contracting myofibril. Future plans include: mapping genes in chromosomes, localization of ion-channels in membranes, and detection of motor-protein conformational changes.

**M-Pos511**

**A NEW WAVELENGTH-RATIOMETRIC $Ca^{2+}$ PROBE WITH LONG WAVELENGTH EXCITATION AND EMISSION.** ((E.U. Akkaya and J.R. Lakowicz)) Univ of Maryland, School of Medicine, Center for Fluorescence Spectroscopy, Department of Biological Chemistry, 108 N. Greene Street, Baltimore, MD 21201. (Spon. by J.R. Lakowicz)

We have synthesized a fluorescent $Ca^{2+}$ probe that contains the highly selective $Ca^{2+}$ chelator BAPTA (1,2-bis-(2-amino-phenoxy)ethane-N,N,N',N',-tetraacetic acid) as an integral part of the fluorophore. On binding to $Ca^{2+}$ ($K_d$=1.8 $\mu$M), emission is mostly unchanged; but the absorbance peak shifts dramatically (from 508 nm to 407 nm) to shorter wavelengths. Hence, wavelength-ratiometric measurements are possible using two excitation wavelengths. Both $Ca^{2+}$-bound and free forms of the probe can be excited at wavelengths where autofluorescence would not be problem in an intracellular environment. As with all polycarboxylate probes, conversion to a cell permeable AM (acetoxymethyl) ester form is feasible. While the quantum yield of the probe is low, we see this probe as the first example of a series of related probes. We intend to optimize its spectral properties by chemical modification of the basic structure. We also appreciate the potential of our approach in the development of wavelength-ratiometric probes for other cations of biological significance.

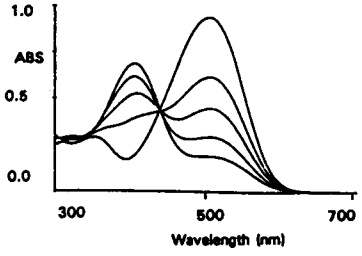


**M-Pos512**

QUANTIFICATION OF CHANGES IN MITOCHONDRIAL SPECIFIC PYRIDINE NUCLEOTIDE FLUORESCENCE FROM SKELETAL MUSCLE CELLS.

((K.N. Richmond*, P.C. Johnson*, and R.M. Lynch*+))Departments of Physiology* and Pharmacology+, University of Arizona, Tucson AZ 85724

Adjustments in cell metabolism elicit changes in pyridine nucleotide (PN) fluorescence from skeletal muscle *in vivo*. The changes in fluorescence are assumed to reflect shifts in the mitochondrial $NAD^+$/NADH redox couple. To test this assumption the distribution of PN fluorescence in enzymatically dissociated single cells from rat spinotrapezius muscle was compared to that for a mitochondrial selective fluorescent probe (Rhodamine 123) using 3-D microscopic imaging techniques. Images were acquired using a liquid cooled CCD camera attached to an Olympus IMT-2 microscope equipped with a motorized focus which provides precise movement in the Z plane. Fluorophore distributions were analyzed by acquiring through-focus image sets consisting of 15 optical sections which were then processed to reduce out of focus blurring using a deconvolution algorithim based on regularization theory. From Rhodamine 123 images the cell volume occupied by mitochondria was estimated to be 21%. This is consistent with reported values for other red muscles analyzed by electron microscopy. A comparison of PN fluorescence to the mitochondrial distribution indicated 30-35% of the PN fluorescence is associated with mitochondria in the resting state. Preliminary studies indicate that increases in PN fluorescence elicited by the mitochondrial inhibitor cyanide also are greatest in these areas. This observation is consistent with the interpretation that changes in PN fluorescence at the tissue level are indicative of changes in the mitochondrial metabolic state. Current studies will quantify mitochondrial PN fluorescence during perturbations in muscle cell metabolism.

**M-Pos513**

IMAGING SUBCELLULAR STRUCTURES WITH THE SCANNING FORCE MICROSCOPE (SFM).

((L. I. Pietrasanta†*, A. Schaper†, F. J. Barrantes* and T. M. Jovin†)) †Department of Molecular Biology, Max Planck Institute for Biophysical Chemistry, P. O. Box 2841, W-3400 Göttingen, Federal Republic of Germany. *Instituto de Investigaciones Bioquimícas (INIBIBB), C. C. 857, 8000 Bahía Blanca, Argentina.

An SFM (NanoScope from Digital Instruments) was used for high resolution imaging of subcellular structures of cultured rat mammary carcinoma cells. We adjusted the conditions of sample preparation so as to selectively visualize the microvilli, the nucleus, the mitochondria, and the various components of the cytoskeletal system, with high resolution and no apparent distortion. The microvilli are well preserved after fixation in glutaraldehyde vapor and are clearly distinguished as abundant 1-2 µm protrusions from the cell surface. To observe the intracellular organelles, the plasma membrane was removed with non-ionic detergent in a buffer system. The nuclei are very well defined; if the nuclear envelope is removed, features of the chromatin are visible. Invariably, the nucleoli appear as higher, discrete structures. The mitochrondria are concentrated primarily in the perinuclear space and exhibit a well defined filamentous shape. The cytoskeletal network is resolved as a complex mesh in which the three major components are distinguishable: actin fibers, microtubules, and intermediate filaments. In all cases, positive identification of the substructures was achieved by imunofluorescence, immunogold, and specific fluorescence probes.

Similar studies are being conducted on cellular systems with specific cell surface receptors.

**M-Pos514**

MEASUREMENT OF MICROSTRUCTURE, ADHESION AND UNBINDING OF GIANT VESICLES BY QUANTITATIVE REFLECTION INTERFERENCE CONTRAST MICROSCOPY.

((J.Rädler)) Physics Department, Technical University Munich, D-8046 Garching/Munich, Germany. (Spon. by E.Sackmann)

Reflection Interference Contrast Microscopy (RICM) allows to study the membrane-substrate separation distance of giant phospholipid vesicles close to an underlying surface with nm resolution. Osmotically swollen vesicles can be regarded as rigid colloidal particles interacting with substrates via long range electrostatic, VdW and gravitational forces. The interaction was determined from the Brownian motion of vesicles tracked by image processing. In the case of adhering vesicles the bound contour shapes were reconstructed from the interference pattern depending on the area to volume ratio and the bending elasticity modulus. Membranes attracted by a weak potential exhibited thermally excited surface undulations. The time-space correlation function was measured and compared with the scaling behaviour predicted for undulation forces and the unbinding transition. A new contrast variation technique based on RICM is presented which allows optical density mapping of bilayers close to a surface with an out of plane resolution of 0.2nm and a lateral resolution of 0.2µm.

## MOLECULAR MECHANISMS OF MEMBRANE FUSION

**Tu-AM-Symi-1**

MEMBRANE FUSION PROTEINS: FROM VIRUS TO SPERM.

((J.M. White)), Univ. of California, San Francisco, CA 94143

The processes of virus-cell and cell-cell fusion are topologically identical. In both cases, membrane leaflets that face the extracellular environment make initial contact. We have therefore hypothesized that proteins involved in important cell-cell fusion events, such as sperm-egg fusion and myoblast fusion, resemble viral membrane fusion proteins. This hypothesis will be discussed.

Most viral membrane fusion proteins share the following characteristics: They are composed of one or two type I integral membrane glycoproteins that form higher order oligomers. They contain a fusion peptide, a relatively hydrophobic stretch of amino acids, in a transmembrane-anchored subunit. Proteolytic processing activates fusion potential. The fusion glycoprotein complex is also involved in binding to the host cell membrane. These features will be illustrated in the context of recent models for how the well characterized influenza virus hemagglutinin promotes membrane fusion.

A sperm surface protein called PH-30 was implicated in the process of sperm-egg fusion based on the ability of an anti-PH-30 monoclonal antibody to prevent sperm-egg fusion. Biochemical, cell biological, and molecular biological studies have revealed that PH-30 shares many properties with viral membrane fusion proteins: PH-30 is a complex of two type I integral membrane glycoproteins. Proteolytic processing of PH-30 correlates with the acquisition of fertilization competence. One subunit of PH-30 contains an apolar sequence that resembles viral fusion peptides. The other subunit contains a receptor binding domain. Possible roles of PH-30 in sperm-egg binding and fusion will be discussed.

**Tu-AM-Symi-2**

**A DISSECTION OF STEPS LEADING TO VIRAL ENVELOPE PROTEIN-MEDIATED MEMBRANE FUSION.**

((Robert Blumenthal)) NCI, NIH, Bethesda, MD, 20892.

The viral fusion process involves a range of steps before the final merging of membranes occurs. Our studies deal with a number of key questions concerning the fusion process such as: How does triggering the event by a pH or temperature change, or receptor binding affect conformation of the viral envelope protein? Do the viral proteins form oligomeric complexes at the site at which fusion is to occur? Can we identify intermediate fusion steps or structures? What sorts of molecular rearrangements occur before, during and after the fusion event? These questions are approached by developing kinetic assays for fusion of fluorescently-labeled virus with a variety of target membranes using spectrofluorometric and video microscopic techniques. We have studied the mode of action of the hemagglutinin (HA) protein of influenza virus, as well as other viral envelope proteins using both intact virus and viral proteins expressed on surfaces of cells. We could identify a number of intermediates in the kinetic pathway, which include a committed pre-fusion state, a fusion junction which allows redistribution of lipids and small aqueous molecules, and a wide opening which allows entry of the nucleocapsid into the cells. The molecular structure of the various intermediates is examined by a combination of biochemical, biophysical and genetic approaches.